Graduate School Form 30
(Updated 11/20/2014)

PURDUE UNIVERSITY
GRADUATE SCHOOL
Thesis/Dissertation Acceptance

This is to certify that the thesis/dissertation prepared

By Xu Han

Entitled
Design and Synthesis of Small-Molecule Protein-Protein Interaction Antagonists

For the degree of Master of Science

Is approved by the final examining committee:

Samy Meroueh

Eric C. Long

Michael J. McLeish

To the best of my knowledge and as understood by the student in the Thesis/Dissertation Agreement, Publication Delay, and Certification/Disclaimer (Graduate School Form 32), this thesis/dissertation adheres to the provisions of Purdue University's "Policy on Integrity in Research" and the use of copyrighted material.

Approved by Major Professor(s): Samy Meroueh

Approved by: Eric C. Long 11/21/2014

Head of the Department Graduate Program Date

DESIGN AND SYNTHESIS OF SMALL-MOLECULE PROTEIN-PROTEIN INTERACTION ANTAGONISTS

A Thesis

Submitted to the Faculty

of

Purdue University

by

Xu Han

In Partial Fulfillment of the

Requirements for the Degree

of

Master of Science

December 2014

Purdue University

Indianapolis, Indiana

Dedicated to my family and friends

ACKNOWLEDGMENTS

I want to thank my academic adviser Dr. Samy Meroueh for assisting me and guiding me through graduate study. I would also like to thank Dr. Tax Georgiadis for his inculcation in my research, including performing synthesis and data analysis. Also I specifically thank his encouragement and assistance in my life in United States.

I would like to thank my great friends Jack (Geno) Samaritoni and Kitty O'Doherty for their friendship and strong help in my current study and future career. I also want to thank my senior colleagues Eric Knabe and Yajun Jian for their friendship, training and guidance to my research in the laboratory.

I sincerely appreciate my parents, younger brother and my undergraduate academic adviser, Dr. Xiaowen Xue for their love, support and encouragement throughout my time in United States. And I would also like to thank my lovely girlfriend, Li Ma, for all her support, encouragement, solicitude and belief in me throughout my life in United States. If without them I wouldn't accomplish my degree in United States.

TABLE OF CONTENTS

Page

Page

LIST OF TABLES

LIST OF FIGURES

Figure Page

Figure Page

Figure Page

LIST OF SCHEMES

LIST OF ABBREVIATIONS

AID	α-interaction domain
Boc	di-*tert*-butyl dicarbonate
BID	β-interaction domain
DCM	dichloromethane
DIAD	diisopropyl azodicarboxylate
DMAP	4-dimethylaminopyridine
DMSO	dimethyl sulfoxide
ECM	extracellular matrix
EDCI	1-ethyl-3-(3-dimethylaminopropyl)carbodiimide hydrochloride
ELISA	enzyme-linked immunosorbent assay
ERK	extracellular signal-regulated kinases
FP	fluorescence polarization
GPI	glycosylphosphatidylinositol
HATU	1-[bis(dimethylamino)methylene]-1*H*-1,2,3-triazolo[4,5-*b*] pyridinium-3-oxid hexafluorophosphate
HOAc	acetic acid
HOBt	hydroxybenzotriazole

HPLC	high-performance liquid chromatography
HRMS	high-resolution mass spectrometry
iPrOH	isopropyl alcohol
LC/MS	liquid chromatography–mass spectrometry
Lys	lysine
MMP	matrix metalloproteinase
NaOEt	sodium ethoxide
NMR	nuclear magnetic resonance
Phe	phenylalanine
SAR	structure–activity relationship
TEA	triethylamine
TFA	trifluoroacetic acid
THF	tetrahydrofuran
Trp	tryptophan
Tyr	tyrosine
uPAR	urokinase receptor
uPA	urokinase-type plasminogen activator
UV	ultraviolet
VGCCs	voltage-gated Ca^{2+} channels

ABSTRACT

Han, Xu. M.S., Purdue University, December 2014. Design and Synthesis of Small-Molecule Protein-Protein Interaction Antagonists. Major Professor: Samy Meroueh.

Protein-protein interactions play a crucial role in a wide range of biological processes. Research on the design and synthesis of small molecules to modulate these protein-protein interactions can lead to new targets and drugs to modulate their function. In Chapter one, we discuss the design and synthesis of small molecules to probe a protein-protein interaction in a voltage-gated Ca^{2+} channel. Virtual screening identified a compound (BTT-3) that contained a 3,4-dihydro-3,4'-pyrazole core. This compound had modest biological activity when tested in a fluorescence polarization (FP) assay. The synthetic route to BTT-3 consisted of six steps. In addition, analogs of BTT-3 were made for a structure-activity study to establish the importance of a carboxylate moiety. We also synthesized a biotinylated benzophenone photo-affinity probe and linked it to BTT-3 to identify additional protein targets of the compound. In Chapter two, small-molecule antagonists targeting uPA-uPAR protein-protein interaction are presented. A total of 500 commercially-available compounds were previously identified by virtual screening and tested by a FP assay. Three classes of compounds were found with biological activity. The first class of compounds contains pyrrolidone core structures represented by IPR-1110, the second class has a novel pyrrolo[3,4-*c*]pyrazole ring system, represented by

IPR-1283 and the last series had compounds with a 1,2-disubstituted 1,2-dihydropyrrolo[3,4-*b*]indol-3(4*H*)-one core structure, represented by IPR-540. Each of these three compounds were synthesized and assessed by FP and ELISA assays. A binding mode of IPR-1110 with uPA was subsequently proposed. Based on this binding mode, another 61 IPR-1110 derivatives were synthesized by us to illustrate the SAR activity. Analogs of the other two series were also synthesized.

CHAPTER 1. STRUCTURE-BASED DRUG DESIGN AND SYNTHESIS TARGETING Ca^{2+} CHANNEL PROTEIN-PROTEIN INTERACTIONS

1.1 Introduction

1.1.1 Antagonists Targeting Ca^{2+} Channel Protein-Protein Interactions

Protein-protein interactions play an essential role in a number of biological processes, such as the formation of protease-inhibitor, antigen-antibody and hormone-receptor complexes.[1] Protein-protein interactions are intrinsically important to study the role of allostery. In addition, protein-protein interactions provide an avenue to understand protein folding. It is known that there are three major forces that drive protein-protein interactions; they include hydrophobicity, hydrogen bonding, and van der Waals interactions. In addition, protein-protein interactions are also an important source of new drug targets.[2-5]

Ca^{2+} plays a crucial role in biological processes and it is the second messenger of electrical signaling. Ca^{2+} can initiate intracellular events including secretion, synaptic transmission and gene expression. In addition, the influx of Ca^{2+} through voltage-gated Ca^{2+} channels (VGCCs) regulates various cellular processes, including tumorigenesis, cell migration and cell death. These VGCCs are the main Ca^{2+} entryways to nerve and

muscle cells.[6,7] These high-voltage Ca^{2+} channels are plasma membrane proteins that consist of four subunits, including α_1, $\alpha_2\delta$, β and γ (Fig. 1.1).[6] $Ca_v\alpha_1$ is the pivotal subunit of voltage-gated Ca^{2+} channels and this subunit contains most drug binding sites and channel pore. The β subunit ($Ca_v\beta$) is essential in regulation of Ca^{2+} channels by G proteins and protein kinases.[8-11] In addition, this subunit also plays a crucial role in regulating the surface expression of high-voltage activated Ca^{2+} channels and directly modulates gene transcription.

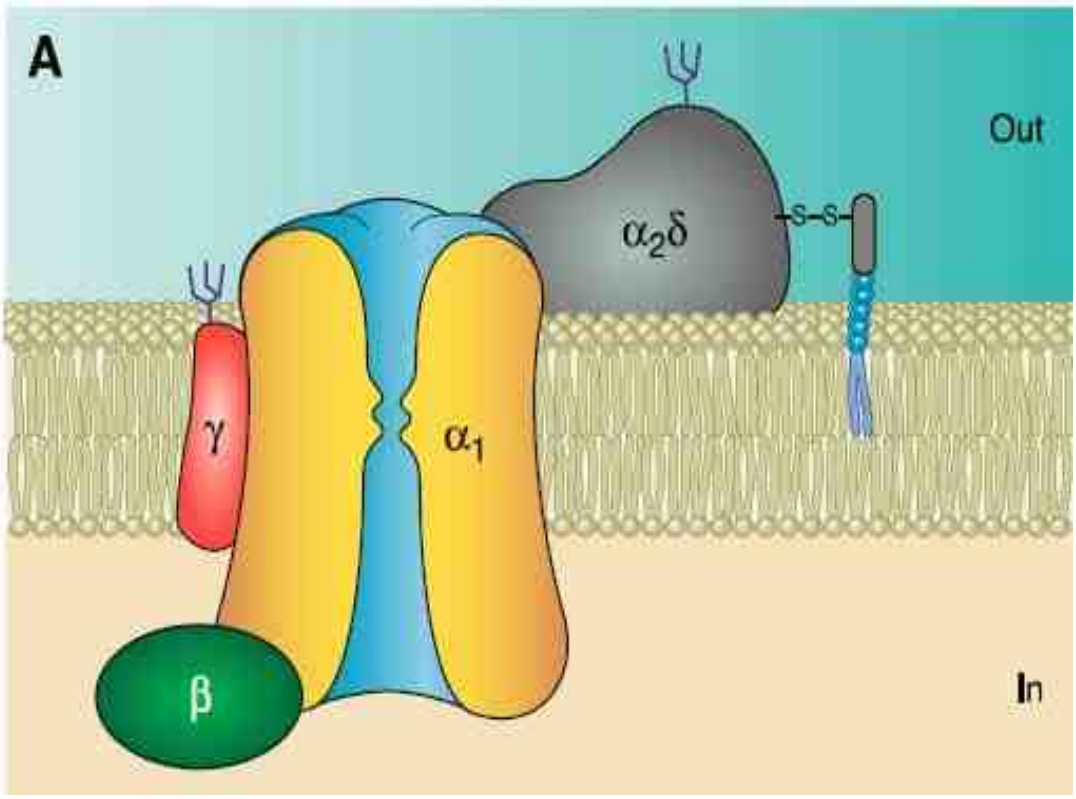

Figure 1.1. Organization of voltage-gated Ca^{2+} channels

The molecular structure of $Ca_v\beta$ was reported in 1998,[12-14] and the crystal structure of $Ca_v\beta$ was also reported in 2004 (Fig. 1.2). The structure showed three main

regions at the N-terminus, including an SH3 domain (residues 60-120 and 170-175, gold), a HOOK region (residues 121-169, purple) and a GK domain (residues 176-360, green).[6,15-17]

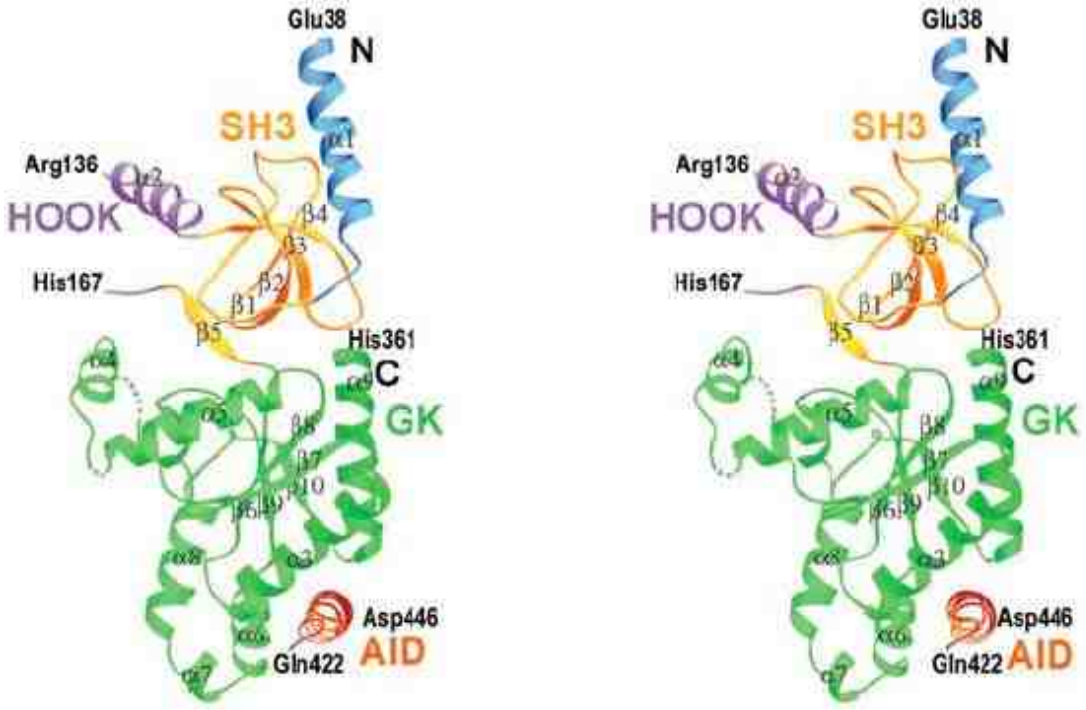

Figure 1.2. Crystal structure of $Ca_v\beta$ core

In the cytoplasmic loop of $Ca_v\alpha_1$, there is a high-affinity site where $Ca_v\beta$ binds. This site is known as the α-interaction domain (AID) and the conformation of AID is an α-helix that binds to a hydrophobic pocket in the GK domain. In addition, there is a β-interaction domain (BID) that directly binds to AID. The BID domain is the primary area that the β-subunit uses to associate with α_1. The significance of this interaction was reported and suggests that interactions between $Ca_v\beta$ and $Ca_v\alpha_1$ can have an effect of normal physiological function and pathophysiological processes.[18-22]

Research in our group mainly focuses on discovering and developing a small molecule to inhibit the interaction of $Ca_v\alpha1$ and $Ca_v\beta$. Screening libraries of 500,000 compounds from ChemDiv were docked to $Ca_v\beta$ protein and ranked according to GlideScore. The top 88 compounds were purchased and assessed by FP (fluorescence polarization) assay at 50 μM. The results yielded one compound (BTT-3) that showed concentration-dependent inhibition of AID binding to $Ca_v\beta$. A binding mode of BTT-3 was proposed (Fig. 1.3). These studies were carried out by members of the Meroueh laboratory.

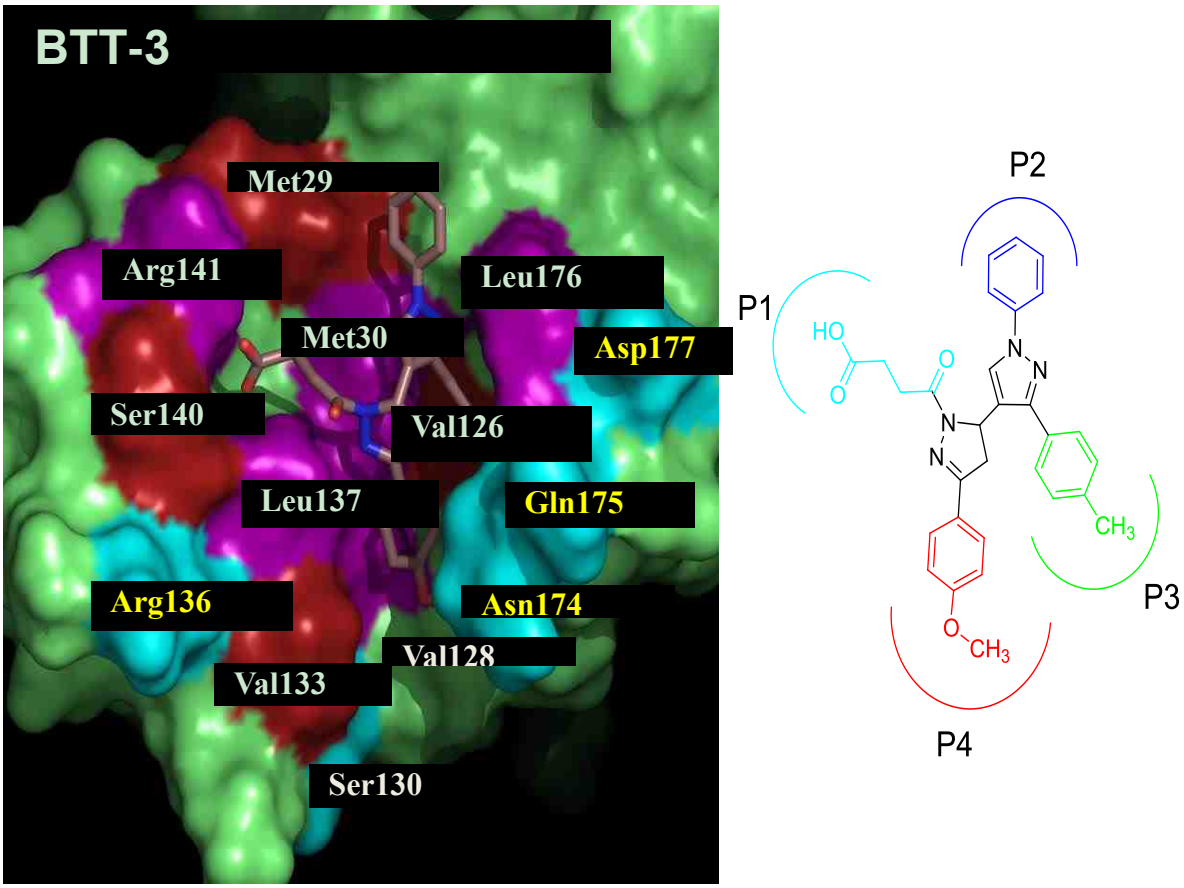

Figure 1.3. **(a)** Binding mode of BTT-3. **(b)** Chemical structure of BTT-3

A synthetic route to BTT-3 and its derivatives was proposed and implemented. To identify additional targets of BTT-3, we developed a biotinylated benzophenone photo-affinity probe that was linked to BTT-3.

1.1.2 Photo-affinity Probe

Photo-affinity labeling was first discovered and reported by F.H.Westheimer in 1962.[23] It has become a highly efficient tool in identification of target proteins of biological molecules,[24,25] and protein-protein complexes.[26-29] A photo-affinity probe is composed by three major parts: a photoreactive functional group, such as diazirines or benzophenones,[30-32] a biological scaffold, and an indicator unit.[33] Generally, a biotin tag is the indicator group in photo-affinity probes because of its specificity and sensitivity to immunological methods.

Although a number of photo-affinity groups have been developed, benzophenones have several advantages. First, benzophenones are chemically stable, even more stable than diazirines.[32] Second, benzophenones can be activated at 350-360 nm, which is a wavelength that is beyond the range of protein-damaging wavelength. The activation of the inert benzophenone group can be triggered by UV light and then highly reactive electrophilic radicals will be created to form a covalent bond with the protein.[34] The mechanism of this activation was reported by Gyorgy Dormtin in 1994.[32]

We have strong interest in identifying additional target protein(s) of BTT-3 in order to gain more knowledge of the biological activity of this compound and to help us design

and explore new derivatives in the future. Thus a biotinylated benzophenone photo-affinity probe was synthesized through a six-step synthesis and its chemical structure is shown in Fig. 1.4.

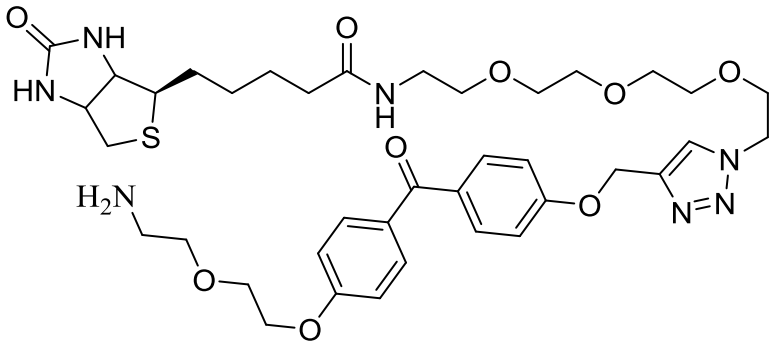

Figure 1.4. Chemical structure of photo-affinity probe

The biotinylated benzophenone photo-affinity probe was linked to the synthesized BTT-3 via a simple coupling reaction and the chemical structure of the BTT-3 photo-affinity reagent is shown in Fig. 1.5.

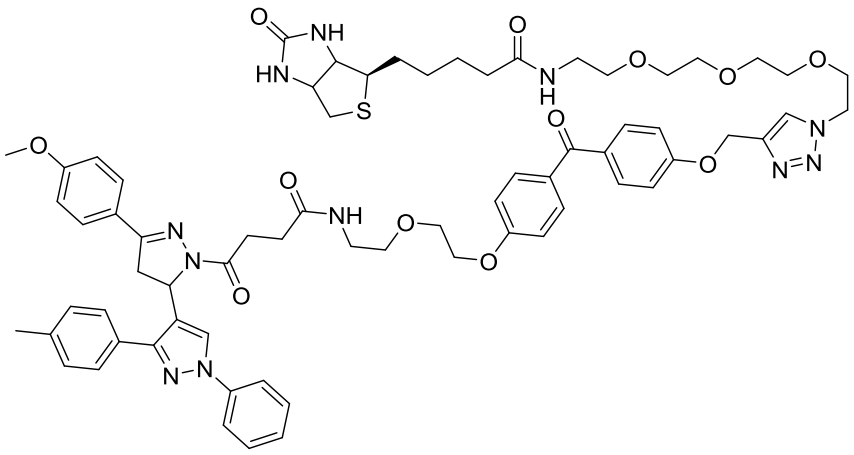

Figure 1.5. Chemical structure of BTT-3 photo-affinity reagent

1.2 Results and Discussion

1.2.1 Chemical Synthesis of BTT-3

BTT-3 is a compound that has biological activity targeting Ca^{2+} channel protein-protein interactions in neuropathic pain. Retrosynthetically, BTT-3 can be synthesized via hydrolysis of its precursor,[35] the methyl ester derivative **5**, which can be achieved via a coupling reaction of commercially available methyl-4-chloro-4-oxobutyrate and a secondary free amine in **4**.[36,37] The secondary amine in 4,5-dihydro-1*H*-pyrazole could in turn be generated via Michael addition by excessive hydrazine hydride, simplifying the structure to **3**.[38] The latter can be prepared from **2** through an Aldol condensation.[39,40] The pyrazole core structure along with free aldehyde group in **3** was accessible from phenylhydrazine and 4'-methylacetophenone[41] involving a condensation/Vilsmeier-Haack reaction sequence (Scheme 1.1).[42,43]

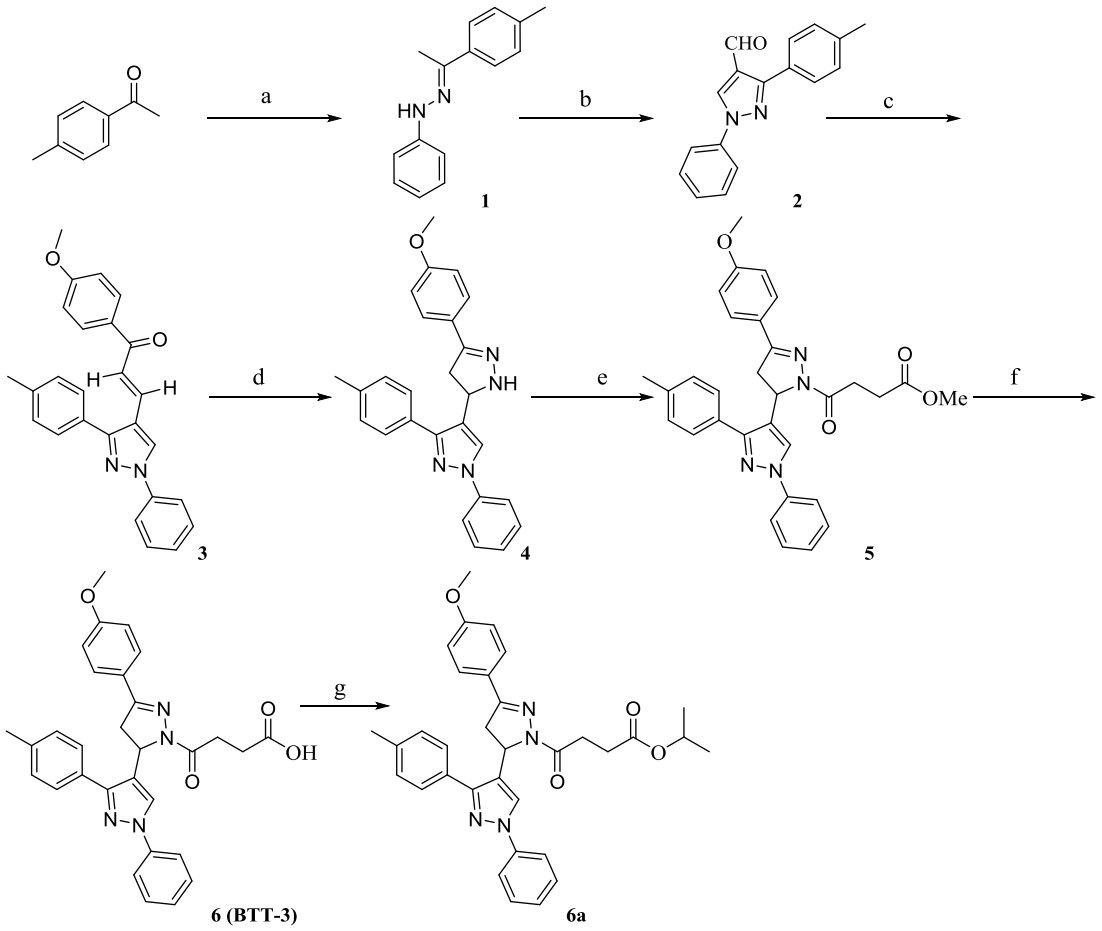

Reagents and conditions: (a) phenylhydrazine, HOAc, ethanol, N_2, 70-80 °C, 6 h, yield 85%; (b) $POCl_3$, DMF, 50-60 °C, 20 h, yield 94%; (c) 4'-methoxyacetophenone, KOH, ethanol, 25 °C, 20 h, yield 81%; (d) 50-60% hydrazine hydrate, ethanol, 80-90 °C, 24 h, yield 72%; (e) methyl-4-chloro-4-oxobutyrate , pyridine, reflux, 4 h, yield 83%; (f) KOH (2M aq), methanol, 80-90 °C, 16 h, yield 87%; (g) $SOCl_2$, i-PrOH, 25 °C, 5 h, yield 85%.

Scheme 1.1. Synthetic scheme of BTT-3

With commercially available phenylhydrazine and 4’-methylacetophenone, the synthesis of **1** was achieved by simple condensation in good yield. But the desired product was very sensitive to visible light. It decomposed when exposed to light and was easily oxidized when exposed to air. Thus, this compound was handled with special care by storing in darkness, under argon gas and at 4 °C.

The second step in Scheme 1.1 is key to generate the pyrazole ring core of BTT-3. This was achieved by adding excess Vilsmeier reagent (DMF+$POCl_3$) to **1**. The reaction occurs through a Vilsmeier-Haack reaction resulting in pyrazole structure **2** that contains a free aldehyde group. Condensation with substituted acetophenones yielded the enone **3**, which was subsequently coupled with excess hydrazine hydride to yield the second 3,4-dihydropyrazole ring **4**.

When exploring the reaction conditions for the acetylation of **4** and commercially-available methyl-4-chloro-4-oxobutyrate, the two common methods employed consisted of using DCM as the solvent followed by addition of 3 equivalents of TEA. Alternatively, the reaction was carried out using anhydrous pyridine as solvent. Pyridine was a good solvent as evidenced by the purity of the desired product **5**.

Finally, the hydrolysis of **5** was achieved by using 2 M KOH aqueous solution in methanol refluxed for 16 h to afford **6** in good yield. It is of interest to note that using 2 M NaOH aqueous solution results in lower yields. Also the procedure was faster when compared to using 2 M LiOH, which required 3 days to go to completion. The disadvantage in using 2 M KOH solution was that the base was strong enough to break down the amide bond formed via acetylation of methyl-4-chloro-4-oxobutyrate and **4**. But this could be avoided by limiting reaction time to less than 16 h.

1.2.2 Structure Based Modification of BTT-3

Based on the binding mode of **6** shown in Fig. 1.3, the terminal carboxylic acid group in P1 interacts with an Arg141 residue on the protein side chain through a salt bridge interaction. To probe this predicted binding mode, four additional BTT-3 derivatives

were prepared, namely **6a** to **6d**. In these derivatives, the carboxylic acid group was replaced with a neutral moiety. The synthetic scheme for preparation of **6b** to **6d** is shown in Scheme 1.2. The efficiency of **6a** to **6d** along with **5** has been assessed in biochemical assays by my colleagues in the Meroueh laboratory. A fluorescence polarization assay was used for this purpose. The assay consisted of a fluorescently-labeled AID peptide (AID-FAM). Active compounds are expected to displace AID-FAM and significantly increase polarization. Testing of the derivatives showed no effect on AID-FAM binding suggesting that the carboxylic acid on BTT-3 is essential for binding to the protein.

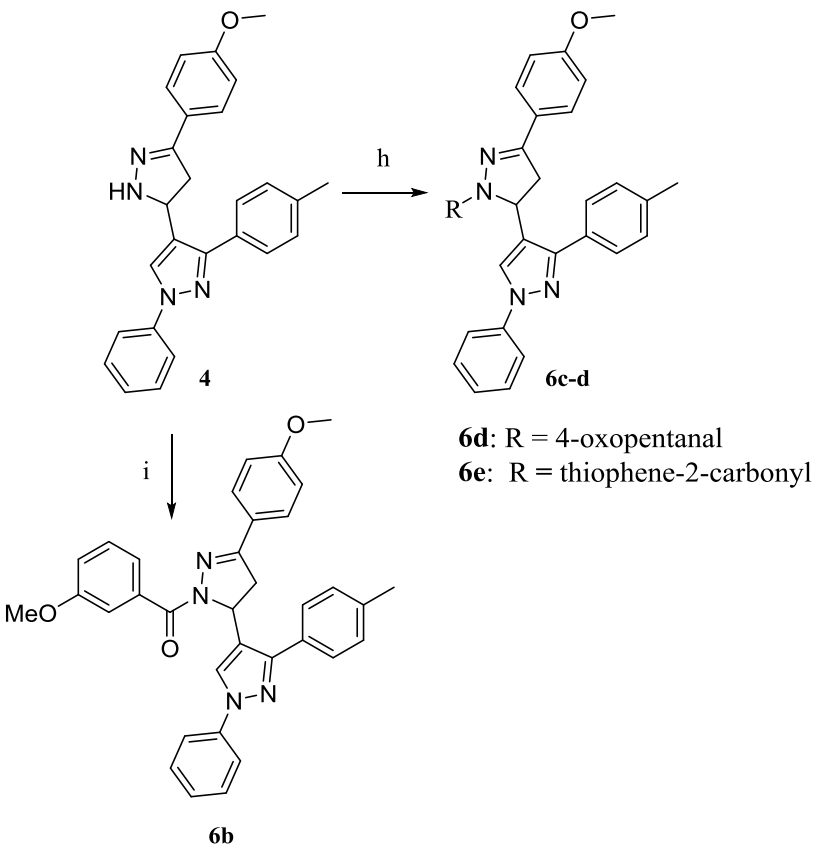

Scheme 1.2. Synthetic scheme of **6b** to **6d**

1.2.3 Synthesis of BTT-3 Photo-affinity Reagent

Photo-affinity probe **12** can be achieved through a six-step synthesis (Scheme 1.3). Compound **7** was prepared with 4,4'-dihydroxybenzophenone and propargyl bromide through a simple S_N2 reaction.[44] Mitsunobu coupling was used staring with DIAD in toluene (40% w/v) added to the mixture of triphenylphosphine, **7** and **8** in anhydrous THF to afford **9**.[45,46] Biotin is coupled with the azide linker using EDCI and HOBt to yield **10**,[47] which in turn reacted with compound **9** through a Huisgen cycloaddition to yield **11**.[48] The protecting group in **11** was removed to afford the final biotinylated benzophenone photo-affinity probe, namely compound **12**.[49]

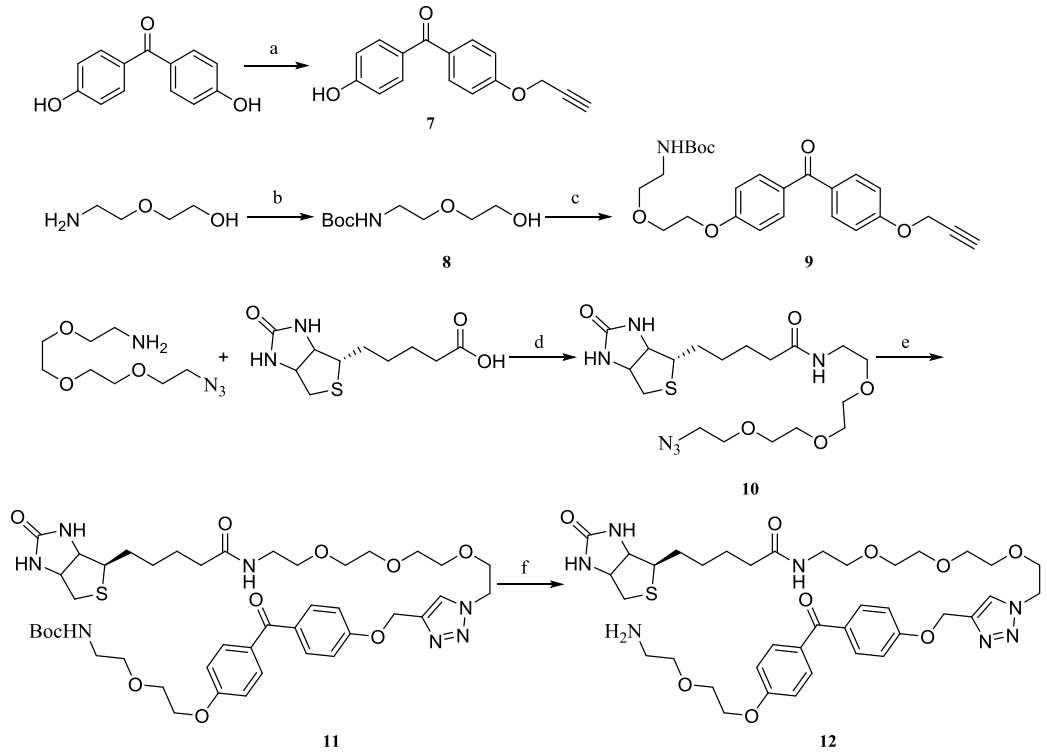

Reagents and conditions: (a) propargyl bromide, K_2CO_3, DMF, 85 °C, 17 h, yield 68%; (b) $(Boc)_2O$, 1 M NaOH(aq), THF, 24 h, yield 96%; (c) **7**, Ph_3P, DIAD, THF, yield 56%; (d) EDCI, HOBt, DMF, 24 h, room temperature, yield 81%; (e) **9**, $CuSO_4$ $5H_2O$, Methanol, sodium ascorbate, r.t. yield 90%; (f) TFA, DCM, 3 h

Scheme 1.3. Synthetic scheme of photo-affinity probe

The final BTT-3 photo-affinity reagent **13** can be prepared through a simple coupling reaction between **6** and the photo-affinity probe **12** (Scheme 1.4).[50] The reagent **13** was characterized by LC/MS.

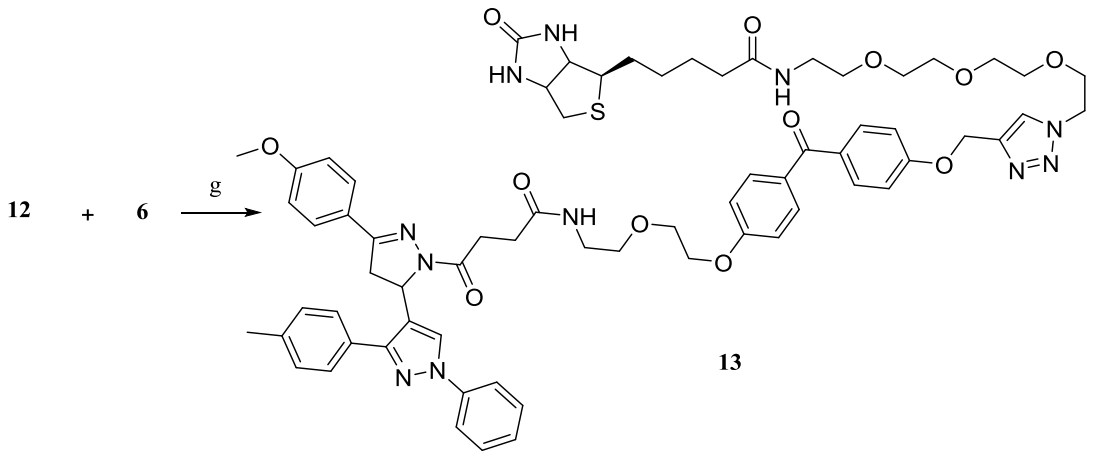

Reagents and conditions: g) HATU, TEA, DMF, 12 h

Scheme 1.4. Synthetic scheme of BTT-3 photo-affinity probe

It should be noted that in the first step, it is unavoidable to get both the desired product **7** and the di-alkyne substituted side product. However, the pure product **7** can be achieved by flash chromatography. In addition, the Mitsunobu coupling reaction always takes a long time and it has to be performed in darkness since the coupling reagent DIAD is very sensitive to visible light and easily decomposes. In the coupling reaction of biotin and the azide linker, because there are no UV-Visible absorption groups in both of the reactants and final product, it is difficult to monitor the reaction progress by either TLC or LC/MS. The final product was visualized by a phosphomolybdate stain. **11** is then achieved through Huisgen cycloaddition of **9** and **10** and was characterized by HRMS, ^{1}H NMR and ^{13}C NMR. Then the protection group in **11** was removed to afford the final photo-affinity probe **12**, which was used in next reaction without further purification to

afford the final BTT-3 photo-affinity reagent. This reagent was only identified by LC/MS and it will be further identified by ^{1}H NMR and ^{13}C NMR in the future.

1.3 Experimental

General Methods: All chemicals were purchased from either Sigma-Aldrich or Acros and used as received. Column chromatography was carried out with silica gel GF254 (25-63μm). Mass Spectra were measured on an Agilent 6520 Mass Q-TOF instrument. ^{1}H NMR and ^{13}C NMR spectra were recorded on a BRUKER 500 MHz spectrometer, using TMS as an internal standard and $CDCl_3$ or DMSO-d_6 as solvents. Chemical shifts (δ values) and coupling constants (J values) are reported in ppm and hertz, respectively. Anhydrous solvent and reagents were all analytically pure and dried through routine protocols. All compounds that were evaluated in biological essays had > 95% purity using HPLC.

1.3.1 Chemical Synthesis of BTT-3

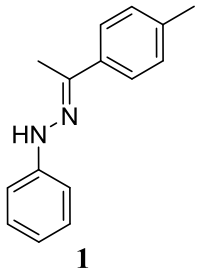

1

4-Methylacetophenone phenylhydrazone (**1**). 4'-Methylacetophenone (0.95 g, 7.1 mmol) was dissolved in 95% ethyl alcohol (7 mL) followed by phenylhydrazine (0.68 mL, 6.9 mmol) and 3-5 drops of HOAc. The mixture was stirred under ambient temperature for

30 min, and then was heated to reflux for an additional 15 h. The resulting brown-yellow solution was cooled to room temperature and then ice-H_2O (20 mL) was added. Grey solid was filtered off, washed with ice-H_2O and hexane, respectively. The solid was then dried under high vacuum (1.31 g, 85%): ^{1}H NMR (500 MHz, $CDCl_3$) δ 7.70 (d, *J* = 8.0 Hz, 2H), 7.28 (t, *J* = 8.0 Hz, 2H), 7.17-7.19 (m, 4H), 6.87 (t, *J* = 7.5 Hz, 1H), 2.37 (s, 3H), 2.23 (s, 3H); ^{13}C NMR (125 MHz, $CDCl_3$) δ 145.45, 141.97, 138.05, 136.38, 129.34, 129.15, 125.62, 120.19, 113.34, 21.30, 12.03; HRMS (ESI) *m/z* for $C_{15}H_{16}N_2$ $[M + H]^+$ calcd 225.1386, found 225.1381.

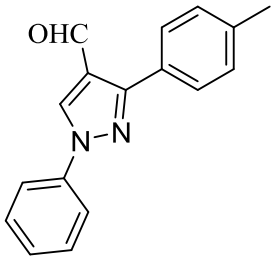

2

3-(4-Methylphenyl)-1-phenyl-4-pyrazolecarboxaldehyde (**2**). To an oven-dried 50 mL round bottom flask was added anhydrous DMF (10 mL) which was cooled to 0 °C in an ice bath before adding $POCl_3$ (2.0 mL, 21.44 mmol) dropwise. Compound **1** (1.20 g, 5.36 mmol) was poured into the solution and the resulting mixture was warmed to room temperature then was heated to 50-60 °C. The reaction was stopped after 20 h and the resulting dark-red solution was quenched by pouring into stirred slurry of ice. Saturated $NaHCO_3$ solution was added dropwise to adjust to afford pH 7. Yellow precipitate was filtered and washed with ice-H_2O to give the desired product and the solid was dried under high vacuum (1.32 g, 94%): ^{1}H NMR (500 MHz, $CDCl_3$) δ 10.05 (s, 1H), 8.53 (s,

1H), 7.79 (d, *J* = 8.5 Hz, 2H), 7.71(d, *J* = 8.5 Hz, 2H), 7.51(t, *J* = 8.5 Hz, 2H), 7.40(t, *J* = 7.5 Hz, 1H), 7.31(d, *J* = 8 Hz, 2H), 2.43(s, 3H); ^{13}C NMR (125 MHz, $CDCl_3$) δ 185.37, 154.95, 139.41, 139.14, 130.93, 129.73, 129.54, 128.92, 128.55, 127.96, 122.55, 119.81, 21.44; HRMS (ESI) *m/z* for $C_{17}H_{14}N_2O$ $[M + H]^+$ calcd 263.1179, found 263.1172.

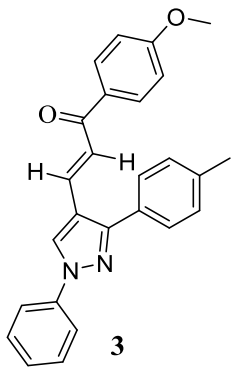

3

1-(4-Methoxyphenyl)-3-[3-(4-methylphenyl)-1-phenyl-1H-pyrazol-4-yl]-2-propen-1-one (**3**). Acetanisole (1.05 g, 4 mmol), aldehyde **2** (600.7 mg, 4 mmol) and KOH pellets (600 mg, 10.7 mmol) were mixed in a 50 mL round bottom flask containing 95% alcohol (20 mL). The mixture was stirred at ambient temperature for 20 h. Yellow solid was filtered off and washed with cold alcohol (3 x 20 mL). The solid was dried under high vacuum to afford the desired product **3** (1.28 g, 81%): ^{1}H NMR (500 MHz, $CDCl_3$) δ 8.32 (s, 1H), 7.97 (d, *J* = 8.5 Hz, 2H), 7.87 (d, *J* = 15.5 Hz, 1H), 7.79 (d, *J* = 8.5 Hz, 2H), 7.61 (d, *J* = 8 Hz, 2H), 7.50 (t, *J* = 8 Hz, 2H), 7.37 (d, *J* = 15.5 Hz, 1H), 7.35 (t, *J* = 7.5 Hz, 1H), 7.30 (d, *J* = 8 Hz, 2H), 6.97 (dd, *J* = 7, 2 Hz, 2H), 3.88 (s, 3H), 2.42 (s, 3H); ^{13}C NMR (125 MHz, $CDCl_3$) δ 188.48, 163.41, 153.93, 139.63, 138.66, 134.77, 131.28, 130.77, 129.64, 129.56, 128.78, 127.20, 126.73, 121.40, 119.43, 118.51, 113.90, 55.58, 21.46; HRMS (ESI) *m/z* for $C_{26}H_{22}N_2O_2$ $[M + H]^+$ calcd 395.1754, found 395.1745.

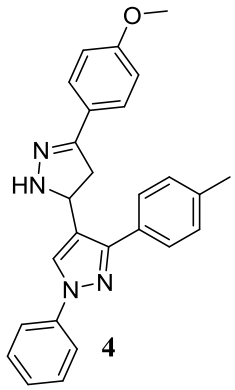

4

5-(4-Methoxyphenyl)-1'-phenyl-3'-(p-tolyl)-3,4-dihydro-1'H,2H-3,4'-bipyrazole (**4**). To a solution of propen-1-one **3** (1.20 g, 3.04 mmol) in 95% ethanol (40 mL) was added 50-60% hydrazine hydrate (0.6 mL, 12.2 mmol) dropwise at room temperature then the resulting mixture was refluxed for 24 h to yield white precipitate. The reaction was then cooled to 0 °C in an ice bath. The resulting precipitate was filtered, washed with ice-water (5 x 20 mL) and dried under high vacuum to give product **4** as a white solid (894 mg, 72%): ^{1}H NMR (500 MHz, $CDCl_3$) δ 8.05 (s, 1H), 7.72 (d, *J* = 7.5 Hz, 2H), 7.60-7.63 (m, 4H), 7.42 (t, *J* = 8 Hz, 2H), 7.27-7.28 (m, 3H), 6.91 (d, *J* = 9 Hz, 2H), 5.14 (t, *J* = 9 Hz, 1H), 3.83 (s, 3H), 3.44-3.49 (dd, *J* = 16, 10 Hz, 1H), 3.03-3.09 (dd, *J* = 16, 8.5 Hz, 1H), 2.41 (s, 3H); ^{13}C NMR (125 MHz, $CDCl_3$) δ 160.48, 152.39, 151.18, 140.06, 138.13, 130.33, 129.49, 128.09, 127.69, 126.49, 125.85, 125.63, 123.22, 119.04, 114.12, 55.81, 55.45, 41.18, 21.41; HRMS (ESI) *m/z* for $C_{26}H_{24}N_4O$ $[M + H]^+$ calcd 409.2023, found 409.2014.

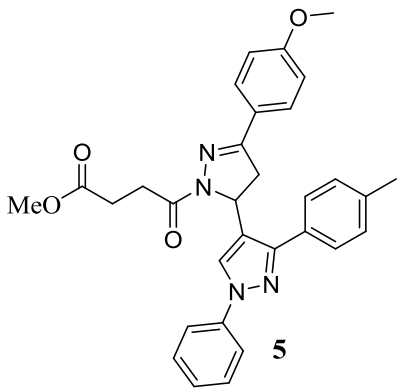

5

Methyl-4-(5-(4-methoxyphenyl)-1'-phenyl-3'-(p-tolyl)-3,4-dihydro-1'H,2H-[3,4'-bipyrazol]-2-yl)-4-oxobutanoate (**5**). Compound **4** (817 mg, 2.0 mmol) was dissolved in anhydrous pyridine (10 mL). The resulting mixture was cooled to 0 °C and methyl-4-chloro-4-oxobutyrate (0.25 mL, 4.0 mmol) was added dropwise. The reaction was heated to reflux for 4 h and then was quenched by pouring the solution into ice-H_2O (20 mL). The resulting precipitate was filtered off and washed with water. The crude solid was purified by flash chromatography eluting with 30% ethyl acetate/hexanes to give a white solid (0.87 g, 83%): $R_{f=}$ 0.15 (30% ethyl acetate/hexanes): ^{1}H NMR (500 MHz, $CDCl_3$) δ 7.92 (s, 1H), 7.77 (d, *J* = 7.5Hz, 2H), 7.65 (d, *J* = 8 Hz, 2H), 7.61 (2H, *J* = 9 Hz, 2H), 7.39 (t, *J* = 8.5 Hz, 2H), 7.21-7.26 (m, 4H), 6.89 (d, *J* = 8.5 Hz, 2H), 5.90-5.93 (dd, *J* = 11.5, 4 Hz, 1H), 3.83 (s, 3H), 3.69 (s, 3H), 3.56-3.62 (dd, *J* = 17, 11.5 Hz, 1H), 3.56-3.42 (m, 1H), 3.03-3.07 (dd, *J* = 17, 4 Hz, 1H), 2.85-2.97 (m, 2H), 2.68-2.73 (m, 1H), 2.39 (s, 3H); ^{13}C NMR (125 MHz, $CDCl_3$) δ 173.94, 169.61, 161.52, 154.42, 150.00, 140.10, 137.94, 130.51, 129.47, 129.30, 128.41, 128.16, 126.24, 124.10, 122.25, 119.01, 114.19, 100.13, 55.52, 52.81, 51.86, 42.11, 29.14, 28.84, 21.43; HRMS (ESI) *m/z* for $C_{31}H_{30}N_4O_4$ $[M + H]^+$ calcd 523.2340, found 523.2339.

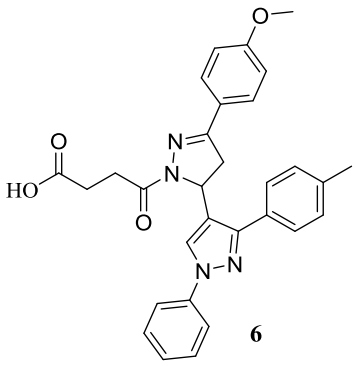

6

4-(5-(4-Methoxyphenyl)-1'-phenyl-3'-(p-tolyl)-3,4-dihydro-1'H,2H-[3,4'-bipyrazol]-2-yl)-4-oxobutanoic acid (**6**). A solution of compound **5** (522.6 mg, 1 mmol) and 2 M KOH aqueous solution (2.4 mL) in methanol (12 mL) was heated to reflux for 16 h. The reaction was cooled to room temperature. Solvent was removed *in vacuo* and the crude residue was acidified with 1 M HCl solution to yield white precipitate. The resulting solid was filtered off, washed with ice-H_2O and dried under high vacuum to afford white solid (442.5 mg, 87%): ^{1}H NMR (500 MHz, DMSO-d_6) δ 8.23 (s, 1H), 7.85 (d, *J* = 8 Hz, 2H), 7.67-7.71 (m, 4H), 7.47 (t, *J* = 8 Hz, 2H), 7.29 (m, 3H), 6.99 (d, *J* = 8.5 Hz, 2H), 5.67-5.70 (dd, *J* = 11.5, 5 Hz, 1H), 3.85-3.88 (m, 1H), 3.82 (s, 3H), 3.11-3.17 (m, 1H), 3.06-3.10 (m, 1H), 2.82-2.88 (m, 1H), 2.53-2.55 (m, 2H), 2.36 (s, 3H); ^{13}C NMR (125 MHz, DMSO-d_6) δ 173.99, 168.75, 160.85, 153.82, 149.15, 139.34, 137.30, 129.99, 129.43, 129.17, 128.29, 127.74, 126.24, 126.09, 123.73, 123.14, 118.09, 114.12, 99.50, 55.31, 51.99, 42.01, 28.73, 28.49, 20.83; HRMS (ESI) *m/z* for $C_{30}H_{28}N_4O_4$ $[M + H]^+$ calcd 509.2183, found 509.2185.

1.3.2 Chemical Synthesis of BTT-3 Derivatives

General procedures for synthesis of **6c** to **6d**: HATU (114 mg, 0.3 mmol), carboxylic acid (0.3 mmol) and TEA (0.08 mL, 0.6 mmol) were dissolved in anhydrous DMF solution (2 mL) and the resulting mixture was stirred for 30 min at room temperature. Compound **4** (82 mg, 0.2 mmol) was then slowly added and the mixture was stirred for 20 h at ambient temperature. Ethyl acetate (5 mL) was added. The mixture was washed with saturated $NaHCO_3$ solution, H_2O and brine, respectively. The collected organic layer was dried over anhydrous $MgSO_4$ and concentrated *in vacuo*. The crude residue was purified by flash column chromatography (3:1 hexane/ethyl acetate) to afford the desired compound.[50]

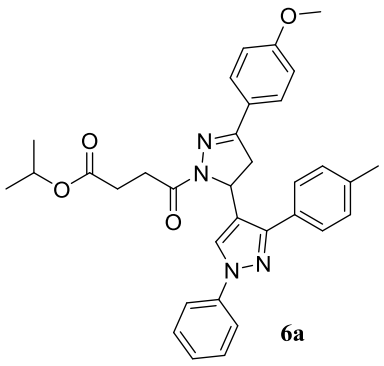

6a

Isopropyl-4-(5-(4-methoxyphenyl)-1'-phenyl-3'-(p-tolyl)-3,4-dihydro-1'H,2H-[3,4'-bipyrazol]-2-yl)-4-oxobutanoate (**6a**). Compound **6** (50 mg, 0.1 mmol) was dissolved in isopropyl alcohol (2 mL) and the mixture was stirred at 0 °C. Thionyl chloride (0.02 mL, 0.3 mmol) was added dropwise. The reaction was warmed to ambient temperature and stirred for 5 h. Solvent was removed *in vacuo* and DCM (2 mL) was then added. The crude residue was basified by saturated $NaHCO_3$ solution and extracted by DCM (2 x 10 mL). The organic extracts were dried over anhydrous $MgSO_4$, and solvent was removed

in vacuo to afford the resulting compound as a white solid (46 mg, 85%): ^{1}H NMR (500 MHz, $CDCl_3$) δ 7.96 (s, 1H), 7.77 (d, *J* = 8 Hz, 2H), 7.65 (d, *J* = 8 Hz, 2H), 7.60 (d, *J* = 9 Hz, 2H), 7.38 (t, *J* = 8.5 Hz, 2H), 7.24 (d, *J* = 8 Hz, 2H), 7.20 (d, *J* = 7.5 Hz, 1H), 6.88 (d, *J* = 8.5 Hz, 2H), 5.91-5.94 (dd, *J* = 11, 4 Hz, 1H), 4.98-5.07 (m, 1H), 3.83 (s, 3H), 3.56-3.61 (m, 1H), 3.35-3.42 (m, 1H), 3.02-3.06 (dd, *J* = 13, 4 Hz, 1H), 2.82-2.93 (m, 2H), 2.63-2.69 (m, 1H), 2.39 (s, 3H), 1.5-1.6 (brs, 1H), 1.25 (d, *J* = 6.5 Hz, 3H), 1.19 (d, *J* = 6 Hz, 3H); ^{13}C NMR (125 MHz, $CDCl_3$) δ 173.05, 169.77, 161.51, 154.30, 149.98, 140.16, 137.91, 130.60, 129.48, 129.27, 128.41, 128.15, 126.36, 126.19, 124.19, 122.27, 119.00, 114.19, 100.15, 68.13, 55.53, 52.84, 42.08, 29.42, 29.14, 21.98, 21.44; HRMS (ESI) *m/z* for $C_{33}H_{34}N_4O_4$ $[M + H]^+$ calcd 551.2653, found 551.2662.

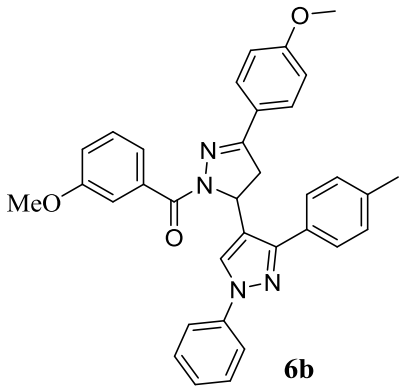

6b

(3-Methoxyphenyl)(5-(4-methoxyphenyl)-1'-phenyl-3'-(p-tolyl)-3,4-dihydro-1'H,2H-[3,4'-bipyrazol]-2-yl)methanone (**6b**). Compound **4** (816 mg, 2 mmol) was dissolved in dry DCM (10 mL) and the mixture was cooled to 0 °C**.** 3-Methoxybenzoyl chloride (0.56 mL, 4 mmol) was added dropwise and followed by TEA (0.84 mL, 6 mmol). The mixture was warmed to ambient temperature and stirred for 12 h. H_2O (5 mL) was added and the mixture was extracted with DCM (2 x 10 mL). The combined organic layer was then

washed with brine and dried over anhydrous $MgSO_4$. Solvent was removed *in vacuo* and the crude residue was purified by flash chromatography eluting with 30% ethyl acetate/hexanes to give a white solid (0.9 g, 82%): R_f = 0.2 (30% ethyl acetate/hexanes): ^{1}H NMR (500 MHz, DMSO-d_6) δ 8.50 (s, 1H), 7.89 (d, *J* = 8 Hz, 2H), 7.71 (d, *J* = 8 Hz, 2H), 7.64 (d, *J* = 8.5 Hz, 2H), 7.46 (t, *J* = 7.5 Hz, 3H), 7.41-7.43 (m, 1H), 7.37-7.40 (m, 1H), 7.28-7.31 (m, 3H), 7.08-7.10 (dd, *J* = 8, 2 Hz, 1H), 7.01 (d, *J* = 9 Hz, 2H), 5.84-5.88 (dd, *J* = 12, 5.5 Hz, 1H), 3.89-3.95 (m, 1H), 3.81 (s, 3H), 3.80 (s, 3H), 3.22-3.27 (m, 1H), 2.38 (s, 3H); ^{13}C NMR (125 MHz, DMSO-d_6) δ 167.10, 164.97, 160.93, 158.46, 154.78, 149.73, 139.36, 136.08, 130.11, 129.40, 129.13, 128.66, 128.35, 128.01, 126.36, 126.13, 123.73, 123.38, 121.89, 121.52, 118.16, 116.37, 114.93, 114.19, 113.89, 55.33, 55.23, 52.97, 41.67, 20.85; HRMS (ESI) *m/z* for $C_{34}H3_0N_4O_3$ $[M + H]^+$ calcd 543.2391, found 543.2396.

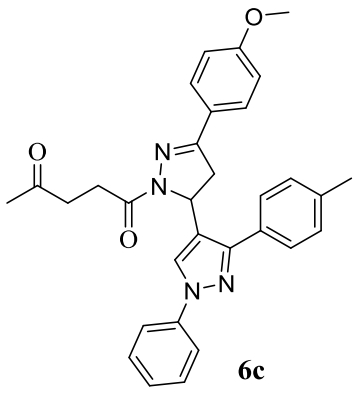

6c

1-(5-(4-Methoxyphenyl)-1'-phenyl-3'-(p-tolyl)-3,4-dihydro-1'H,2H-[3,4'-bipyrazol]-2-yl)pentane-1,4-dione (**6c**). Compound **6c** was prepared through a coupling reaction of **4** and levulinic acid in a manner similar to that described in general procedures for synthesis of **6c** to **6d.** Yield 46%, white solid: ^{1}H NMR (500 MHz, $CDCl_3$) δ 7.90 (s, 1H),

7.77 (d, *J* = 7.5 Hz, 2H), 7.65 (d, *J* = 8 Hz, 2H), 7.60 (d, *J* = 8.5 Hz, 2H), 7.40 (t, *J* = 7.5 Hz, 2H), 7.21-7.25 (m, 3H), 6.88 (d, *J* = 8.5 Hz, 2H), 5.88-5.91 (dd, *J* = 11, 4 Hz, 1H), 3.83 (s, 3H), 3.56-3.61 (m, 1H), 3.30-3.35 (m, 1H), 3.02-3.06 (m, 1H), 2.95-3.00 (m, 1H), 2.87-2.93 (m, 1H), 2.78-2.84 (m, 1H), 2.39 (s, 3H), 2.23 (m, 3H); ^{13}C NMR (125 MHz, $CDCl_3$) δ 207.91, 169.98, 161.50, 154.29, 149.97, 140.10, 137.91, 130.51, 129.45, 129.32, 128.38, 128.15, 126.23, 126.12, 124.15, 122.32, 119.03, 114.18, 100.12, 55.50, 52.77, 42.13, 38.03, 30.16, 28.21, 21.40; HRMS (ESI) *m/z* for $C_{31}H_{30}N_4O_3$ $[M + H]^+$ calcd 507.2391, found 507.2384.

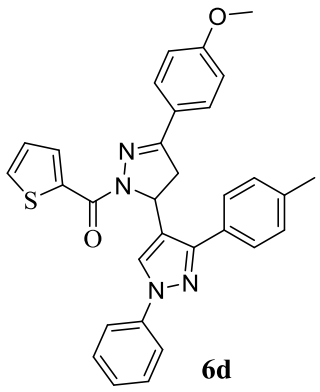

6d

(5-(4-Methoxyphenyl)-1'-phenyl-3'-(p-tolyl)-3,4-dihydro-1'H,2H-[3,4'-bipyrazol]-2-yl)(thiophen-2-yl)methanone (**6d**). Compound **6d** was prepared through a coupling reaction of **4** and 2-thiophenecarboxylic acid in a manner similar to that described in general procedures for synthesis of **6c** to **6d.** Yield 62%, brown red solid: ^{1}H NMR (500 MHz, DMSO-d_6) δ 8.41 (s, 1H), 8.01-8.02 (dd, *J* = 4, 1.5 Hz, 1H), 7.91-7.92 (dd, *J* = 5, 1 Hz, 1H), 7.86 (d, *J* = 8 Hz, 2H), 7.82 (d, *J* = 9 Hz, 2H), 7.71 (d, *J* = 8 Hz, 2H), 7.44 (t, *J* = 7.5 Hz, 2H), 7.29 (d, *J* = 8 Hz, 2H), 7.26 (d, *J* = 7.5 Hz, 1H), 7.19-7.21 (dd, *J* = 5, 3.5 Hz, 1H), 7.08 (d, *J* = 9 Hz, 2H), 5.82-5.85 (dd, *J* = 11.5, 5.5 Hz, 1H), 3.92-3.97 (m, 1H),

3.83 (s, 3H), 3.25-3.29 (m, 1H), 2.36 (s, 3H); ^{13}C NMR (125 MHz, DMSO-d_6) δ 161.11, 157.77, 155.16, 149.78, 139.32, 137.34, 135.17, 133.96, 133.88, 130.03, 129.38, 129.12, 128.69, 128.08, 126.85, 126.43, 126.13, 123.63, 123.20, 118.14, 114.28, 55.39, 52.99, 41.76, 20.85; HRMS (ESI) *m/z* for $C_{31}H_{26}N_4O_2S$ $[M + H]^+$ calcd 519.1849, found 519.1849.

1.3.3 Synthesis of BTT-3 Photo-affinity Reagent

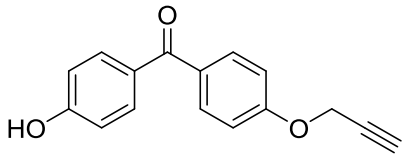

7

(4-Hydroxyphenyl)[4-(2-propyn-1-yloxy)phenyl]-methanone (**7**). To a solution of 4,4'-dihydroxybenzophenone (1.7 g, 8 mmol) and K_2CO_3 (552 mg, 4.0 mmol) in dry DMF (20 mL) was added propargyl bromide (80 wt % in toluene, 0.52 mL, 4.0 mmol) at room temperature over 15 minutes. The resulting mixture was stirred at 80-85 °C for 17 h. The reaction was cooled to room temperature and quenched with H_2O (20 mL). The solution was extracted with ethyl acetate (3 x 20 mL) and the combined organic extracts were washed with saturated $NaHCO_3$ solution (2 x 30 mL) and brine (2 x 30 mL), respectively. The organic layer was dried over anhydrous $MgSO_4$ and concentrated *in vacuo*. Flash column chromatography (3:1, hexane/ethyl acetate) afforded compound **7** as a white powder (686 mg, 68%): R_f = 0.2 (30% ethyl acetate/hexanes); ^{1}H NMR (500 MHz, DMSO-d_6) δ 7.70 (d, *J* = 9 Hz, 2H), 7.63 (d, *J* = 8.5 Hz, 2H), 7.12 (d, *J* = 8.5 Hz, 2H), 6.89 (d, *J* = 8.5 Hz, 2H), 4.92 (s, 2H), 3.64 (s, 1H); ^{13}C NMR (125 MHz, DMSO-d_6) δ

193.16, 161.65, 160.26, 132.29, 131.61, 131.10, 128.47, 115.22, 114.58, 78.88, 78.75, 66.76; HRMS (ESI) *m/z* for $C_{16}H_{12}O_3$ $[M + H]^+$ calcd 253.0859, found 253.0853.

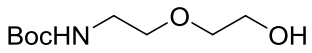

8

Tert-butyl-(2-(2-hydroxyethoxy)ethyl)carbamate (**8**). 2-(2-Aminoethoxy)-ethanol (1.00 mL, 10 mmol) was dissolved in THF (20 mL) at 0 °C and 1 M NaOH aqueous solution (5.0 mL) was added and followed by di-*tert*-butyl dicarbonate (2.46 g, 11.3 mmol). Ice bath was removed and the resulting mixture was stirred at ambient temperature for 20 h. After removal of the solvent, the resulting mixture was extracted with ethyl acetate (3 x 20 mL). The combined organic extracts were washed with brine, dried over anhydrous $MgSO_4$ and concentrated *in vacuo*. The crude residue was purified by flash chromatography (100% ethyl acetate) to give the desired product **8** (1.97 g, 96%) as a colorless oil: ^{1}H NMR (500 MHz, $CDCl_3$) δ 3.73 (t, *J* = 4 Hz, 2H), 3.57 (t, *J* = 4.5 Hz, 2H), 3.54 (t, *J* = 5 Hz, 2H), 3.32 (t, *J* = 5 Hz, 2H), 1.44 (s, 9H); ^{13}C NMR (125 MHz, DMSO-d_6) δ 156.12, 72.21, 70.30, 61.70, 40.37, 28.39, 27.40; HRMS (ESI) *m/z* for $C_9H_{19}NO_4$ $[M + Na]^+$ calcd 228.1206, found 228.1206.

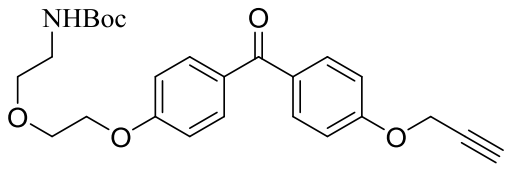

9

Tert-butyl(2-(2-(4-(4-(prop-2-yn-1-yloxy)benzoyl)phenoxy)ethoxy)ethyl)carbamate (**9**). To a mixture of compound **7** (1.39 g, 5.5 mmol)**, 8** (1.13 g, 5.5 mmol) and Ph_3P (1.73 g,

6.6 mmol) in anhydrous THF (20 mL) was added diisopropyl azodicarboxylate (DIAD) in anhydrous toluene solution (1.4 mL, 7.2 mmol, 40% w/v) dropwise under 0 °C. The ice bath was removed and the reaction was kept in darkness and stirred at ambient temperature for 48 h. The reaction was diluted with ethyl acetate (20 mL) then washed by H_2O (20 mL) and brine (20 mL), respectively. The combined organic layers were dried over anhydrous $MgSO_4$ and concentrated *in vacuo*. The crude residue was purified by flash column chromatography (3:1 hexane/acetate) to afford **9** (1.36 g, 56%) as a white foam: R_f = 0.2 (3:1 hexane/ ethyl acetate); ^{1}H NMR (500 MHz, $CDCl_3$) δ 7.79 (d, *J* = 8.5 Hz, 2H), 7.78 (d, *J* = 9 Hz, 2H), 7.04 (d, *J* = 9 Hz, 2H), 6.99 (d, *J* = 9 Hz, 2H), 4.97 (brs, 1H), 4.78 (s, 2H), 4.20 (t, *J* = 4.5 Hz, 2H), 3.85 (t, *J* = 4.5 Hz, 2H), 3.63 (t, *J* = 5 Hz, 2H), 3.36 (m, 2H), 2.56 (s, 1H), 1.44 (s, 9H); ^{13}C NMR (125 MHz, $CDCl_3$) δ 194.31, 162.05, 160.67, 155.97, 132.24, 132.10, 131.53, 130.85, 114.37, 114.09, 77.89, 76.11, 70.50, 69.26, 67.53, 55.88, 28.41, 22.05, 21.99; HRMS (ESI) *m/z* for $C_{25}H_{29}NO_6$ $[M + H]^+$ calcd 440.2068, found 440.2083.

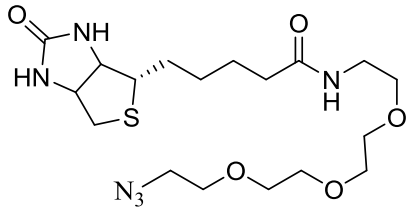

10

Biotin-azide (**10**). Biotin (800 mg, 3.3 mmol), EDCI (1.05 g, 5.5 mmol) and HOBt (836 mg, 5.5 mmol) were dissolved in anhydrous DMF (18 mL) at 0 °C. 1-amino-11-azido-3, 6, 9-trioxaundecane (0.54 mL, 2.7 mmol) dissolved in anhydrous DMF (5 mL) was then added dropwise. The resulting mixture was stirred at 0 °C for 0.5 h. The ice bath was

removed and the resulting mixture was stirred at ambient temperature for 24 h. DCM (20 mL) was added and the mixture was washed with saturated $NaHCO_3$ solution and brine, respectively. The combined DCM layers were dried over anhydrous $MgSO_4$ and removed *in vacuo*. The resulting oil residue was purified by flash column chromatography (9:1 DCM/CH_3OH, spots were visualized by a phosphmolybdate stain) to give desired product **10** as a white solid (0.98 g, 81%): ^{1}H NMR (500 MHz, $CDCl_3$) δ 6.64 (t, *J* = 5 Hz, 1H), 6.30 (s, 1H), 5.33 (s, 1H), 4.49 (m, 1H), 4.31-4.33 (m, 1H), 3.62-3.68 (m, 10H), 3.56 (t, *J* = 5 Hz, 2H), 3.44 (t, *J* = 5.5 Hz, 2H), 3.40 (t, *J* = 5 Hz, 2H), 3.14–3.16 (m, 1H), 2.92 (dd, *J* = 13, 5 Hz, 1H), 2.74 (d, *J* = 13 Hz, 1H), 2.21-2.24 (m, 2H), 1.67-1.79 (m, 4H), 1.44-1.47 (m, 2H); ^{13}C NMR (125 MHz, $CDCl_3$) δ 173.40, 164.20, 70.67, 70.48, 70.10, 70.03, 69.96, 61.81, 60.27, 55.67, 50.69, 40.53, 39.16, 35.99, 28.26, 28.11, 25.64; HRMS (ESI) *m/z* for $C_{18}H_{32}N_6O_5S$ $[M + H]^+$ calcd 445.2228, found 445.2219.

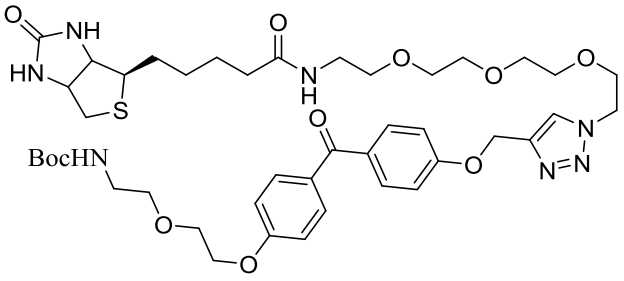

11

Boc-probe (**11**). To a solution of biotin-azide **10** (464 mg, 0.8 mmol) and benzophenone alkyne **9** (480 mg, 0.8 mmol) in methanol (20 mL) was added $CuSO_4 \cdot 5H_2O$ (40 mg, 0.16 mmol) and sodium ascorbate (79.2 mg, 0.4 mmol). The reaction mixture was stirred at room temperature for 24 h. The resulting light-blue solution was filtered through a pad of diatomaceous earth which was washed with MeOH. The filtrate was concentrated *in*

vacuo and the crude residue was dissolved in DCM. The mixture was then washed by brine and dried over anhydrous $MgSO_4$. Solvent was removed *in vacuo* and the resulting residue was purified by flash column chromatography (9:1 DCM/CH_3OH) to yield the desired product **11** (636 mg, 90%) as a white solid: ^{1}H NMR (500 MHz, $CDCl_3$) δ 7.87 (s, 1H), 7.77 (d, *J* = 9 Hz, 4H), 7.06 (d, *J* = 9 Hz, 2H), 6.98 (d, *J* = 9 Hz, 2H), 5.28 (s, 2H), 4.57 (t, *J* = 5 Hz, 2H), 4.46-4.49 (dd, *J* = 7, 6 Hz, 1H), 4.27-4.30 (dd, *J* = 8, 4.5 Hz, 1H), 4.19 (t, *J* = 5 Hz, 2H), 3.89 (t, *J* = 5 Hz, 2H), 3.85 (t, *J* = 4.5 Hz, 2H), 3.55-3.66 (m, 10H), 3.52 (m, 2H), 3.37-3.39 (m, 2H) , 3.34 (m, 2H), 3.10-3.13 (m, 1H), 2.85-2.89 (m, 1H), 2.71-2.75 (m, 1H), 2.17-2.21 (m, 2H), 1.60-1.69 (m, 4H), 1.38-1.43 (m, 11H); ^{13}C NMR (125 MHz, $CDCl_3$) δ 194.46, 173.51, 173.48, 164.03, 162.19, 161.58, 156.09, 143.37, 132.35, 132.33, 131.32, 130.90, 124.42, 114.45, 114.23, 70.78, 70.61, 70.47, 70.24, 70.16, 69.98, 69.49, 69.36, 67.66, 65.94, 62.17, 61.98, 60.37, 55.65, 50.80, 50.51, 40.59, 39.27, 36.02, 35.95, 28.53, 28.29, 28.18, 25.67; HRMS (ESI) *m/z* for $C_{43}H_{61}N_7O_{11}S$ $[M + H]^+$ calcd 884.4223, found 884.4229.

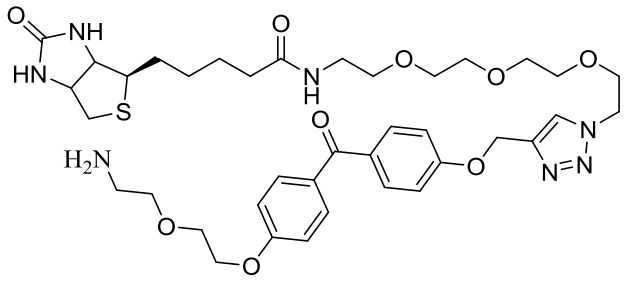

12

Photo-affinity probe (**12**). Compound **11** (106 mg, 0.12 mmol) was dissolved in DCM (3.0 mL) and TFA (3.0 mL) was added dropwise at room temperature. The mixture was stirred for 3 h and then saturated $NaHCO_3$ solution was added dropwise to adjust to

afford pH 7. The mixture was extracted with DCM and the combined organic layer was washed with brine and dried over anhydrous $MgSO_4$. Solvent was removed *in vacuo* and dried under high vacuum to afford compound **12**. MS (ESI) *m/z* 806.1 $[M+Na]^+$. The crude material **12** was used to react with **6** in the next step without further purification.

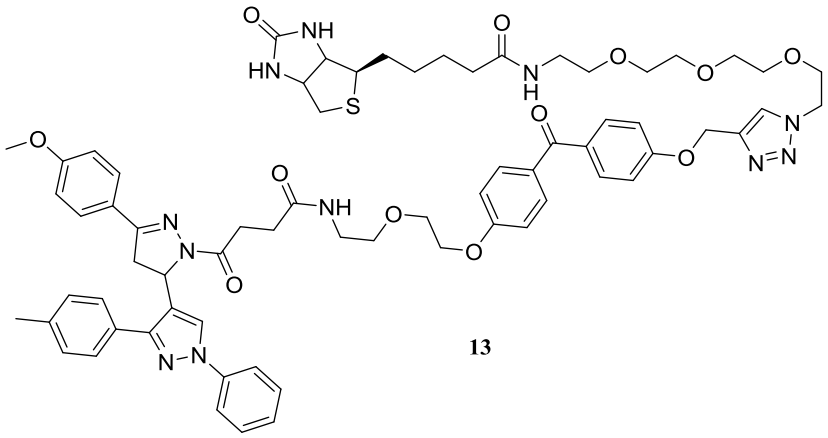

13

BTT-3 photo-affinity reagent (**13**). Compound **6a** (102 mg, 0.2 mmol), HATU (114 mg, 0.3 mmol) and TEA (0.06 mL, 0.4 mmol) were mixed in dry DMF (2 mL) and the resulting mixture was stirred at room temperature for 10 minutes. Photo-affinity probe **12** (156.8 mg, 0.2 mmol) was then added and the resulting solution was stirred at ambient temperature for 12 h. DCM (5 mL) was added and the mixture was washed with H_2O and brine, respectively. The combined DCM layer was dried over anhydrous $MgSO_4$ and solvent was removed *in vacuo*. The crude residue was purified by flash chromatography (9:1 DCM/methanol) and dried under high vacuum to afford the desired product **13** as a grey solid. MS (ESI) *m/z* 1274.8 $[M+1]^+$.

1.4 List of References

1. Stites, W. E. Proteinminus signProtein Interactions: Interface Structure, Binding Thermodynamics, and Mutational Analysis. *Chem. Rev.* **1997,** 97, 1233-1250.
2. Yin, H.; Hamilton, A. D. Strategies for targeting protein-protein interactions with synthetic agents. *Angew. Chem. Int. Ed.* **2005,** 44, 4130-63.
3. Arkin, M. R.; Wells, J. A. Small-molecule inhibitors of protein-protein interactions: progressing towards the dream. *Nat. Rev. Drug. Discov.* **2004,** 3, 301-17.
4. Boger, D. L.; Desharnais, J.; Capps, K. Solution-phase combinatorial libraries: modulating cellular signaling by targeting protein-protein or protein-DNA interactions. *Angew. Chem. Int. Ed.* **2003,** 42, 4138-76.
5. Berg, T. Modulation of protein-protein interactions with small organic molecules. *Angew. Chem. Int .Ed* .**2003,** 42, 2462-81.
6. Buraei, Z.; Yang, J. The βsubunit of voltage-gated Ca^{2+} channels. *Physiol. Rev.* **2010,** 90, 1461-506.
7. Berrou, L.; Bernatchez, G.; Parent, L. Molecular determinants of inactivation within the I-II linker of α_1E ($Ca_V2.3$) calcium channels. *Biophys. J.* **2001,** 80, 215-28.
8. Campbell, V.; Berrow, N. S.; Fitzgerald, E. M.; Brickley, K.; Dolphin, A. C. Inhibition of the interaction of G protein G(o) with calcium channels by the calcium channel beta-subunit in rat neurones. *J. Physiol.* **1995,** 485 (Pt 2), 365-72.
9. De Waard, M.; Liu, H.; Walker, D.; Scott, V. E.; Gurnett, C. A.; Campbell, K. P. Direct binding of G-protein betagamma complex to voltage-dependent calcium channels. *Nature.* **1997,** 385, 446-50.

10. Dolphin, A. C. Mechanisms of modulation of voltage-dependent calcium channels by G proteins. *J. Physiol.* **1998,** 506 (Pt 1), 3-11.

11. Zhang, J. F.; Ellinor, P. T.; Aldrich, R. W.; Tsien, R. W. Multiple structural elements in voltage-dependent Ca^{2+} channels support their inhibition by G proteins. *Neuron.* **1996,** 17, 991-1003.

12. Birnbaumer, L.; Qin, N.; Olcese, R.; Tareilus, E.; Platano, D.; Costantin, J.; Stefani, E. Structures and functions of calcium channel beta subunits. *J. Bioenerg. Biomembr.* **1998,** 30, 357-75.

13. Colecraft, H. M.; Alseikhan, B.; Takahashi, S. X.; Chaudhuri, D.; Mittman, S.; Yegnasubramanian, V.; Alvania, R. S.; Johns, D. C.; Marban, E.; Yue, D. T. Novel functional properties of Ca($^{2+}$) channel beta subunits revealed by their expression in adult rat heart cells. *J. Physiol.* **2002,** 541, 435-52.

14. De Waard, M.; Pragnell, M.; Campbell, K. P. Ca^{2+} channel regulation by a conserved β subunit domain. *Neuron.* **1994,** 13, 495-503.

15. Chen, Y. H.; Li, M. H.; Zhang, Y.; He, L. L.; Yamada, Y.; Fitzmaurice, A.; Shen, Y.; Zhang, H.; Tong, L.; Yang, J. Structural basis of the alpha1-beta subunit interaction of voltage-gated Ca^{2+} channels. *Nature.* **2004,** 429, 675-80.

16. Opatowsky, Y.; Chen, C. C.; Campbell, K. P.; Hirsch, J. A. Structural analysis of the voltage-dependent calcium channel β subunit functional core and its complex with the α 1 interaction domain. *Neuron.* **2004,** 42, 387-99.

17. Van Petegem, F.; Clark, K. A.; Chatelain, F. C.; Minor, D. L., Jr. Structure of a complex between a voltage-gated calcium channel β-subunit and an α-subunit domain. *Nature.* **2004,** 429, 671-5.

18. De Waard, M.; Witcher, D. R.; Pragnell, M.; Liu, H.; Campbell, K. P. Properties of the alpha 1-beta anchoring site in voltage-dependent Ca^{2+} channels. *J. Biol. Chem.* **1995,** 270, 12056-64.

19. Pragnell, M.; De Waard, M.; Mori, Y.; Tanabe, T.; Snutch, T. P.; Campbell, K. P. Calcium channel beta-subunit binds to a conserved motif in the I-II cytoplasmic linker of the alpha 1-subunit. *Nature.* **1994,** 368, 67-70.

20. Witcher, D. R.; De Waard, M.; Liu, H.; Pragnell, M.; Campbell, K. P. Association of native Ca^{2+} channel beta subunits with the alpha 1 subunit interaction domain. *J. Biol. Chem.* **1995,** 270, 18088-93.

21. Washbourne, P. Greasing transmission: palmitoylation at the synapse. *Neuron.* **2004,** 44, 901-2.

22. Hurley, J. H.; Cahill, A. L.; Currie, K. P.; Fox, A. P. The role of dynamic palmitoylation in Ca^{2+} channel inactivation. *Pro.c Natl. Acad. Sci. U. S. A.* **2000,** 97, 9293-8.

23. Singh, A.; Thornton, E. R.; Westheimer, F. H. The photolysis of diazoacetylchymotrypsin. *J. Biol. Chem.* **1962,** 237, 3006-8.

24. Lin, W.; Li, K.; Doughty, M. B. Characterization of a binding site for template competitive inhibitors of HIV-1 reverse transcriptase using photolabeling derivatives. *Bioorg. Med. Chem.* **2002,** 10, 4131-41.

25. Al-Mawsawi, L. Q.; Fikkert, V.; Dayam, R.; Witvrouw, M.; Burke, T. R., Jr.; Borchers, C. H.; Neamati, N. Discovery of a small-molecule HIV-1 integrase inhibitor-binding site. *Proc. Natl. Acad .Sci. U. S .A.* **2006,** 103, 10080-5.

26. Vervacke, J. S.; Funk, A. L.; Wang, Y. C.; Strom, M.; Hrycyna, C. A.; Distefano, M. D. Diazirine-containing photoactivatable isoprenoid: synthesis and application in studies with isoprenylcysteine carboxyl methyltransferase. *J. Org. Chem.* **2014,** 79, 1971-8.

27. Gubbens, J.; Ruijter, E.; de Fays, L. E.; Damen, J. M.; de Kruijff, B.; Slijper, M.; Rijkers, D. T.; Liskamp, R. M.; de Kroon, A. I. Photocrosslinking and click chemistry enable the specific detection of proteins interacting with phospholipids at the membrane interface. *Chem. Biol.* **2009,** 16, 3-14.

28. Kita, M.; Hirayama, Y.; Yamagishi, K.; Yoneda, K.; Fujisawa, R.; Kigoshi, H. Interactions of the antitumor macrolide aplyronine A with actin and actin-related proteins established by its versatile photoaffinity derivatives. *J. Am. Chem. Soc.* **2012,** 134, 20314-7.

29. Bond, M. R.; Zhang, H.; Vu, P. D.; Kohler, J. J. Photocrosslinking of glycoconjugates using metabolically incorporated diazirine-containing sugars. *Nat. Protoc.* **2009,** 4, 1044-63.

30. Das, J. Aliphatic diazirines as photoaffinity probes for proteins: recent developments. *Chem. Rev.* **2011,** 111, 4405-17.

31. Brunner, J. New photolabeling and crosslinking methods. *Annu. Rev. Biochem.* **1993,** 62, 483-514.

32. Dorman, G.; Prestwich, G. D. Benzophenone photophores in biochemistry. *Biochemistry.* **1994,** 33, 5661-73.

33. Mizuhara, T.; Oishi, S.; Ohno, H.; Shimura, K.; Matsuoka, M.; Fujii, N. Design and synthesis of biotin- or alkyne-conjugated photoaffinity probes for studying the target molecules of PD 404182. *Bioorg. Med. Chem.* **2013,** 21, 2079-87.

34. Shreder, K. R.; Wong, M. S.; Nomanbhoy, T.; Leventhal, P. S.; Fuller, S. R. Synthesis of AX7593, a quinazoline-derived photoaffinity probe for EGFR. *Org. Lett.* **2004,** 6, 3715-8.

35. Song, J. J.; Tan, Z.; Xu, J.; Reeves, J. T.; Yee, N. K.; Ramdas, R.; Gallou, F.; Kuzmich, K.; Delattre, L.; Lee, H.; Feng, X.; Senanayake, C. H. Practical stereoselective synthesis of an alpha-trifluoromethyl-alpha-alkyl epoxide via a diastereoselective trifluoromethylation reaction. *J. Org. Chem.* **2007,** 72, 292-4.

36. Lee, H.; Park, W.; Lim, D. Synthesis and SOD activity of manganese complexes of substituted pyridino pentaaza macrocycles that contain axial auxiliary. *Bioorg. Med. Chem. Lett.* **2010,** 20, 2421-4.

37. Fort, S.; Kim, H. S.; Hindsgaul, O. Screening for galectin-3 inhibitors from synthetic lacto-N-biose libraries using microscale affinity chromatography coupled to mass spectrometry. *J. Org. Chem.* **2006,** 71, 7146-54.

38. Khunt, R. C.; Khedkar, V. M.; Chawda, R. S.; Chauhan, N. A.; Parikh, A. R.; Coutinho, E. C. Synthesis, antitubercular evaluation and 3D-QSAR study of N-phenyl-3-(4-fluorophenyl)-4-substituted pyrazole derivatives. *Bioorg. Med. Chem. Lett.* **2012,** 22, 666-78.

39. Insuasty, B.; Garcia, A.; Quiroga, J.; Abonia, R.; Nogueras, M.; Cobo, J. Synthesis of novel 6,6a,7,8-tetrahydro-5H-naphtho[1,2-e]pyrimido[4,5-b][1,4]diazepines under microwave irradiation as potential anti-tumor agents. *Eur. J. Med .Chem.* **2010,** 45, 2841-6.

40. Bekhit, A. A.; Abdel-Aziem, T. Design, synthesis and biological evaluation of some pyrazole derivatives as anti-inflammatory-antimicrobial agents. *Bioorg. Med. Chem.* **2004,** 12, 1935-45.

41. Zhang, G.; Miao, J.; Zhao, Y.; Ge, H. Copper-catalyzed aerobic dehydrogenative cyclization of N-methyl-N-phenylhydrazones: synthesis of cinnolines. *Angew. Chem. Int. Ed.* **2012,** 51, 8318-21.

42. Yu, D. D.; Lin, W.; Forman, B. M.; Chen, T. Identification of trisubstituted-pyrazol carboxamide analogs as novel and potent antagonists of farnesoid X receptor. *Bioorg. Med. Chem.* **2014,** 22, 2919-38.

43. El-Sayed, W. A.; Ali, O. M.; Zyada, R. A.; Mohamed, A. A.; Abdel-Rahman, A. A. Synthesis and antimicrobial activity of new substituted thienopyrimidines, their tetrazolyl and sugar derivatives. *Acta. Pol. Pharm.* **2012,** 69, 439-47.

44. Tae, H. S.; Hines, J.; Schneekloth, A. R.; Crews, C. M. Total synthesis and biological evaluation of tyroscherin. *Org. Lett.* **2010,** 12, 4308-11.

45. Buchini, S.; Buschiazzo, A.; Withers, S. G. A new generation of specific Trypanosoma cruzi trans-sialidase inhibitors. *Angew. Chem. Int. Ed.* **2008,** 47, 2700-3.

46. Bui, T.-T.; Garreau-de Bonneval, B.; Moineau-Chane Ching, K. I. Synthesis and preliminary physical properties of new neutral tetraalkoxy-substituted nickel bis(1,2-dithiolene) complexes. *New J. Chem.* **2010,** 34, 337.

47. Tantama, M.; Lin, W. C.; Licht, S. An activity-based protein profiling probe for the nicotinic acetylcholine receptor. *J. Am. Chem. Soc.* **2008,** 130, 15766-7.

48. Rostovtsev, V. V.; Green, L. G.; Fokin, V. V.; Sharpless, K. B. A stepwise huisgen cycloaddition process: copper(I)-catalyzed regioselective "ligation" of azides and terminal alkynes. *Angew. Chem. Int. Ed.* **2002,** 41, 2596-9.

49. Park, K. D.; Morieux, P.; Salome, C.; Cotten, S. W.; Reamtong, O.; Eyers, C.; Gaskell, S. J.; Stables, J. P.; Liu, R.; Kohn, H. Lacosamide isothiocyanate-based agents: novel agents to target and identify lacosamide receptors. *J. Med. Chem.* **2009,** 52, 6897-911.

50. Nicolaou, K. C.; Stepan, A. F.; Lister, T.; Li, A.; Montero, A.; Tria, G. S.; Turner, C. I.; Tang, Y.; Wang, J.; Denton, R. M.; Edmonds, D. J. Design, synthesis, and biological evaluation of platensimycin analogues with varying degrees of molecular complexity. *J. Am. Chem. Soc.* **2008,** 130, 13110-9.

CHAPTER 2. DESIGN AND SYNTHESIS OF SMALL-MOLECULE ANTAGONISTS TARGETING UPAR-UPA INTERACTION

2.1 Introduction

The urokinase-type plasminogen activator (uPA) is a serine protease that was first discovered in 1947 by McFarlane and it was initially isolated from human urine. uPA has a cell surface receptor known as the urokinase-type plasminogen activator receptor (uPAR). uPAR is a glycosylphosphatidylinositol (GPI) anchored protein containing three domains (D_1, D_2 and D_3) (Fig. 2.1).[1,2] D_1 and D_3 domains provide the binding site of uPA.

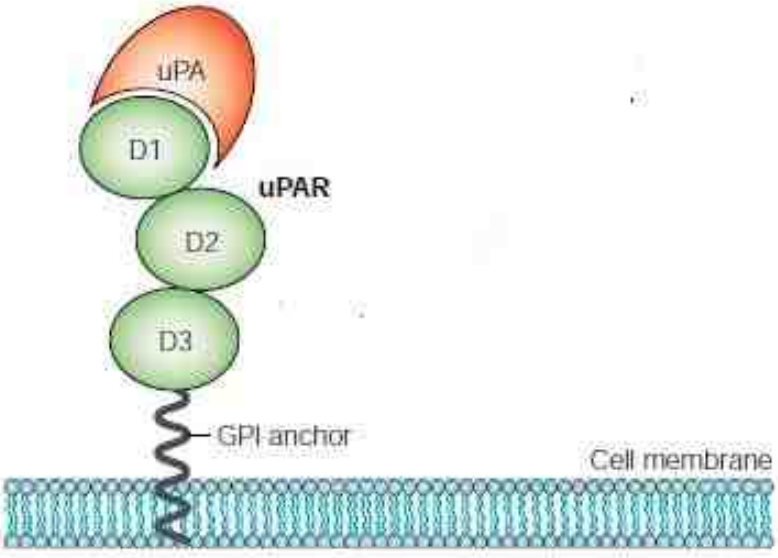

Figure 2.1. Schematic representation of uPAR

Only the intact urokinase receptor (uPAR) has a high affinity binding to uPA (1 nM). When uPA binds to uPAR, it is activated by other proteases. Active uPA will subsequently activate plasminogen to trigger the cascade of signaling events that promote tumor cell metastasis.[3,4] It is known that the migration and invasion of tumor cells into surrounding tissues are the most common interdependent processes of cancer metastasis.[5] There are studies showing that uPAR can be expressed in ECM remodeling,[6-9] and it plays a role in inflammatory and immune responses.[10,11] This causes cellular stress, injury and inflammation.[12] uPAR is also highly expressed in human cancers,[13-15] and the interaction between GPI anchored-uPAR and uPA is implicated in tumorigenesis,[16] invasion,[17-20] and angiogenesis.[21,22]

The interaction between uPA and uPAR is believed to lead to activation of cell signaling (Fig. 2.2).[2] On the surface of migrating cells, uPAR binds inactive urokinase

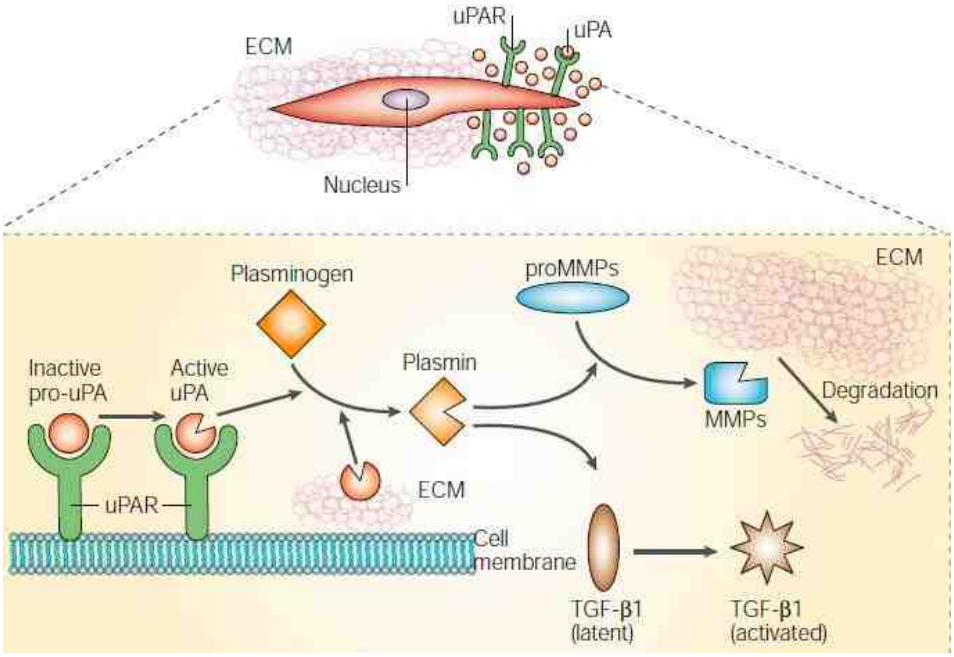

Figure 2.2. The role of uPAR as a protease receptor

(pro-uPA), which is converted to active uPA. Active uPA will activate plasminogen to plasmin. The activation of plasmin then triggers a proteolytic cascade that leads to further extracellular matrix (ECM) degradation. Active plasmin can activate latent growth factors β1 and it can also activate matrix metalloproteinases (MMPs). This process will result in the degradation of extracellular matrix that further promotes cancer metastasis.

We are interested in developing novel uPA antagonists that can bind into the cavity between uPA and its receptor uPAR to modulate the uPA-uPAR interaction and block the signaling pathway in cancer cell that are responsible for promoting metastasis (Fig. 2.3).

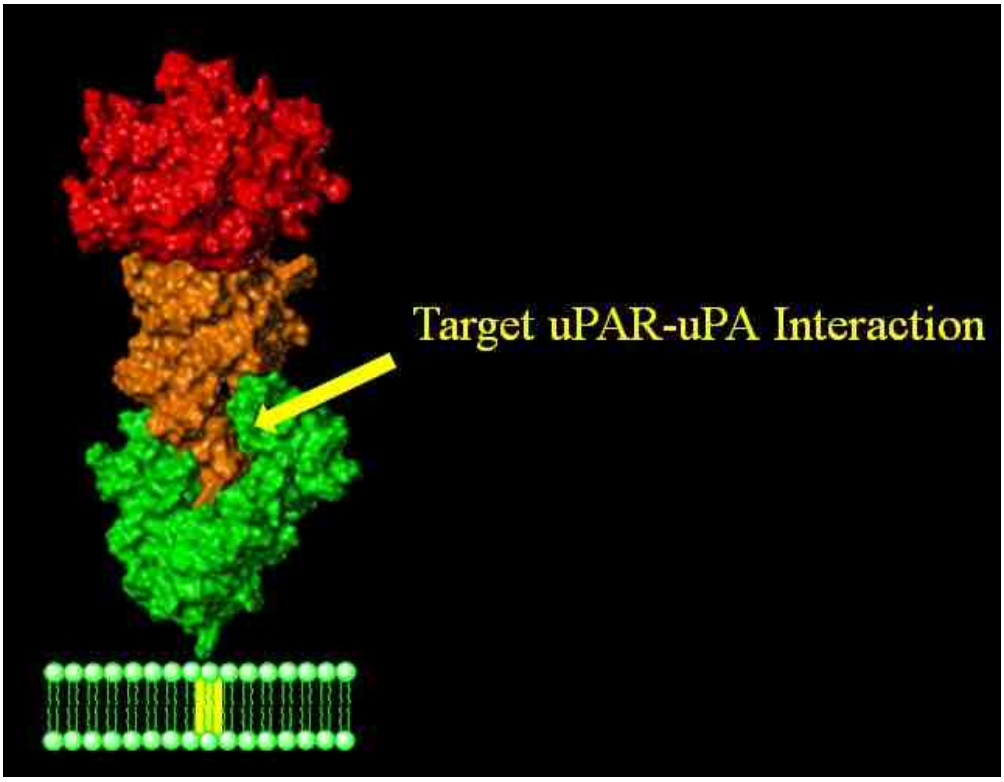

Figure 2.3. Target of uPAR-uPA interaction

The rational design and synthesis of small molecules targeting uPAR-uPA interaction was carried out using docking-based virtual screening.[17,23] Based on our

previously-published papers, small molecules with 6*H*-anthra[1,9-*cd*]isoxazol-6-one core structure (IPR-803) and pyrazole core structure (IPR-69) (Fig. 2.4) were discovered and synthesized by members of the Meroueh laboratory. These two compounds have shown good activity in inhibiting uPAR-uPA protein-protein interaction in cancer cell invasion but they did not show very potent *in vivo* activity. Thus, we are developing antagonists with novel structures that bind at higher affinity to uPAR and exhibit greater efficacy.

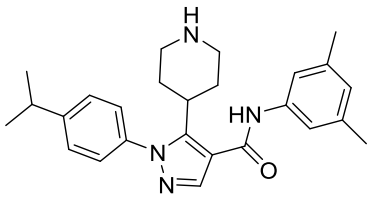

IPR-69

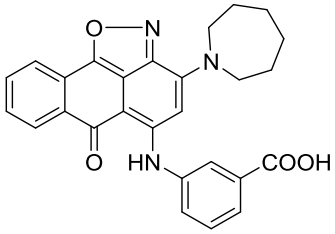

IPR-803

Figure 2.4. Chemical structures of IPR-69 and IPR-803

Towards the goal of discovering small molecules with novel core structure and better affinity to inhibit uPAR-uPA protein-protein interaction, 500 commercially-available compounds were purchased and computationally docked in the uPAR. These compounds were also tested in the biological assay by members of the Meroueh laboratory and three series were found to have modest activity. Their chemical structure is shown in Fig. 2.5. The first series is represented by IPR-1110, which has a pyrrolidone core structure. The second series contains a pyrrolo[3,4- *c*]pyrazole scaffold and it is represented by IPR-1283, and last series contains a 1,2-disubstituted 1,2-dihydropyrrolo[3,4-*b*]indol-3(4*H*)-one core structure and is represented by IPR-540.

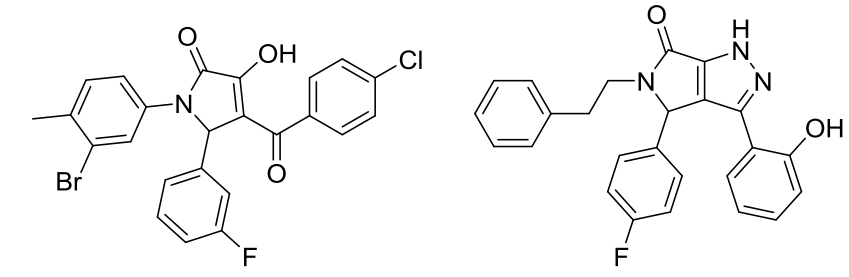

IPR-1110

IPR-1283

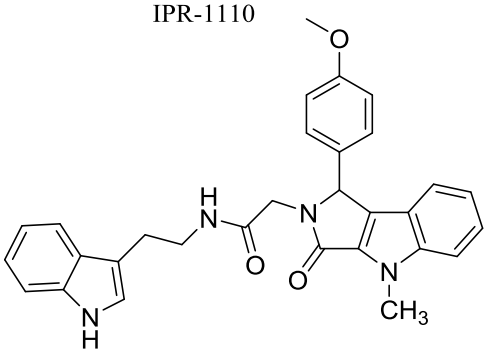

IPR-540

Figure 2.5 Chemical structures of IPR-1110, IPR-1283 and IPR-540

More IPR-1110 derivatives that emerged from a library were docked to uPAR and a binding mode of IPR-1110 with uPAR protein was proposed (Fig. 2.6). Judging from the binding mode in Fig. 2.6, there are four hot spot residues on uPA side chain that the molecule IPR-1110 mimics. In the structure of IPR-1110, R_1 mimics Trp30, R_2 mimics Phe25 and R_3 mimics Tyr24, respectively. Based on this binding mode, the synthetic routes to each of the three series compounds that are shown in Fig. 2.5 were proposed and derivatives were also designed and synthesized.

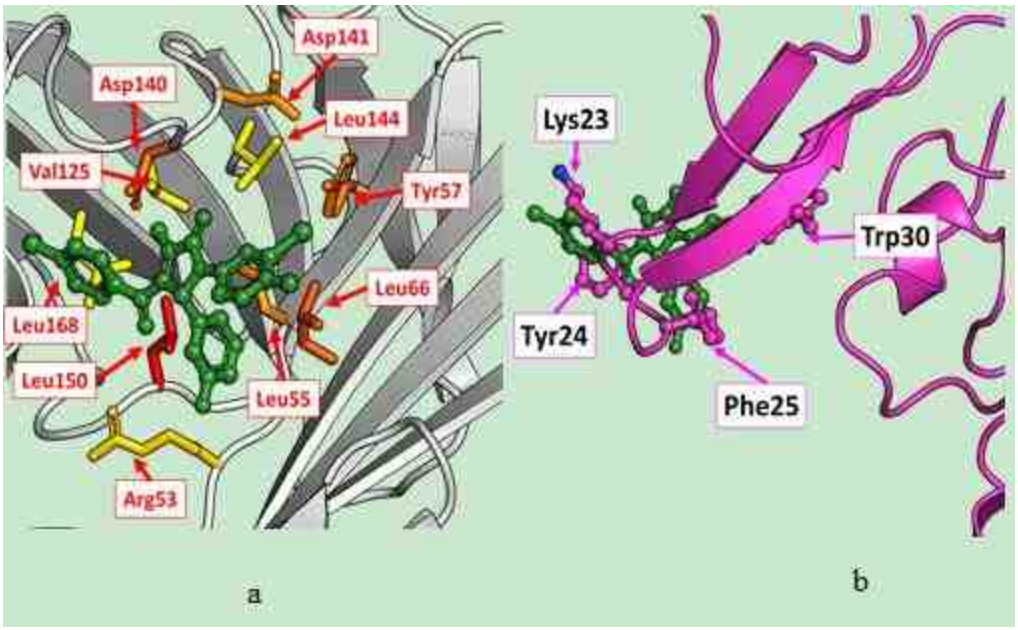

Figure 2.6. (a) Binding mode of IPR-1110 shown in capped-sticks. **(b)** Binding mode of IPR-1110 shown in green ball-and-stick rendering.

The chemical structure of IPR-1110 is shown in Fig. 2.5 and its binding mode to uPAR was proposed (Fig. 2.6). The binding mode of IPR-1110 with uPAR is shown in capped-sticks in (Fig. 2.6a). uPAR is shown in grey ribbon and uPAR hot spots are shown in capped sticks (orange and red). Here we define hot spots as residues that contribute an order of magnitude or more to the binding affinity. Binding mode of IPR-1110, which is shown in green ball-and-stick rendering, is shown in (Fig. 2.6b). uPA is shown in purple ribbon representation and uPAR is removed for clarity. In addition, the labels correspond to the four hot spots on uPA.

2.2 Results and Discussion

2.2.1 Compounds with Pyrrolidone Core Structure

In this series, IPR-1110 and various derivatives were prepared in a two-step procedure. Acetophenone derivatives were first treated with diethyl oxalate then followed by the addition of sodium ethoxide to afford the reactive intermediate **1**, which exists in an enone conformation. Then a three-component Knoevenagel condensation reaction with enone **1**, benzaldehyde derivatives and free amines was carried out to afford the pyrrolidone structures **2** (Scheme 2.1).[24]

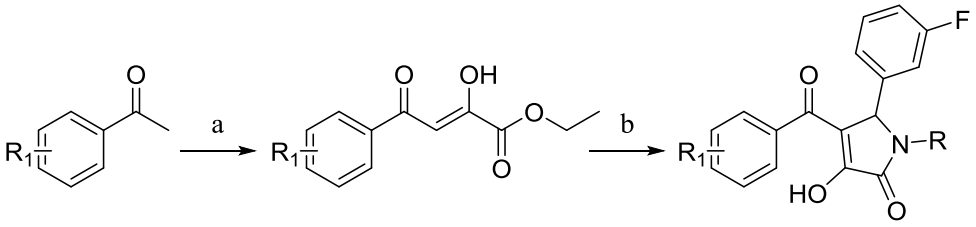

1a-b **2a-k**

1a:R_1 = 4'-Cl
1b:R_1 = 3'-Cl

Reagents and conditions: a) NaOEt (3 M in ethanol), diethyl oxalate, anhydrous THF, room temperature, 20 h; b) 3-F-PhCHO, RNH_2 , acetonitrile, room temperature, 20 h.

Scheme 2.1. Synthetic scheme of IPR-1110 series

In the first step, enone **1** can be made through a simple Aldol condensation. The α-proton of acetophenone is first deprotonated by the strong base sodium ethoxide to form a carbanion intermediate. And this carbanion, which is a strong nucleophile will subsequently react with diethyl oxalate to afford the desired enone compound. This compound was used for next reaction without further purification. It should be noted that the enone **1** is very reactive and it will decompose on the TLC plate. Therefore, this

compound cannot be purified by flash chromatography. This reaction is straightforward and in good yield. However, the only disadvantage of this reaction is that the acetophenone sometimes will not completely be converted to the desired product because of insufficient sodium ethoxide. Thus, when performing this chemistry, the ratio of diethyl oxalate and acetophenone was kept at 1 equivalent and followed by 1.3 equivalent of sodium ethoxide. The excess sodium ethoxide will be quenched by adding 2 M HCl solution to form ethanol which can be removed under high vacuum conditions.

In the second step, the mechanism can be divided into two half reactions. The first half is a Knoevenagel condensation reaction. Compound **1** is deprotonated to form reactive carbanion intermediate that will subsequently react with free benzaldehyde derivatives to form an enoate intermediate. In the second half of the reaction, the free amine acts as a nucleophile. It will first react with the enoate intermediate through Michael addition and then react with the intermolecular carboxylic ester functional group to yield the final pyrrolidone compounds. The detailed mechanism of the second step in Scheme 2.1 is proposed in Fig. 2.7 using IPR-1110 as example.

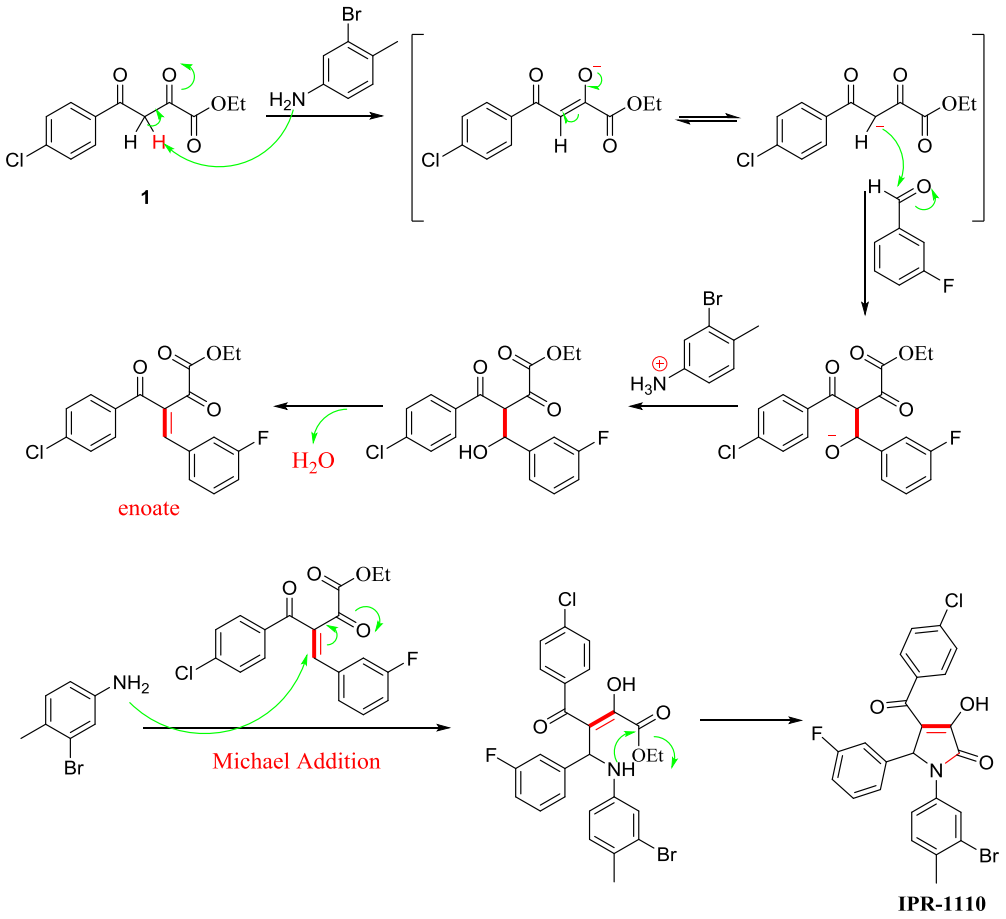

Figure 2.7. Proposed mechanism of Knoevenagel reaction

A library containing more than 100,000 compounds that includes the pyrrolidone ring system was docked to uPAR protein by computational chemists in the Meroueh laboratory. Based on the rankings of Glide scores of various compounds in this library, the top 51 compounds were synthesized by other members of Meroueh laboratory following Scheme 2.1. They are included here to illustrate to the variation of substituents at R_1, R_2 and R_3 that were explored. These compounds were subsequently tested with FP and ELISA assays. In addition, SAR study of these 51 compounds was also developed (Table 1).

Table 1. SAR Study of 51 Synthesized Compounds[a]

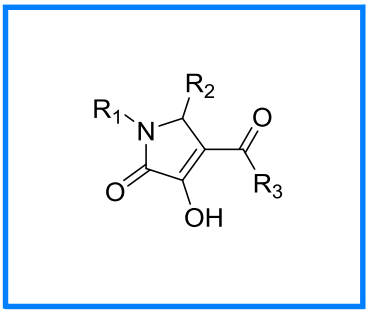

Compounds	R_1	R_2	R_3	IC_{50} (μM)	K_i (μM)
1(IPR-1110)	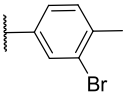	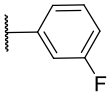	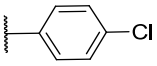	18	0.7
2	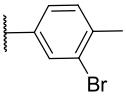	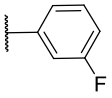	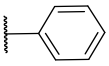	30	4
3	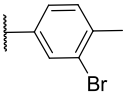	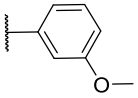	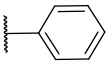	91	13
4	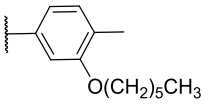	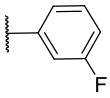	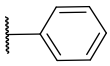	60	5
5	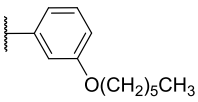	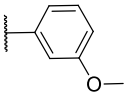	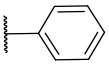	56	4
6	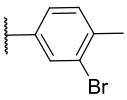	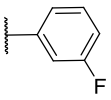	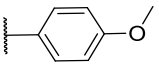	26	0.8
7	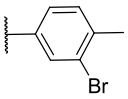	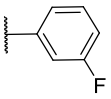	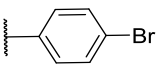	29	2
8	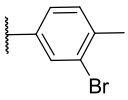	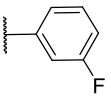	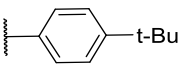	27	3

Table 1. continued

Compounds	R_1	R_2	R_3	IC_{50} (μM)	K_i (μM)
9	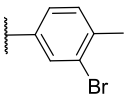	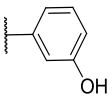	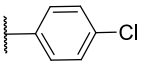	29	2
10	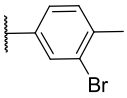	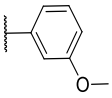	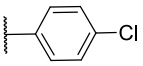	21	1
11	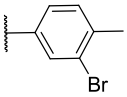	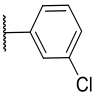	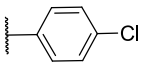	20	1
12	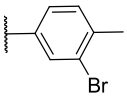	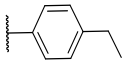	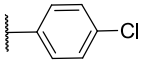	26	3
13	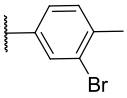	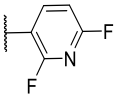	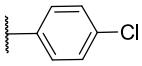	35	2
14	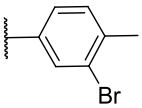		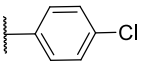	30	2
15	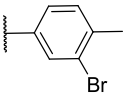	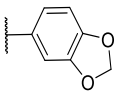	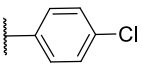	58	2
16	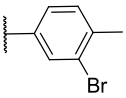	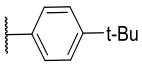	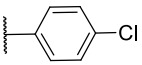	N/D	16
17	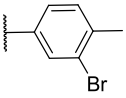	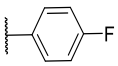	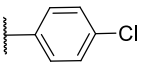	N/D	12
18	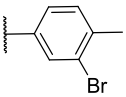	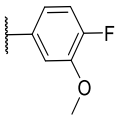	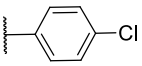	21	3

Table 1. continued

Compounds	R_1	R_2	R_3	IC_{50} (μM)	K_i (μM)
19	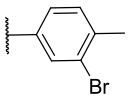	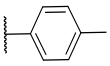	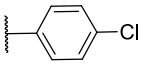	N/D	18
20	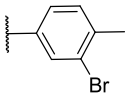	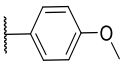	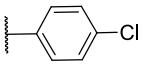	N/D	N/D
21	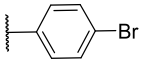	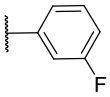	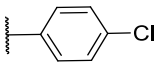	N/D	N/D
22	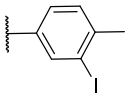		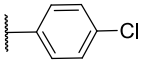	23	1
23	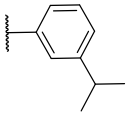		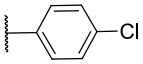	67	4
24	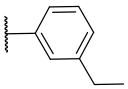		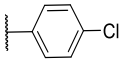	77	6
25	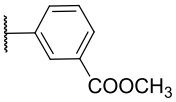		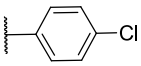	98	8
26	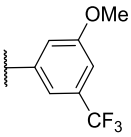		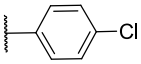	88	19
27	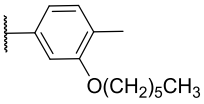		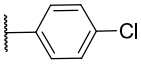	17	1
28	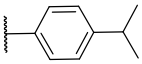		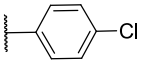	45	2

Table 1. continued

Compounds	R_1	R_2	R_3	IC_{50} (μM)	K_i (μM)
29	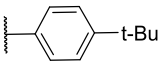		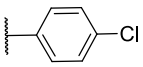	62	2
30	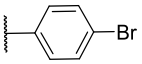		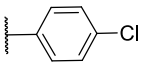	N/D	N/D
31	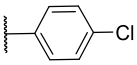		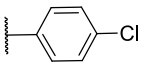	69	32
32	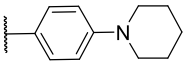		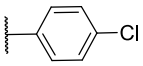	67	8
33	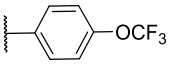		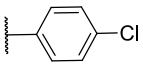	93	4
34	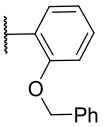		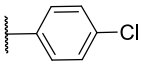	35	2
35	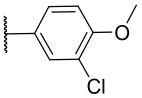		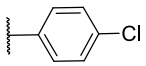	37	1
36	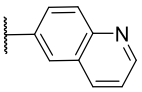		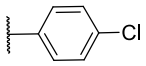	N/D	2
37	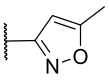		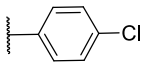	N/D	55
38	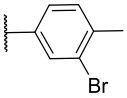	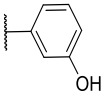	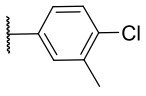	16	0.9

Table 1. continued

Compounds	R_1	R_2	R_3	$IC_{50}(\mu M)$	$K_i(\mu M)$
39	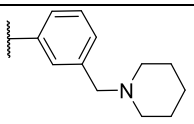		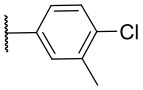	N/D	4
40	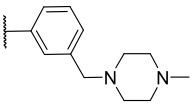		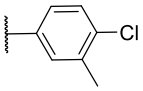	N/D	6
41	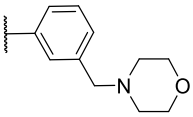		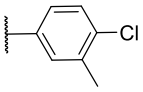	N/D	11
42	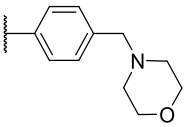		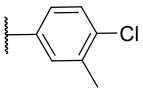	N/D	11
43	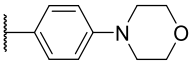		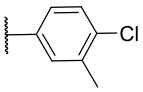	N/D	17
44	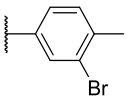	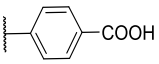	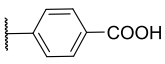	N/D	53
45	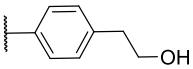		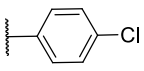	N/D	95
46	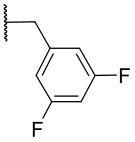		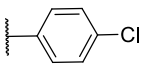	N/D	2
47	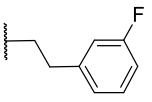		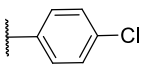	N/D	2
48	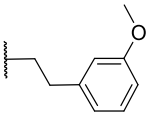		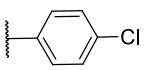	47	4

Table 1. continued

Compounds	R_1	R_2	R_3	IC_{50} (μM)	K_i (μM)
49	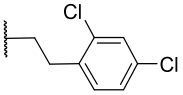		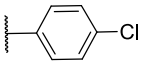	N/D	2
50	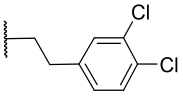		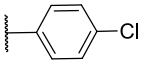	23	0.9
51			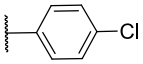	47	4

[a]N/D: not determined

From the SAR results in Table 1, IPR-1110 shows the highest inhibition to uPAR-uPA interaction according to IC_{50}. This suggests that R_2 with 3-fluorobenzene and R_3 with a 4-chloro substituted benzene group are desirable for high affinity interaction with uPAR. Introducing a phenethyl moiety into R_1 could be an efficient strategy to mimic Trp30 hot spot on uPA. An alternative way to modify R_1 is to introduce some more rigid aromatic groups that can form stronger hydrophobic interaction with Trp30 hot spot into R_1. Thus, another 8 pyrrolidone derivatives were designed and I synthesized the compounds. These compounds were also evaluated for binding and inhibition using a fluorescence polarization and ELISA assay as we have described previously.[17] The biochemical studies were conducted by Dr. Degang Liu in the Meroueh laboratory and the results are shown in Table 2.

Table 2. SAR Study of 8 Synthesized Compounds

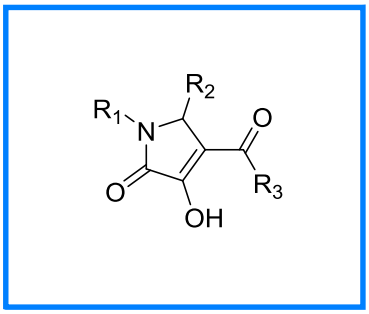

Compounds	R_1	R_2	R_3	IC_{50} (μM)	K_i (μM)
2b	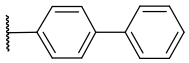		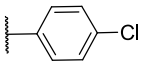	24	0.8
2c	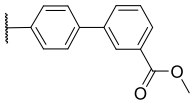		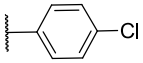	16	N/D
2e	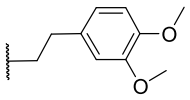		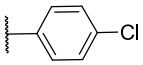	N/D	8
2f	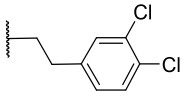		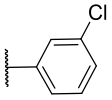	22	0.6
2g	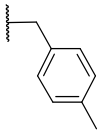		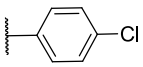	N/A	N/D
2h	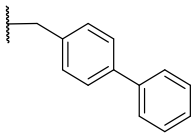		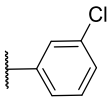	N/A	N/D
2i	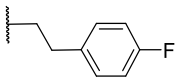		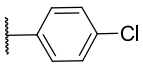	N/A	N/D
2j	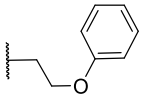		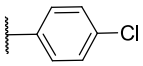	N/A	N/D

Each of the compounds in Table 2 was tested by Dr. Liu in the Meroueh laboratory and used IPR-1110 as control and results were analyzed and summarized in Table 3.

Table 3. Inhibition Activity of 8 Synthesized Compounds[b]

Compound	$IC_{50}(\mu M)$	$K_i(\mu M)$
2a	18	0.7
2b	24	0.8
2c	16	N/D
2e	N/D	8
2f	22	0.6
2g	N/A	N/D
2h	N/A	N/D
2i	N/A	N/D
2j	N/A	N/D

[a]N/D: not determined; [b]N/A: no activity

According to results in Table 3, the IC_{50} of **2c** was 16 μM comparing with our best compound IPR-1110, compound **2c** showed a slight improvement over IPR-1110. These result motivated us to do more research on developing new compounds. It was concluded that introducing a biphenyl group with a strong electron withdrawing group could be a potential breakthrough. Herein, our future work will mainly focus on modification of compound **2c** by converting the methyl ester on the biphenyl group into different amides.

2.2.2 Compounds with Pyrrolo[3, 4- *c*]pyrazole Scaffold

The structure of compound IPR-1283 is shown in Fig. 2.5. It was prepared by a two-step synthesis. In the first step, pyrrolidone **2** was made with the procedure in Scheme 2.1. The synthesized compound **2** is added to hydrazine hydride to afford the corresponding pyrrolo [3,4-*c*] pyrazole ring system, namely **3** (Scheme 2.2).[25,26]

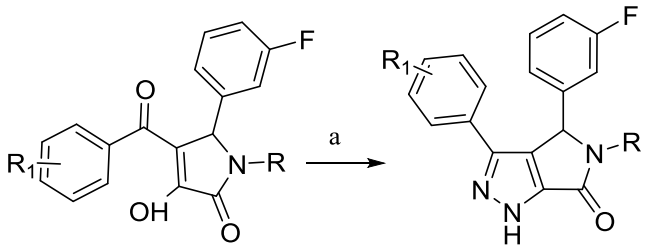

2a-b **3a-b**

Reagents and conditions: a) 50-60 % hydrazine hydride, HOAc, 0 °C to reflux, 6 h

Scheme 2.2. Synthetic scheme of IPR-1283 series

By following the synthetic route in Scheme 2.2, we synthesized compounds **3a** and **3b** and their chemical structures are shown in Fig. 2.8. But these two compounds did not show activity in the ELISA.

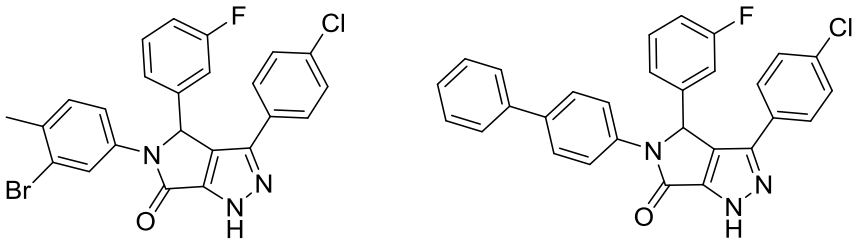

3a 3b

Figure 2.8 Chemical structures of **3a** and **3b**

This is likely due to the fact that the pyrrolo[3,4-*c*]pyrazole scaffold is too rigid too enable the R_3 group to rotate to fit properly into the cavity on uPAR. The structure forces the moiety in R_3 to stretch out of the binding pocket on uPAR and move away from the position occupied by the Tyr24 hot spot.

2.2.3 Compounds with 1, 2-Disubstituted 1, 2- dihydropyrrolo [3, 4-*b*]indol-3(4*H*)-one Core Structure

IPR-540 is a potential uPA inhibitor that was discovered in the Meroueh laboratory by screening commercially-available compounds and its structure is shown in Fig 2.5. The synthetic route to IPR-540 derivatives has been proposed (Scheme 2.3).

The final compound can be prepared by a two-step synthesis. The first step is a Mannich reaction. Aldehyde derivatives and free amines will first react to form a Schiff base. Then 1H-Indole-2-carboxylic acid is performing as a nucleophile reacted with the Schiff base intermediate to afford the final Mannich reaction products.[27]

In the second step reaction, the Mannich reaction products afforded in step 1 will in turn be dehydrated to generate the final product.[27,28]

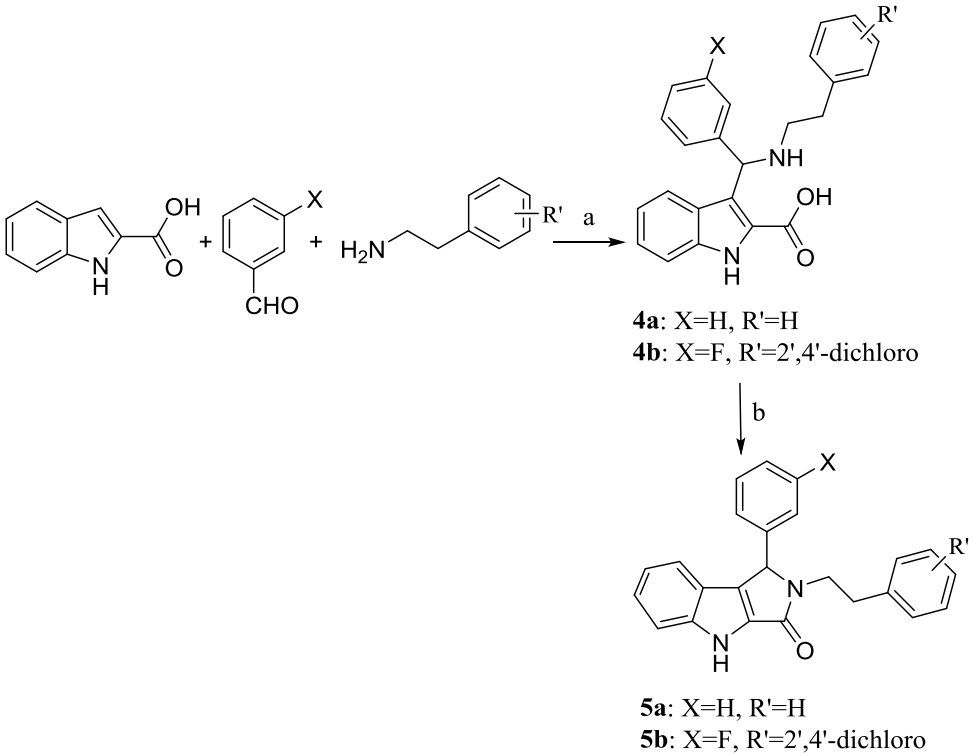

Reagents and conditions: a) ethanol, reflux, 8 h; b) HATU, TEA, DMF,room temperature, 20 h

Scheme 2.3. Synthetic scheme of IPR-540 series

Unfortunately, the synthesized compounds did not inhibit the uPAR-uPA interaction but they did bind to uPAR. Comparing the chemical structure of IPR-540, the only difference is the methyl group on the indole moiety is removed in the synthesized compounds. Without the methyl group on the nitrogen atom in the indole moiety, the secondary amine could form strong hydrogen bond with Asn22 on uPA and this hydrogen bonding interaction will prevent the molecule binding with the hydrophobic pocket in R_3. Thus, protecting the N atom on indole moiety with a hydrophobic group is indispensable.

2.3 Experimental

General Methods: All chemicals were purchased from either Sigma-Aldrich or Acros and used as received. Column chromatography was carried out with silica gel GF254 (25-63μm). Mass Spectra were measured on an Agilent 6520 Mass Q-TOF instrument. ^{1}H NMR and ^{13}C NMR spectra were recorded on a BRUKER 500 MHz spectrometer, using TMS as an internal standard and $CDCl_3$ or DMSO-d_6 as solvents. Chemical shifts (δ values) and coupling constants (*J* values) are reported in ppm and hertz, respectively. Anhydrous solvent and reagents were all analytically pure and dried through routine protocols. All compounds that were evaluated in biological essays had > 95% purity using HPLC.

2.31. Chemical Synthesis of IPR-1110 Derivatives

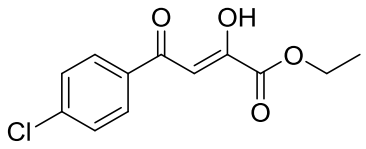

1a

Ethyl (Z)-4-(4-chlorophenyl)-2-hydroxy-4-oxobut-2-enoate (**1a)**. To a stirred solution of 4'-chloroacetophenone (773 mg, 6 mmol) and diethyl oxalate (0.81 mL, 6 mmol) in anhydrous THF (12 mL) was added sodium ethoxide (3 M in ethanol) (2.7 mL, 7.8 mmol) at 0 °C over 15min. The mixture was warmed to ambient temperature and stirred for 20 h. The resulting dark red solution was cooled to 0 °C in an ice bath, quenched with 2 M HCl solution and extracted with ethyl acetate (3 x 15 mL). The combined organic layer was

dried over anhydrous $MgSO_4$ and removed *in vacuo*. Crude residue was kept in refrigerator for 24 h and triturated with hexane. The resulting product was dried under high vacuum to give a light yellow power (1.34 g, 88%): ^{1}H NMR (500 MHz, $CDCl_3$) δ 7.92 (d, *J* = 8.5 Hz, 2H), 7.46 (d, *J* = 8.5 Hz, 2H), 7.02 (s, 1H), 4.37-4.41 (q, *J* = 7 Hz, 2H), 1.40 (t, *J* = 7 Hz, 3H); ^{13}C NMR (125 MHz, $CDCl_3$) δ 189.34, 169.94, 162.00, 140.26, 133.24, 129.22, 129.18, 97.72, 62.68, 14.04; HRMS (ESI) *m/z* for $C_{12}H_{11}ClO_4$ $[M + H]^+$ calcd 255.0419, found 255.0421.

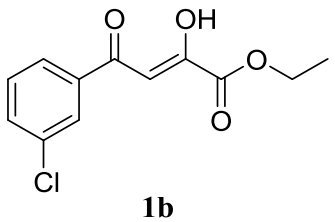

1b

Ethyl (Z)-4-(3-chlorophenyl)-2-hydroxy-4-oxobut-2-enoate (**1b**). Compound **1b** was prepared from 3'-chloroacetophenone in a manner similar to that described for compound **1a.** Yield 92%, light yellow solid: ^{1}H NMR (500 MHz, $CDCl_3$) δ 15.09 (brs, 1H), 7.96 (t, *J* = 2 Hz, 1H), 7.85-7.87 (m, 1H), 7.56-7.58 (m, 1H), 7.44 (t, *J* = 8 Hz, 1H), 7.02 (s, 1H), 4.38-4.43 (q, *J* = 7 Hz, 2H), 1.41 (t, *J* = 7.5 Hz, 3H); ^{13}C NMR (125 MHz, $CDCl_3$) δ 189.12, 170.32, 161.96, 136.58, 136.26, 133.60, 130.20, 127.90, 125.93, 97.95, 62.78, 14.08; HRMS (ESI) *m/z* for $C_{12}H_{11}ClO_4$ $[M + H]^+$ calcd 255.0419, found 255.0423.

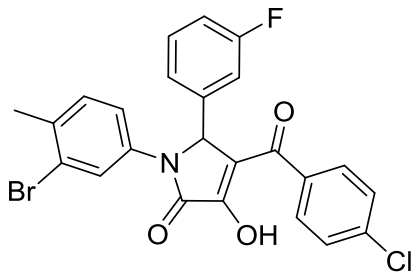

2a

1-(3-Bromo-4-methylphenyl)-4-(4-chlorobenzoyl)-5-(3-fluorophenyl)-3-hydroxy-1,5-dihydro-2H-pyrrol-2-one (**2a**). Compound **1a** (50.9 mg, 0.2 mmol) was dissolved in acetonitrile (2 mL) and 3-bromo-4-methylaniline (37.2 mg, 0.2 mmol) was added subsequently. Yellow precipitate was formed in the solution and the mixture was stirred under room temperature for 30 min. 3-Fluorobenzaldehyde (21.2 μL, 0.2 mmol) was added and the resulting mixture was stirred at ambient temperature for 20 h. Solvent was removed *in vacuo* to yield yellow solid and the residue was triturated with ice-cold diethyl ether. The resulting product was filtered, washed with ice-cold diethyl ether and dried under high vacuum to give a snow-white solid (27.9 mg, 28%): ^{1}H NMR (500 MHz, DMSO-d_6) δ 7.94 (d, *J* = 2 Hz, 1H), 7.74 (d, *J* = 8.5 Hz, 2H), 7.53 (d, *J* = 8.5 Hz, 2H), 7.48-7.50 (dd, *J* = 8, 2 Hz, 1H), 7.30 (t, *J* = 8.5 Hz, 2H), 7.24-7.26 (m, 2H), 6.94-6.98 (m, 1H), 6.33 (s, 1H), 2.25 (s, 3H); ^{13}C NMR (125 MHz, DMSO-d_6) δ 187.77, 164.53, 162.89, 160.95, 137.45, 136.63, 136.20, 134.37, 130.92, 130.62, 130.30, 130.23, 128.31, 125.71, 123.89, 123.70, 121.56, 115.02, 114.85, 114.66, 99.50, 60.45, 21.75; HRMS (ESI) *m/z* for $C_{24}H_{16}BrClFNO_3$ $[M + H]^+$ calcd 500.0059, found 500.0058.

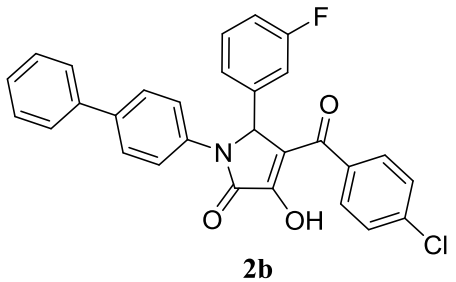

2b

1-([1,1'-Biphenyl]-4-yl)-4-(4-chlorobenzoyl)-5-(3-fluorophenyl)-3-hydroxy-1,5-dihydro-2H-pyrrol-2-one (**2b**). Compound **2b** was prepared by a three-component Knoevenagel condensation of **1a**, 4-aminobiphenyl and 3-fluorobenzaldehyde in a manner similar to that described for **2a**. And 20% DMAP was added. Yield 37%, white solid: ^{1}H NMR (500 MHz, DMSO-d_6) δ 7.73-7.76 (m, 4H), 7.62-7.65 (m, 4H), 7.53 (d, *J* = 8.5 Hz, 2H), 7.43 (t, *J* = 7.5 Hz, 2H), 7.32-7.36 (m, 2H), 7.27-7.30 (m, 1H), 7.23-7.26 (m, 1H), 6.96 (t, *J* = 8 Hz, 1H), 6.40 (s, 1H); ^{13}C NMR (125 MHz, DMSO-d_6) δ 187.88, 164.49, 162.90, 160.96, 151.05, 139.58, 137.50, 137.03, 136.63, 135.54, 130.62, 128.86, 128.32, 127.39, 126.88, 126.44, 123.85, 122.77, 119.14, 114.98, 114.82, 114.66, 60.47; HRMS (ESI) *m/z* for $C_{29}H_{19}ClFNO_3$ $[M + H]^+$ calcd 484.1110, found 484.1067.

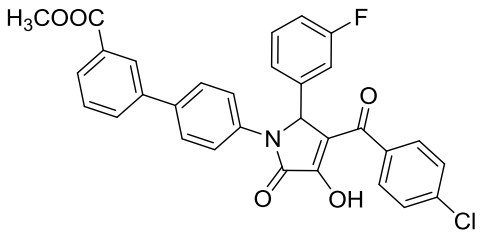

2c

Methyl-4'-(3-(4-chlorobenzoyl)-2-(3-fluorophenyl)-4-hydroxy-5-oxo-2,5-dihydro-1H-pyrrol-1-yl)-[1,1'-biphenyl]-3-carboxylate (**2c**). Compound **2c** was prepared by a three-component Knoevenagel condensation of **1a**, methyl 4'-amino-(1,1'-biphenyl)-3-

carboxylate and 3-fluorobenzaldehyde in a manner similar to that described for **2a**. And 20% DMAP was added. Yield 34%, white solid: ^{1}H NMR (500 MHz, DMSO-d_6) δ 8.14 (s, 1H), 7.92 (m, 2H), 7.69-7.77 (m, 6H), 7.54-7.59 (m, 3H), 7.30-7.36 (m, 3H), 6.96 (s, 1H), 6.41 (s, 1H), 3.88 (s, 3H); ^{13}C NMR (125 MHz, DMSO-d_6) δ 187.83, 166.08, 164.57, 162.89, 160.95, 139.69, 127.47, 136.64, 136.03, 135.83, 131.27, 130.63, 130.32, 129.45, 128.31, 128.01, 127.09, 126.92, 123.86, 122.83, 119.08, 114.83, 114.66, 78.94, 60.42, 52.20; HRMS (ESI) *m/z* for $C_{31}H_{21}ClFNO_5$ $[M + H]^+$ calcd 542.1165, found 542.1149.

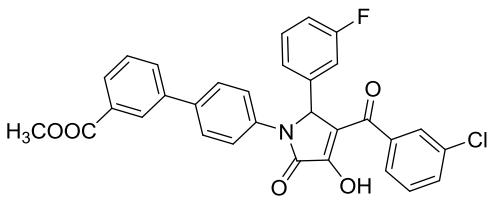

2d

Methyl-4'-(3-(3-chlorobenzoyl)-2-(3-fluorophenyl)-4-hydroxy-5-oxo-2,5-dihydro-1H-pyrrol-1-yl)-[1,1'-biphenyl]-3-carboxylate (**2d**)**.** Compound **2d** was prepared by a three-component Knoevenagel condensation of **1a**, methyl 4'-amino-(1,1'-biphenyl)-3-carboxylate and 3-fluorobenzaldehyde in a manner similar to that described for **2a**. And 20% DMAP was added. Yield 36%, white solid: ^{1}H NMR (500 MHz, DMSO-d_6) δ 8.14 (s, 1H), 7.92 (d, *J* = 7 Hz, 2H), 7.77 (d, *J* = 8 Hz, 2H), 7.74 (s, 1H), 7.68 (d, *J* = 7.5 Hz, 3H), 7.64 (d, *J* = 7.5 Hz, 1H), 7.59 (t, *J* = 7.5 Hz, 1H), 7.50 (t, *J* = 7.5 Hz, 1H), 7.38 (d, *J* = 9.5 Hz, 1H), 7.32 (d, *J* = 7 Hz, 1H), 7.26 (d, *J* = 6 Hz, 1H), 6.96 (m, 1H), 6.39 (s, 1H), 3.87 (s, 3H); ^{13}C NMR (125 MHz, DMSO-d_6) δ 187.86, 166.09, 160.95, 139.70, 136.05, 135.85, 132.97, 132.20, 131.30, 130.33, 130.19, 129.48, 128.29, 128.02, 127.31, 127.10,

126.93, 123.95, 122.89, 114.94, 114.78, 60.42, 52.22; HRMS (ESI) *m/z* for $C_{31}H_{21}ClFNO_5$ $[M + H]^+$ calcd 542.1165, found 542.1166.

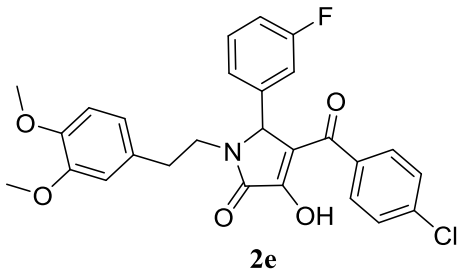

2e

4-(4-Chlorobenzoyl)-1-(3,4-dimethoxyphenethyl)-5-(3-fluorophenyl)-3-hydroxy-1,5-dihydro-2H-pyrrol-2-one (**2e**). Compound **2e** was prepared by a three-component Knoevenagel condensation of **1a**, 3,4-dimethoxyphenethylamine and 3-fluorobenzaldehyde in a manner similar to that described for **2a**. Yield 66%, white solid: ^{1}H NMR (500 MHz, DMSO-d_6) δ 7.69 (d, *J* = 8.5 Hz, 2H), 7.49 (d, *J* = 8 Hz, 2H), 7.34-7.38 (m, 1H), 7.13-7.16 (m, 3H), 6.83 (d, *J* = 8 Hz, 1H), 6.71 (d, *J* = 1.5 Hz, 1H), 6.63-6.65 (dd, *J* = 8.5, 1.5 Hz, 1H), 3.81-3.87 (m, 1H), 3.70 (s, 3H), 3.69 (s, 3H), 2.81-2.84 (m, 1H), 2.73-2.76 (m, 1H), 2.62-2.65 (m, 1H); ^{13}C NMR (125 MHz, DMSO-d_6) δ 188.12, 163. 94, 166.13, 161.66, 149.14, 147.89, 137.55, 137.41, 131.45, 131.04, 128.64, 124.28, 120.97, 112.83, 112.38, 60.68, 55.97, 55.83, 42.20, 33.49; HRMS (ESI) *m/z* for $C_{27}H_{23}ClFNO_5$ $[M + H]^+$ calcd 496.1322, found 496.1321.

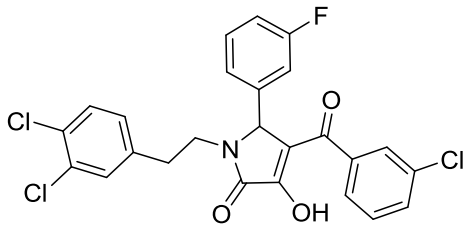

2f

4-(3-Chlorobenzoyl)-1-(3,4-dichlorophenethyl)-5-(3-fluorophenyl)-3-hydroxy-1,5-dihydro-2H-pyrrol-2-one (**2f**). Compound **2f** was prepared by a three-component Knoevenagel condensation of **1b**, 3-fluorobenzaldehyde and 3, 4-dichlorophenethylamine in a manner similar to that described for **2a**. Yield 68%, white solid: ^{1}H NMR (500 MHz, DMSO-d_6) δ 7.98 (s, 1H), 7.70 (s, 1H), 7.63 (d, *J* = 8.5 Hz, 1H), 7.54-7.56 (m, 1H), 7.50 (d, *J* = 8.5 Hz, 1H), 7.42-7.44 (m, 2H), 7.35-7.36 (m, 1H), 7.14-7.20 (m, 2H), 7.09 (t, *J* = 7.5 Hz, 1H), 5.42 (s, 1H), 3.82-3.86 (m, 1H), 2.86-2.88 (m, 1H), 2.79 (m, 2H); ^{13}C NMR (125 MHz, DMSO-d_6) δ 186.10, 165.96, 163.08, 161.14, 150.73, 140.04, 138.53, 132.61, 131.31, 131.04, 130.81, 130,65, 130.33, 129.77, 129.40, 129.28, 129.09, 128.90, 128.23, 127.19, 123.74, 114.75, 59.95, 41.09, 32.28; HRMS (ESI) *m/z* for $C_{25}H_{17}Cl_3FNO_3$ [M + H]$^+$ calcd 504.0331, found 504.0334.

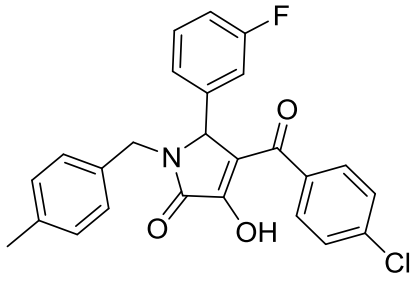

2g

4-(4-Chlorobenzoyl)-5-(3-fluorophenyl)-3-hydroxy-1-(4-methylbenzyl)-1,5-dihydro-2H-pyrrol-2-one (**2g**). Compound **2g** was prepared by a three-component Knoevenagel

condensation of **1a**, 4-methylbenzylamine and 3-fluorobenzaldehyde in a manner similar to that described for **2a**. Yield 59%, light yellow solid: ^{1}H NMR (500 MHz, DMSO-d_6) δ 7.71 (d, *J* = 7.5 Hz, 2H), 7.49 (d, *J* = 8 Hz, 2H), 7.34-7.35 (m, 1H), 7.09-7.11 (m, 5H), 6.98 (d, *J* = 7 Hz, 2H), 5.20 (s, 1H), 4.83 (d, *J* = 15 Hz, 1H), 3.73 (d, *J* = 15 Hz, 1H), 2.27 (s, 3H); HRMS (ESI) *m/z* for $C_{25}H_{19}ClFNO_3$ $[M + H]^+$ calcd 436.1110, found 436.1111.

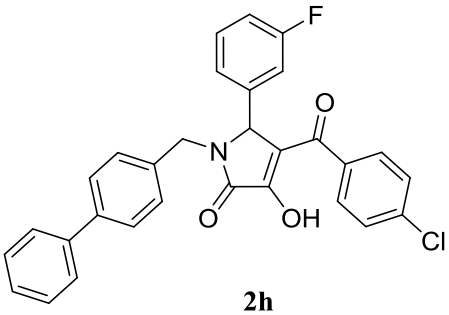

2h

1-([1,1'-Biphenyl]-4-ylmethyl)-4-(4-chlorobenzoyl)-5-(3-fluorophenyl)-3-hydroxy-1,5-dihydro-2H-pyrrol-2-one (**2h**). Compound **2h** was prepared by a three-component Knoevenagel condensation of **1a**, 4-phenylbenzylamine and 3-fluorobenzaldehyde in a manner similar to that described for **2a**. Yield 62%, white solid: ^{1}H NMR (500 MHz, DMSO-d_6) δ 7.72 (d, *J* = 8.5 Hz, 2H), 7.63 (d, *J* = 7.5 Hz, 2H), 7.59 (d, *J* = 8 Hz, 2H), 7.49 (d, *J* = 8.5 Hz, 2H), 7.46 (t, *J* = 7.5 Hz, 2H), 7.32-7.37 (m, 2H), 7.18 (d, *J* = 8 Hz, 2H), 7.14 (d, *J* = 8 Hz, 2H), 7.09 (t, *J* = 8.5 Hz, 1H), 5.31 (s, 1H), 4.86 (d, *J* = 15.5 Hz, 1H), 3.90 (d, *J* = 15 Hz, 1H); HRMS (ESI) *m/z* for $C_{30}H_{21}ClFNO_3$ $[M + H]^+$ calcd 498.1267, found 498.1272.

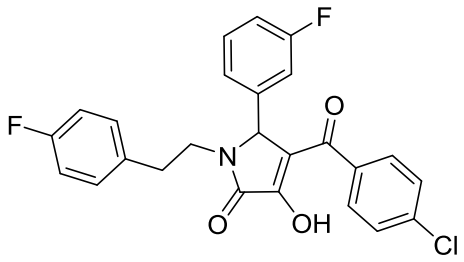

2i

4-(4-Chlorobenzoyl)-1-(4-fluorophenethyl)-5-(3-fluorophenyl)-3-hydroxy-1,5-dihydro-2H-pyrrol-2-one (**2i**). Compound **2i** was prepared by a three-component Knoevenagel condensation of **1a**, 4-fluorophenethylamine and 3-fluorobenzaldehyde in a manner similar to that described for **2a**. Yield 73%, yellow-white solid: ^{1}H NMR (500 MHz, DMSO-d_6) δ 7.70 (d, *J* = 8.5 Hz, 2H), 7.50 (d, *J* = 8.5 Hz, 2H), 7.35-7.39 (m, 1H), 7.16-7.20 (m, 4H), 7.07-7.13 (m, 3H), 5.41 (s, 1H), 3.80-3.86 (m, 1H), 2.79-2.87 (m, 2H), 2.71-2.75 (m, 1H); HRMS (ESI) *m/z* for $C_{25}H_{18}ClF_2NO_3$ $[M + H]^+$ calcd 454.1016, found 454.1008.

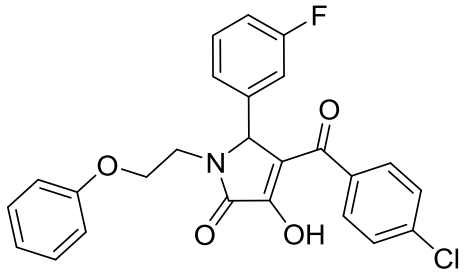

2j

4-(4-Chlorobenzoyl)-5-(3-fluorophenyl)-3-hydroxy-1-(2-phenoxyethyl)-1,5-dihydro-2H-pyrrol-2-one (**2j**). Compound **2j** was prepared by a three-component Knoevenagel condensation of **1a**, 2-phenoxyethylamine, and 3-fluorobenzaldehyde in a manner similar to that described for **2a**. Yield 72%, white solid: ^{1}H NMR (500 MHz, DMSO-d_6) δ 7.97

(s, 1H), 7.72 (d, *J* = 8 Hz, 2H), 7.47 (d, *J* = 8 Hz, 2H), 7.35 (m, 1H), 7.27-7.28 (m, 2H), 7.19 (d, *J* = 7.5 Hz, 1H), 7.09 (m, 1H), 6.97-6.99 (m, 1H), 6.93-6.94 (m, 1H), 6.90 (d, *J* = 7 Hz, 1H), 5.56 (s, 1H), 3.93-4.15 (m, 2H), 3.02 (m, 2H); HRMS (ESI) *m/z* for $C_{25}H_{19}ClFNO_4$ $[M + H]^+$ calcd 452.1059, found 452.1036.

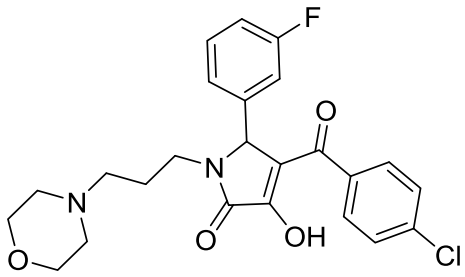

2k

4-(4-Chlorobenzoyl)-5-(3-fluorophenyl)-3-hydroxy-1-(3-morpholinopropyl)-1,5-dihydro-2H-pyrrol-2-one (**2k**). Compound **2k** was prepared by a three-component Knoevenagel condensation of **1a**, 3-morpholinopropylamine and 3-fluorobenzaldehyde in a manner similar to that described for **2a**. Yield 67%, white solid: ^{1}H NMR (500 MHz, DMSO-d_6) δ 7.82 (s, 1H), 7.63 (d, *J* = 8.5 Hz, 1H), 7.45 (d, *J* = 8 Hz, 1H), 7.33 (t, *J* = 8 Hz, 2H), 7.14 (t, *J* = 9 Hz, 2H), 7.04-7.07 (m, 1H), 5.32 (s, 1H), 3.72 (m, 4H), 2.89 (m, 4H), 2.75 (m, 2H), 2.63-2.69 (m, 2H), 1.77 (m, 1H), 1.71 (m, 1H); HRMS (ESI) *m/z* for $C_{24}H_{24}ClFN_2O_4$ $[M + H]^+$ calcd 459.1481, found 459.1489.

2.32. Chemical Synthesis of IPR-1283 Derivatives

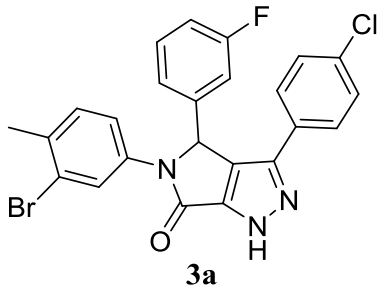

3a

5-(3-Bromo-4-methylphenyl)-3-(4-chlorophenyl)-4-(3-fluorophenyl)-4,5-dihydropyrrolo[3,4-c]pyrazol-6(1H)-one (**3a**). Compound **2a** (49.8 mg, 0.1 mmol) was dissolved in acetic acid (2 mL) and the mixture was cooled to 0 °C in an ice bath. To the solution was added 50-60% hydrazine hydride (0.3 mL, 1.0 mmol) over 5 min. The resulting solution was stirred at 0 °C for 15 min then was heated to reflux for 6 h. The reaction was monitored by LC/MS. After the reaction was completed, the mixture was cooled to room temperature and ice-cold H_2O (2 mL) was added to yield white precipitate. The resulting solid was filtered off, washed with ice-cold H_2O and dried under high vacuum to afford the desired product **3a** as a white solid (30.7 mg, 62%): ^{1}H NMR (500 MHz, DMSO-d_6) δ 7.94 (d, *J* = 2 Hz, 1H), 7.74 (d, *J* = 8.5 Hz, 2H), 7.53 (d, *J* = 8.5 Hz, 2H), 7.48-7.50 (dd, *J* = 8, 2 Hz, 1H), 7.29-7.32 (m, 2H), 7.24-7.26 (m, 2H), 6.94-6.98 (m, 1H), 6.33 (s, 1H), 2.25 (s, 3H); ^{13}C NMR (125 MHz, DMSO-d_6) δ 187.77, 164.53, 162.89, 160.95, 137.45, 136.63, 135.20, 134.37, 130.92, 130.62, 130.30, 130.23, 128.31, 125.71, 123.89, 123.70, 121.56, 115.02, 114.85, 114.66, 99.50, 60.45, 21.75; HRMS (ESI) *m/z* for $C_{24}H_{16}BrClFN_3O$ $[M + H]^+$ calcd 496.0222, found 496.0208.

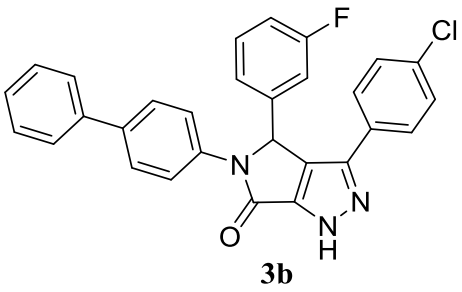

3b

5-([1,1'-Biphenyl]-4-yl)-3-(4-chlorophenyl)-4-(3-fluorophenyl)-4,5-dihydropyrrolo[3,4-c]pyrazol-6(1H)-one (**3b**). Compound **3b** was prepared from **2b** in a manner similar to that described for **3a**. Yield 59%, white solid: ^{1}H NMR (500 MHz, DMSO-d_6) δ 14.24 (brs, 1H), 7.68 (d, *J* = 9 Hz, 2H), 7.64 (m, 4H), 7.59 (d, *J* = 8 Hz, 2H), 7.47 (m, 2H), 7.42 (t, *J* = 7.5 Hz, 2H), 7.32 (t, *J* = 7.5 Hz, 1H), 7.22-7.27 (m, 3H), 6.98 (t, *J* = 8.5 Hz, 1H), 6.92 (s, 1H); ^{13}C NMR (125 MHz, DMSO-d_6) δ 162.98, 161.04, 139.59, 139.20, 136.77, 136.63, 133.18, 130.77, 130.71, 128.84, 127.67, 127.31, 126.79, 126.41, 123.45, 115.40, 115.23, 114.67, 114.49, 58.90, 30.62; HRMS (ESI) *m/z* for $C_{29}H_{19}ClFN_3O$ $[M + H]^+$ calcd 480.1273, found 480.1275.

2.33. Chemical Synthesis of IPR-540 Derivatives

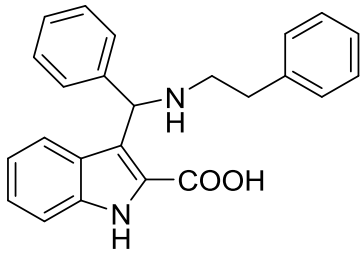

4a

3-((Phenethylamino)(phenyl)methyl)-1H-indole-2-carboxylic acid (**4a**). Indole-2-carboxylic acid (483.5 mg, 3.0 mmol), benzaldehyde (0.37 mL, 3.6 mmol) and phenylethylamine (0.57 mL, 4.5 mmol) were mixed in 95% ethanol (6 mL) and the resulting solution was heated to reflux for 8 h. The reaction was cooled to room temperature and placed into freezer for 48 h. The resulting white precipitate was filtered and washed with minimum amount of ice-cold ethanol. The solid was dried under high vacuum to yield the desired product **4a** (233 mg, 21%): ^{1}H NMR (500 MHz, DMSO-d_6) δ 11.40 (s, 1H), 7.69 (d, *J* = 7.5 Hz, 2H), 7.61 (d, *J* = 8 Hz, 1H), 7.36 (t, *J* = 7.5 Hz, 3H), 7.28-7.31 (m, 2H), 7.26 (d, *J* = 7.5 Hz, 2H), 7.20-7.22 (m, 1H), 7.17 (d, *J* = 7 Hz, 2H), 7.11-7.14 (m, 1H), 6.96-6.99 (m, 1H), 5.74 (s, 1H), 3.01-3.08 (m, 1H), 2.96-3.00 (m, 2H), 2.91-2.95 (m, 1H); ^{13}C NMR (125 MHz, DMSO-d_6) δ 164.59, 138.88, 137.70, 134.49, 131.17, 128.74, 128.57, 128.43, 128.32, 127.91, 126.57, 126.52, 123.17, 119.31, 118.97, 112.31, 112.07, 57.36, 46.93, 32.35; HRMS (ESI) *m/z* for $C_{24}H_{22}N_2O_2$ $[M + H]^+$ calcd 371.1754, found 371.1752.

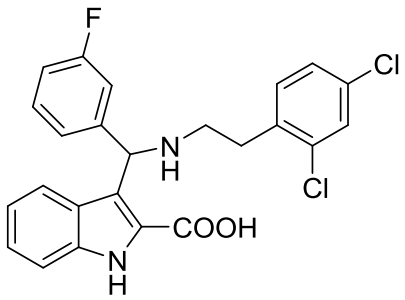

4b

3-(((2,4-Dichlorophenethyl)amino)(3-fluorophenyl)methyl)-1H-indole-2-carboxylic acid (**4b**). Compound **4b** was prepared in a manner similar to that described for **4a**. Yield 33.8%, white solid: ^{1}H NMR (500 MHz, DMSO-d_6) δ 11.47 (s, 1H), 7.68 (d, *J* = 8.5 Hz, 1H), 7.55 (s, 1H), 7.51 (d, *J* = 8.5 Hz, 2H), 7.42 (t, *J* = 8 Hz, 1H), 7.37 (d, *J* = 8.5 Hz, 1H), 7.35 (d, *J* = 1 Hz, 2H), 7.14 (t, *J* = 8 Hz, 2H), 7.00 (t, *J* = 7.5 Hz, 1H), 5.81 (s, 1H), 2.97-3.10 (m, 4H); ^{13}C NMR (125 MHz, DMSO-d_6) δ 164.30, 163.03, 161.08, 141.74, 134.58, 134.35, 133.97, 132.25, 130.80, 128.79, 127.58, 126.46, 123.94, 123.38, 119.47, 119.07, 115.20, 115.04, 114.68, 114.50, 112.37, 56.64, 44.86, 29.92; HRMS (ESI) *m/z* for $C_{24}H_{19}Cl_2FN_2O_2$ $[M + H]^+$ calcd 457.0880, found 457.0883.

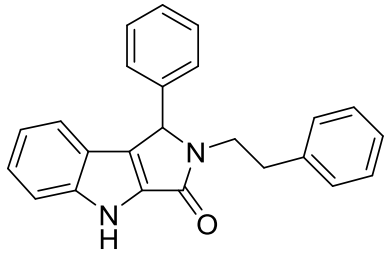

5a

2-Phenethyl-1-phenyl-1,4-dihydropyrrolo[3,4-b]indol-3(2H)-one (**5a**). Compound **4a** (111 mg, 0.3 mmol)**,** HATU (171 mg, 0.45 mmol) and TEA (0.08 mL, 0.6 mmol) were dissolved in anhydrous DMF (5 mL) and the resulting mixture was stirred at room

temperature for 20 h. H_2O was added and the mixture was extracted with ethyl acetate. The combined organic layer was washed with saturated $NaHCO_3$ solution and brine, respectively. The organic extracts were dried over anhydrous $MgSO_4$ and concentrated *in vacuo*. The crude residue was purified by flash chromatography (hexane/ethyl acetate = 3:1) to afford desired compound **5a** as a white solid (26.4 mg, 25%): ^{1}H NMR (500 MHz, DMSO-d_6) δ 11.96 (s, 1H), 7.45 (d, *J* = 8 Hz, 1H), 7.39 (t, *J* = 7.5 Hz, 2H), 7.33-7.34 (m, 1H), 7.26 (t, *J* = 7 Hz, 2H), 7.23-7.24 (m, 1H), 7.22 (m, 1H), 7.19 (d, *J* = 8 Hz, 3H), 7.15-7.16 (m, 2H), 6.97- 7.00 (m, 1H), 5.62 (s, 1H), 3.92-3.98 (m, 1H), 2.96-3.02 (m, 1H), 2.88-2.92 (m, 1H), 2.69-2.75 (m, 1H); ^{13}C NMR matched that previously reported;[27] HRMS (ESI) *m/z* for $C_{24}H_{20}N_2O$ $[M + H]^+$ calcd 353.1648, found 353.1660.

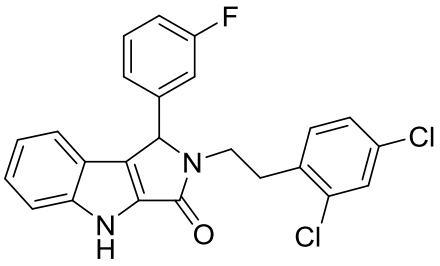

5b

2-(2,4-Dichlorophenethyl)-1-(3-fluorophenyl)-1,4-dihydropyrrolo[3,4-b]indol-3(2H)-one (**5b**). Compound **5b** was prepared from **4b** in a manner similar to that described for **5a**. Yield 19.6%, white solid: ^{1}H NMR (500 MHz, DMSO-d_6) δ 11.99 (s, 1H), 7.52 (s, 1H), 7.44 (d, *J* = 9.5 Hz, 1H), 7.38-7.41 (m, 1H), 7.31 (d, *J* = 1.5 Hz, 2H), 7.22-7.25 (m, 2H), 7.13-7.17 (m, 1H), 7.07-7.09 (m, 2H), 7.00 (t, *J* = 7 Hz, 1H), 5.79 (s, 1H), 3.91-3.97 (m, 1H), 3.06-3.11 (m, 1H), 2.98-3.03 (m, 1H), 2.86-2.93 (m, 1H); ^{13}C NMR (125 MHz, DMSO-d_6) δ 163.31, 162.10, 161.37, 141.32, 140.35, 135.54, 134.00, 133.22, 132.33,

131.87, 131.02, 129.36, 128.65, 127.38, 124.00, 123.24, 120.76, 120.16, 119.10, 115.17, 114.13, 113.52, 59.39, 31.64; HRMS (ESI) *m/z* for $C_{24}H_{17}Cl_2FN_2O$ $[M + H]^+$ calcd 439.0775, found 439.0773.

2.4 List of References

1. Ploug, M.; Ellis, V. Structure-function relationships in the receptor for urokinase-type plasminogen activator. Comparison to other members of the Ly-6 family and snake venom alpha-neurotoxins. *FEBS. Lett.* **1994,** 349, 163-8.
2. Blasi, F.; Carmeliet, P. uPAR: a versatile signalling orchestrator. *Nat. Rev. Mol. Cell. Biol.* **2002,** 3, 932-43.
3. Resnati, M.; Pallavicini, I.; Wang, J. M.; Oppenheim, J.; Serhan, C. N.; Romano, M.; Blasi, F. The fibrinolytic receptor for urokinase activates the G protein-coupled chemotactic receptor FPRL1/LXA4R. *Proc. Natl. Acad .Sci. U. S. A.* **2002,** 99, 1359-64.
4. Liu, D.; Aguirre Ghiso, J.; Estrada, Y.; Ossowski, L. EGFR is a transducer of the urokinase receptor initiated signal that is required for in vivo growth of a human carcinoma. *Cancer. Cell.* **2002,** 1, 445-57.
5. Andreasen, P. A.; Kjoller, L.; Christensen, L.; Duffy, M. J. The urokinase-type plasminogen activator system in cancer metastasis: a review. *Int. J. Cancer.* **1997,** 72, 1-22.
6. Solberg, H.; Ploug, M.; Hoyer-Hansen, G.; Nielsen, B. S.; Lund, L. R. The murine receptor for urokinase-type plasminogen activator is primarily expressed in tissues actively undergoing remodeling. *J. Histochem. Cytochem.* **2001,** 49, 237-46.
7. Floridon, C.; Nielsen, O.; Holund, B.; Sunde, L.; Westergaard, J. G.; Thomsen, S. G.; Teisner, B. Localization and significance of urokinase plasminogen activator and its receptor in placental tissue from intrauterine, ectopic and molar pregnancies. *Placenta.* **1999,** 20, 711-21.

8. Uszynski, M.; Perlik, M.; Uszynski, W.; Zekanowska, E. Urokinase plasminogen activator (uPA) and its receptor (uPAR) in gestational tissues; Measurements and clinical implications. *Eur. J. Obstet. Gynecol. Reprod. Biol.* **2004,** 114, 54-8.

9. Romer, J.; Lund, L. R.; Eriksen, J.; Pyke, C.; Kristensen, P.; Dano, K. The receptor for urokinase-type plasminogen activator is expressed by keratinocytes at the leading edge during re-epithelialization of mouse skin wounds. *J. Invest. Dermatol.* **1994,** 102, 519-22.

10. Plesner, T.; Ralfkiaer, E.; Wittrup, M.; Johnsen, H.; Pyke, C.; Pedersen, T. L.; Hansen, N. E.; Dano, K. Expression of the receptor for urokinase-type plasminogen activator in normal and neoplastic blood cells and hematopoietic tissue. *Am. J. Clin. Pathol.* **1994,** 102, 835-41.

11. Nykjaer, A.; Moller, B.; Todd, R. F., 3rd; Christensen, T.; Andreasen, P. A.; Gliemann, J.; Petersen, C. M. Urokinase receptor. An activation antigen in human T lymphocytes. *J. Immunol.* **1994,** 152, 505-16.

12. Wei, C.; Moller, C. C.; Altintas, M. M.; Li, J.; Schwarz, K.; Zacchigna, S.; Xie, L.; Henger, A.; Schmid, H.; Rastaldi, M. P.; Cowan, P.; Kretzler, M.; Parrilla, R.; Bendayan, M.; Gupta, V.; Nikolic, B.; Kalluri, R.; Carmeliet, P.; Mundel, P.; Reiser, J. Modification of kidney barrier function by the urokinase receptor. *Nat. Med.* **2008,** 14, 55-63.

13. Bene, M. C.; Castoldi, G.; Knapp, W.; Rigolin, G. M.; Escribano, L.; Lemez, P.; Ludwig, W. D.; Matutes, E.; Orfao, A.; Lanza, F.; van't Veer, M.; Egil, E. G. o. I. C. o. L. CD87 (urokinase-type plasminogen activator receptor), function and pathology in hematological disorders: a review. *Leukemia.* **2004,** 18, 394-400.

14. Jacobsen, B.; Ploug, M. The urokinase receptor and its structural homologue C4.4A in human cancer: expression, prognosis and pharmacological inhibition. *Curr. Med. Chem.* **2008,** 15, 2559-73.

15. Rasch, M. G.; Lund, I. K.; Almasi, C. E.; Hoyer-Hansen, G. Intact and cleaved uPAR forms: diagnostic and prognostic value in cancer. *Front. Biosci.* **2008,** 13, 6752-62.

16. Shapiro, R. L.; Duquette, J. G.; Nunes, I.; Roses, D. F.; Harris, M. N.; Wilson, E. L.; Rifkin, D. B. Urokinase-type plasminogen activator-deficient mice are predisposed to staphylococcal botryomycosis, pleuritis, and effacement of lymphoid follicles. *Am. J. Pathol.* **1997,** 150, 359-69.

17. Mani, T.; Wang, F.; Knabe, W. E.; Sinn, A. L.; Khanna, M.; Jo, I.; Sandusky, G. E.; Sledge, G. W., Jr.; Jones, D. R.; Khanna, R.; Pollok, K. E.; Meroueh, S. O. Small-molecule inhibition of the uPAR.uPA interaction: synthesis, biochemical, cellular, in vivo pharmacokinetics and efficacy studies in breast cancer metastasis. *Bioorg. Med. Chem.* **2013,** 21, 2145-55.

18. Kondraganti, S.; Gondi, C. S.; McCutcheon, I.; Dinh, D. H.; Gujrati, M.; Rao, J. S.; Olivero, W. C. RNAi-mediated downregulation of urokinase plasminogen activator and its receptor in human meningioma cells inhibits tumor invasion and growth. *Int. J. Oncol.* **2006,** 28, 1353-60.

19. Subramanian, R.; Gondi, C. S.; Lakka, S. S.; Jutla, A.; Rao, J. S. siRNA-mediated simultaneous downregulation of uPA and its receptor inhibits angiogenesis and invasiveness triggering apoptosis in breast cancer cells. *Int. J. Oncol.* **2006,** 28, 831-9.

20. Kunigal, S.; Lakka, S. S.; Gondi, C. S.; Estes, N.; Rao, J. S. RNAi-mediated downregulation of urokinase plasminogen activator receptor and matrix metalloprotease-9 in human breast cancer cells results in decreased tumor invasion, angiogenesis and growth. *Int. J. Cancer.* **2007,** 121, 2307-16.

21. Mignatti, P.; Rifkin, D. B. Plasminogen activators and matrix metalloproteinases in angiogenesis. *Enzyme. Protein.* **1996,** 49, 117-37.

22. Rabbani, S. A.; Mazar, A. P. The role of the plasminogen activation system in angiogenesis and metastasis. *Surg. Oncol. Clin. N. Am.* **2001,** 10, 393-415, x.

23. Wang, F.; Li, J.; Sinn, A. L.; Knabe, W. E.; Khanna, M.; Jo, I.; Silver, J. M.; Oh, K.; Li, L.; Sandusky, G. E.; Sledge, G. W.; Nakshatri, H.; Jones, D. R.; Pollok, K. E.; Meroueh, S. O. Virtual screening targeting the urokinase receptor, biochemical and cell-based studies, synthesis, pharmacokinetic characterization, and effect on breast tumor metastasis. *J. Med. Chem.* **2011,** 54, 7193-205.

24. Ma, K.; Wang, P.; Fu, W.; Wan, X.; Zhou, L.; Chu, Y.; Ye, D. Rational design of 2-pyrrolinones as inhibitors of HIV-1 integrase. *Bioorg. Med. Chem. Lett.* **2011,** 21, 6724-7.

25. Zhuang, C.; Miao, Z.; Wu, Y.; Guo, Z.; Li, J.; Yao, J.; Xing, C.; Sheng, C.; Zhang, W. Double-edged swords as cancer therapeutics: novel, orally active, small molecules simultaneously inhibit p53-MDM2 interaction and the NF-kappaB pathway. *J. Med. Chem.* **2014,** 57, 567-77.

26. Richter, A.; Rose, R.; Hedberg, C.; Waldmann, H.; Ottmann, C. An optimised small-molecule stabiliser of the 14-3-3-PMA2 protein-protein interaction. *Chemistry.* **2012,** 18, 6520-7.

27. Ma, F.; Ma, L.; Lei, M.; Hu, L. Synthesis of 1,2-disubstituted 1,2-dihydropyrrolo[3,4-*b*]indol-3(4H)-one derivatives. *Monatsh. Chem.* **2014,** 145, 1035-1041.

28. Nicolaou, K. C.; Stepan, A. F.; Lister, T.; Li, A.; Montero, A.; Tria, G. S.; Turner, C. I.; Tang, Y.; Wang, J.; Denton, R. M.; Edmonds, D. J. Design, synthesis, and biological evaluation of platensimycin analogues with varying degrees of molecular complexity. *J. Am. Chem. Soc.* **2008,** 130, 13110-9.

APPENDICES

Appendix-A. ^{1}H NMR and ^{13}C NMR of Compounds in Chapter **1**

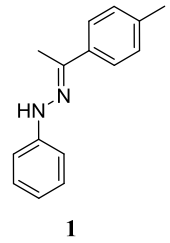

1

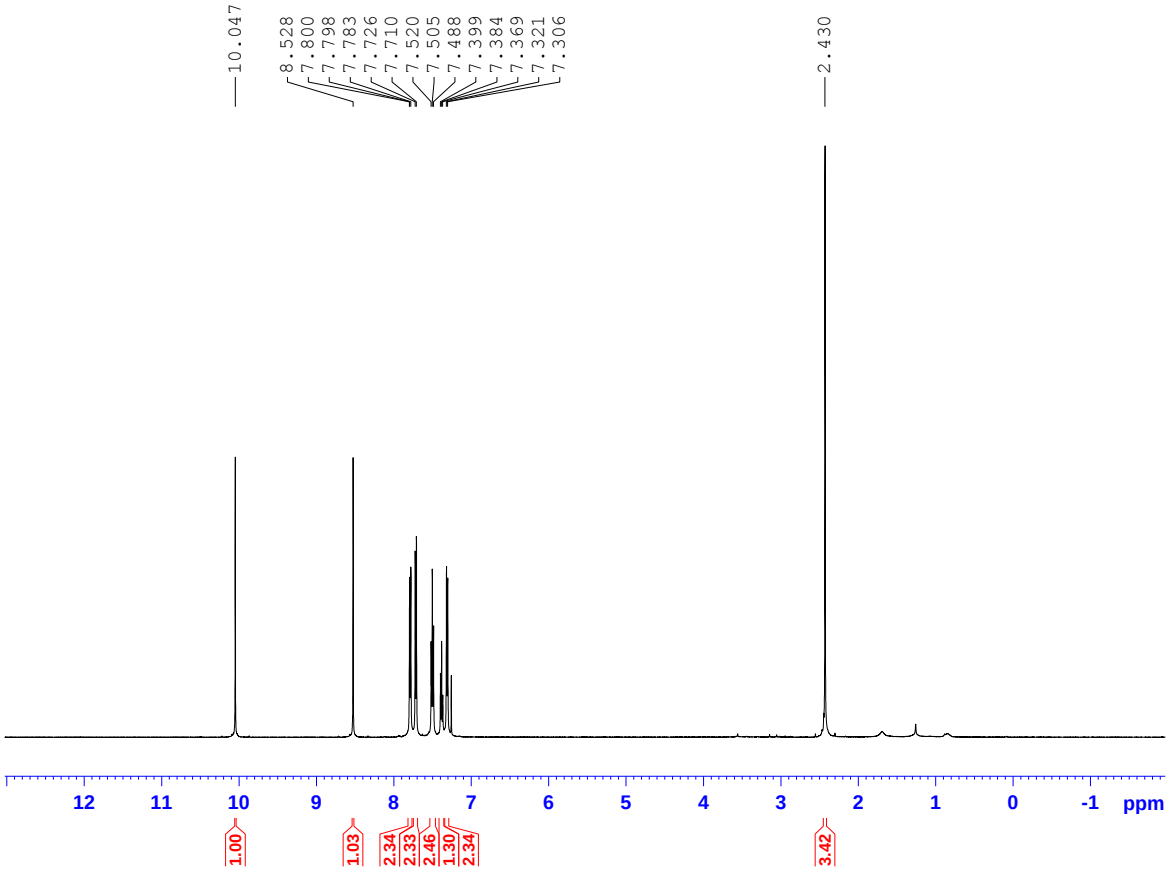

Figure A1. The 500 MHz ^{1}H NMR spectrum of **1** in $CDCl_3$

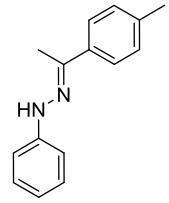

1

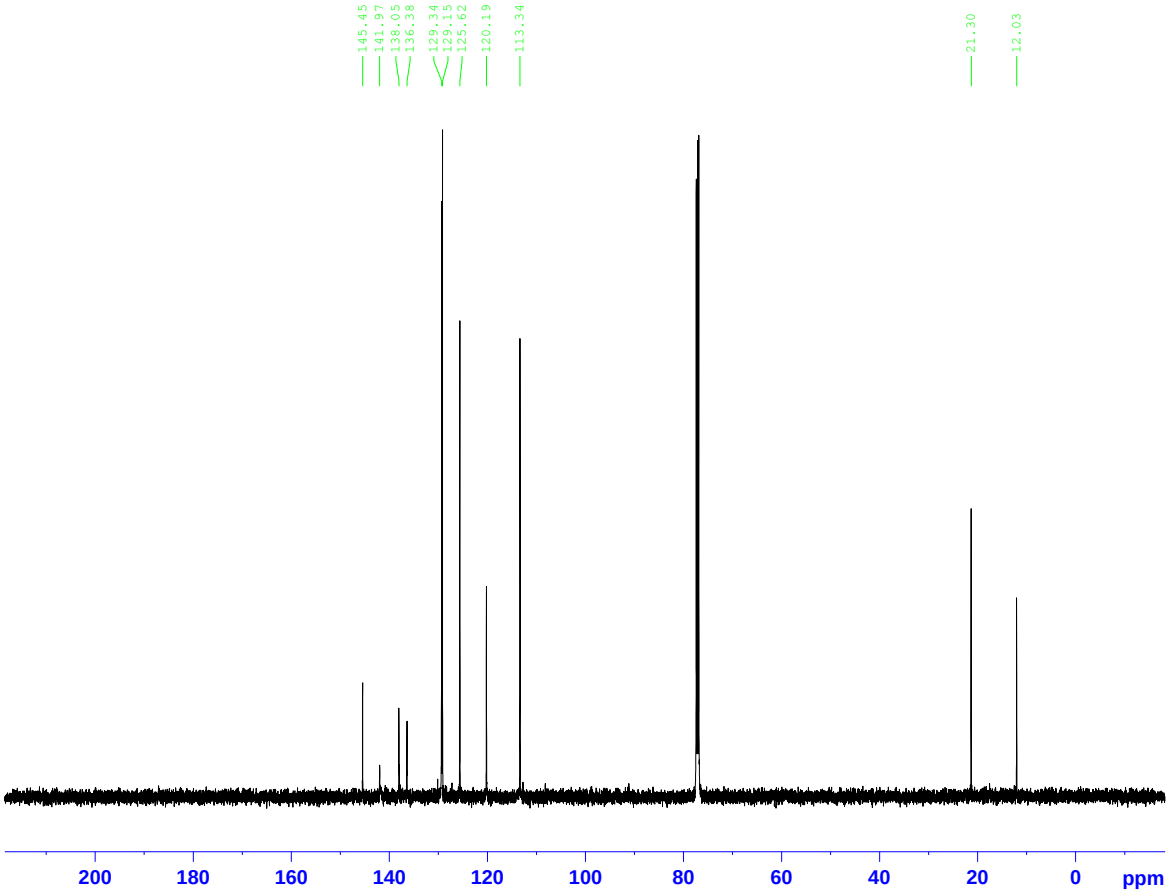

Figure A2. The 125 MHz ^{13}C NMR spectrum of **1** in $CDCl_3$

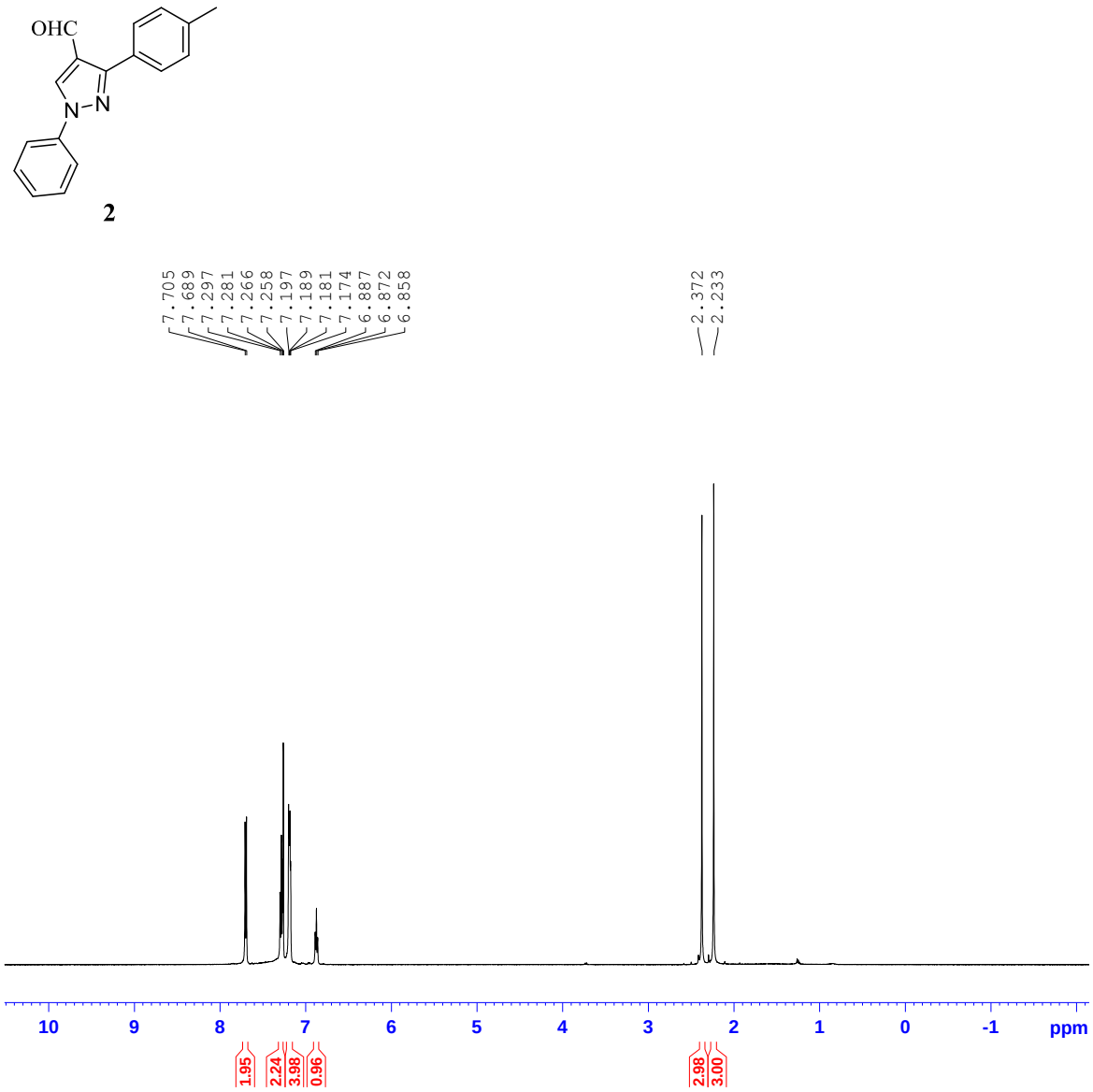

Figure A3. The 500 MHz ^{1}H NMR spectrum of **2** in $CDCl_3$

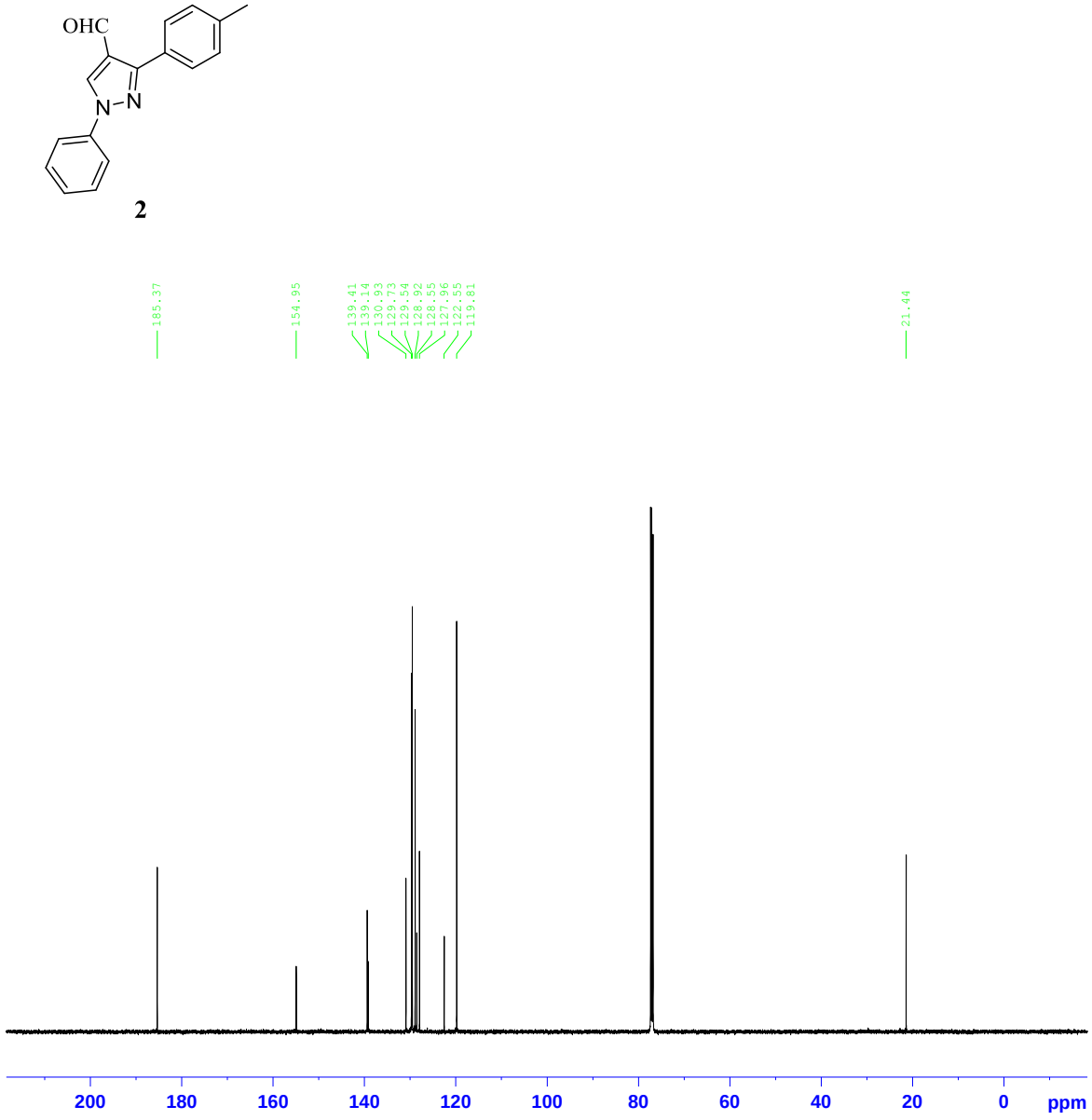

Figure A4. The 125 MHz ^{13}C NMR spectrum of **2** in $CDCl_3$

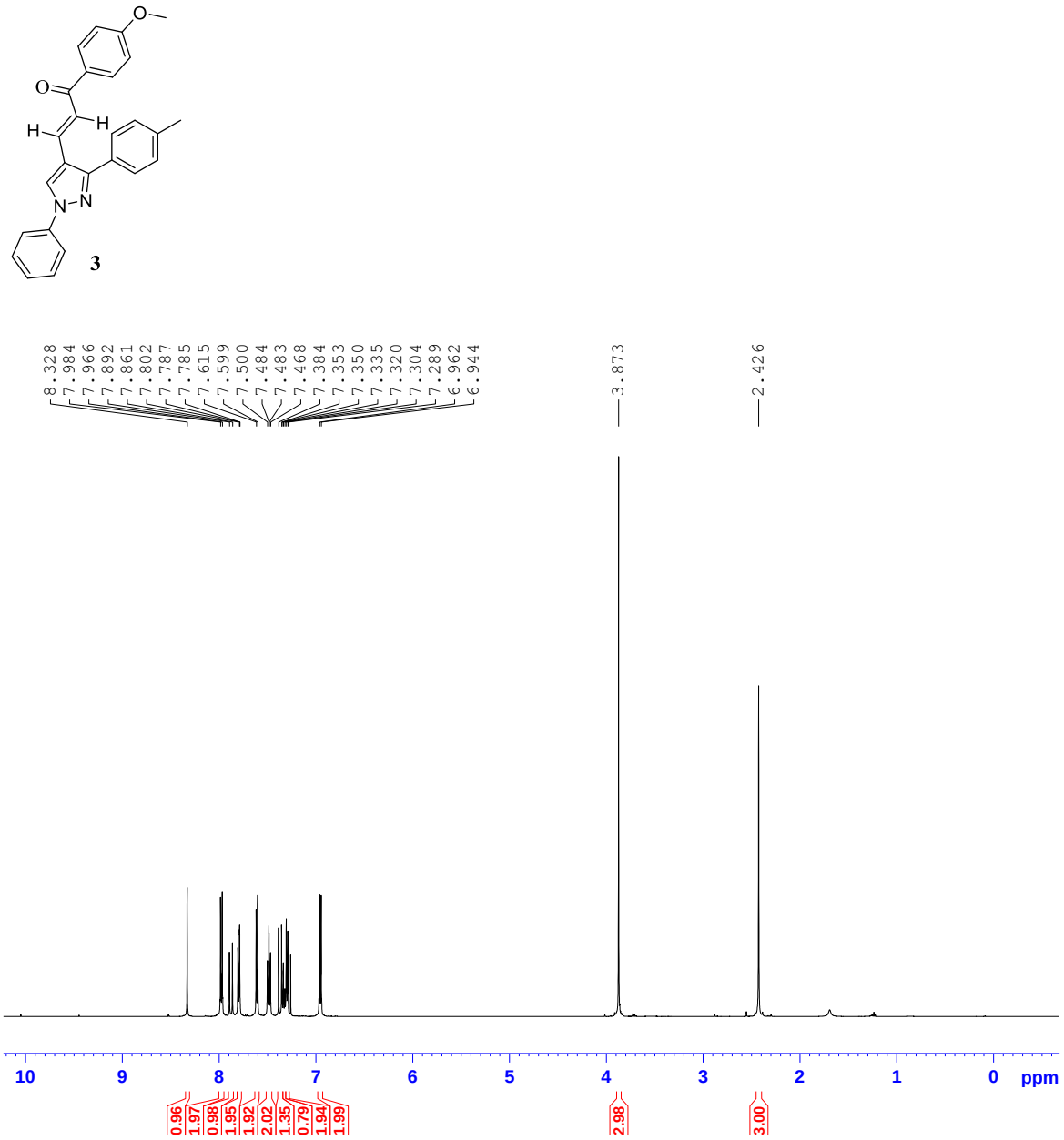

Figure A5. The 500 MHz ^{1}H NMR spectrum of 3 in $CDCl_3$

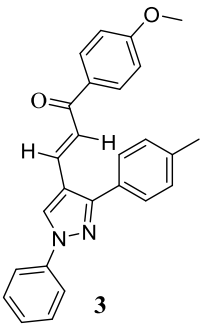

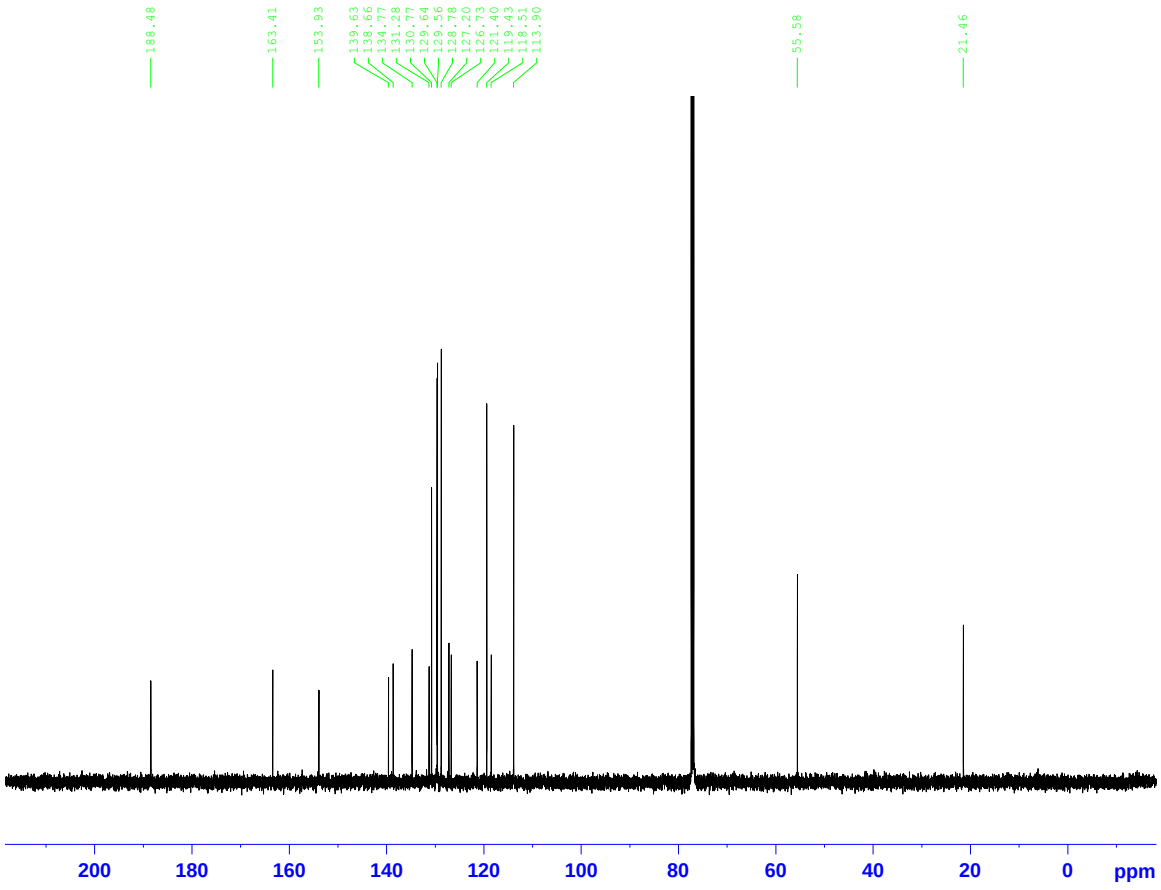

Figure A6. The 125 MHz ^{13}C NMR spectrum of **3** in $CDCl_3$

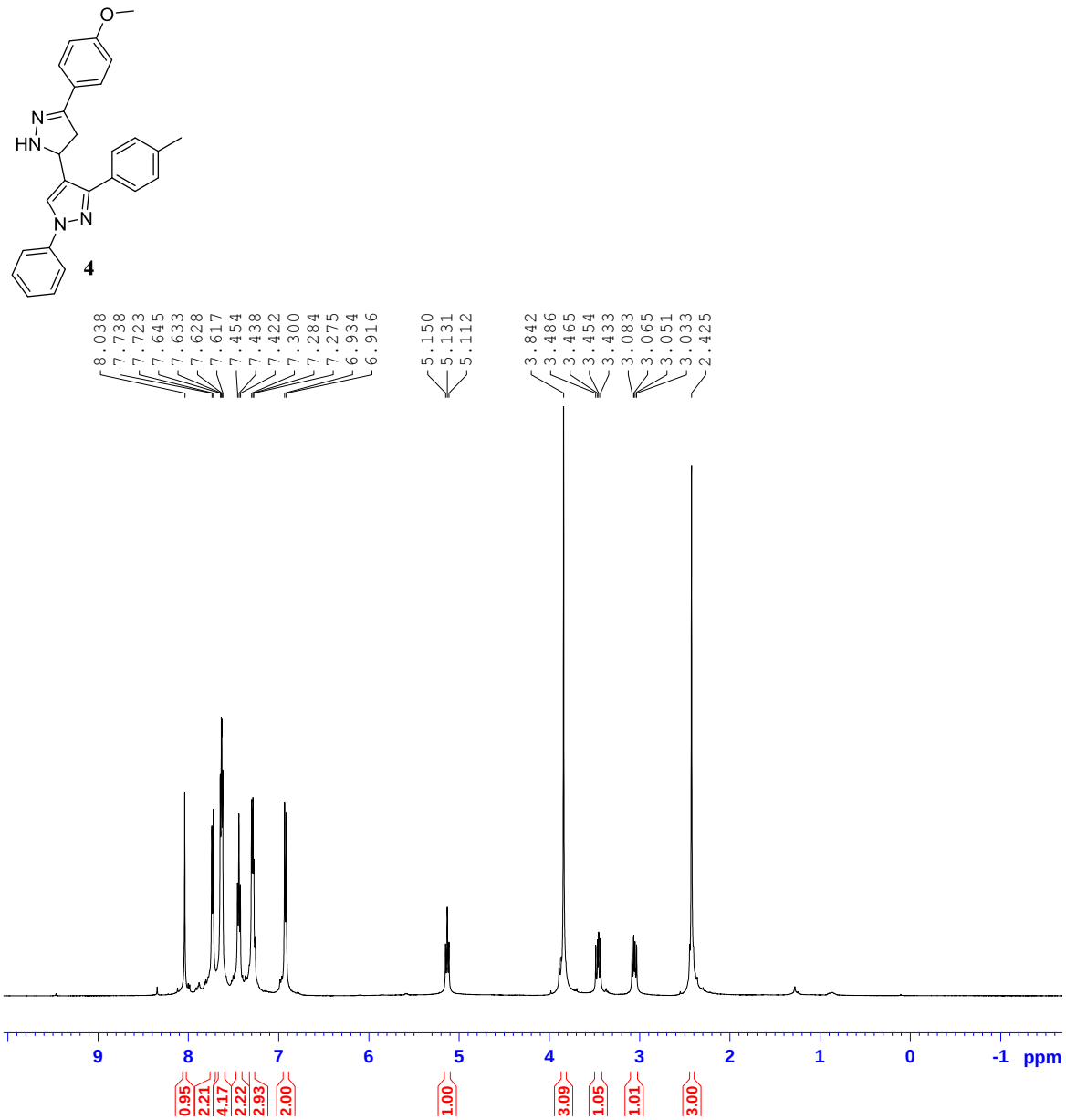

Figure A7. The 500 MHz ^{1}H NMR spectrum of **4** in $CDCl_3$

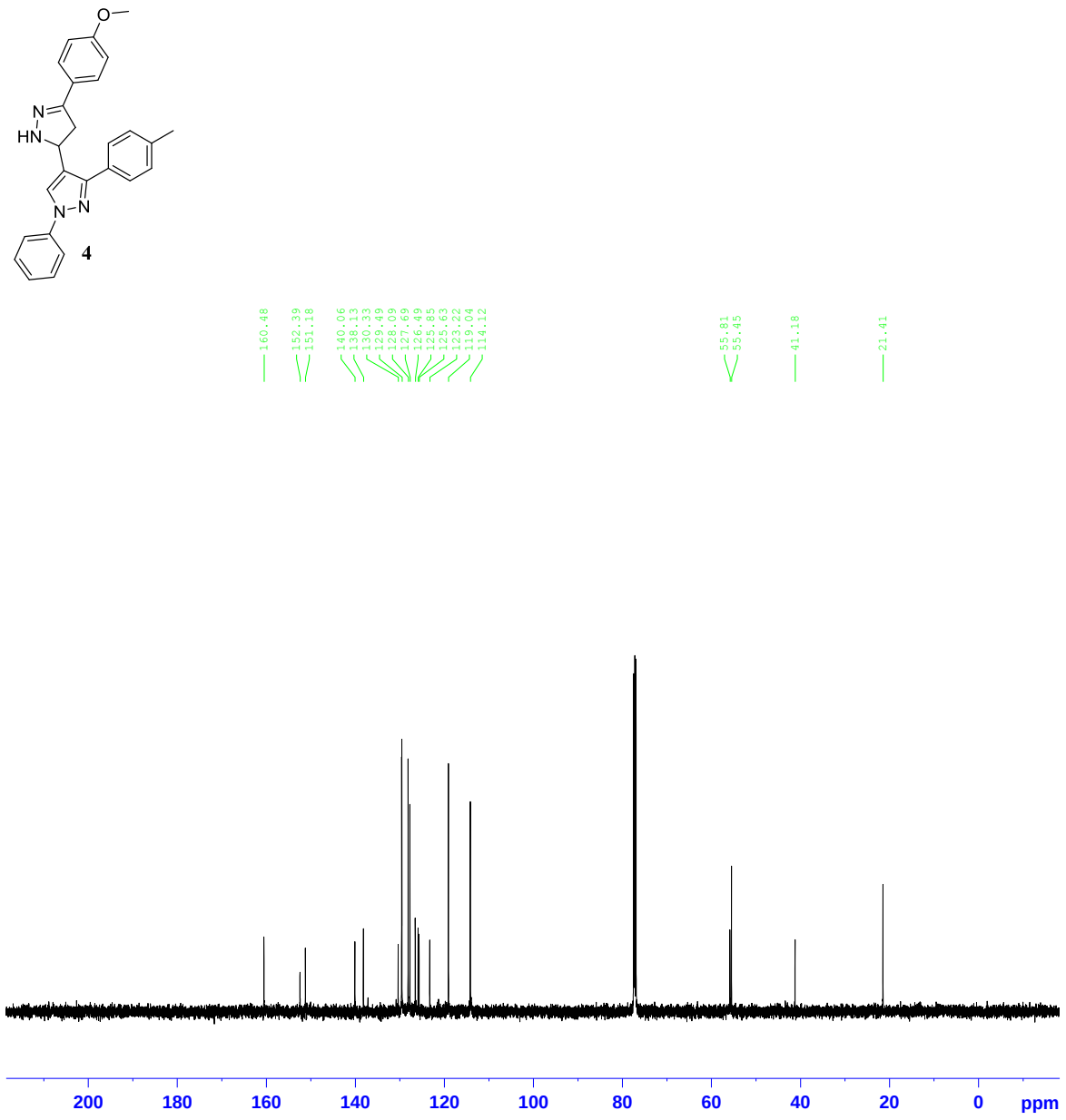

Figure A8. The 125 MHz ^{13}C NMR spectrum of **4** in $CDCl_3$

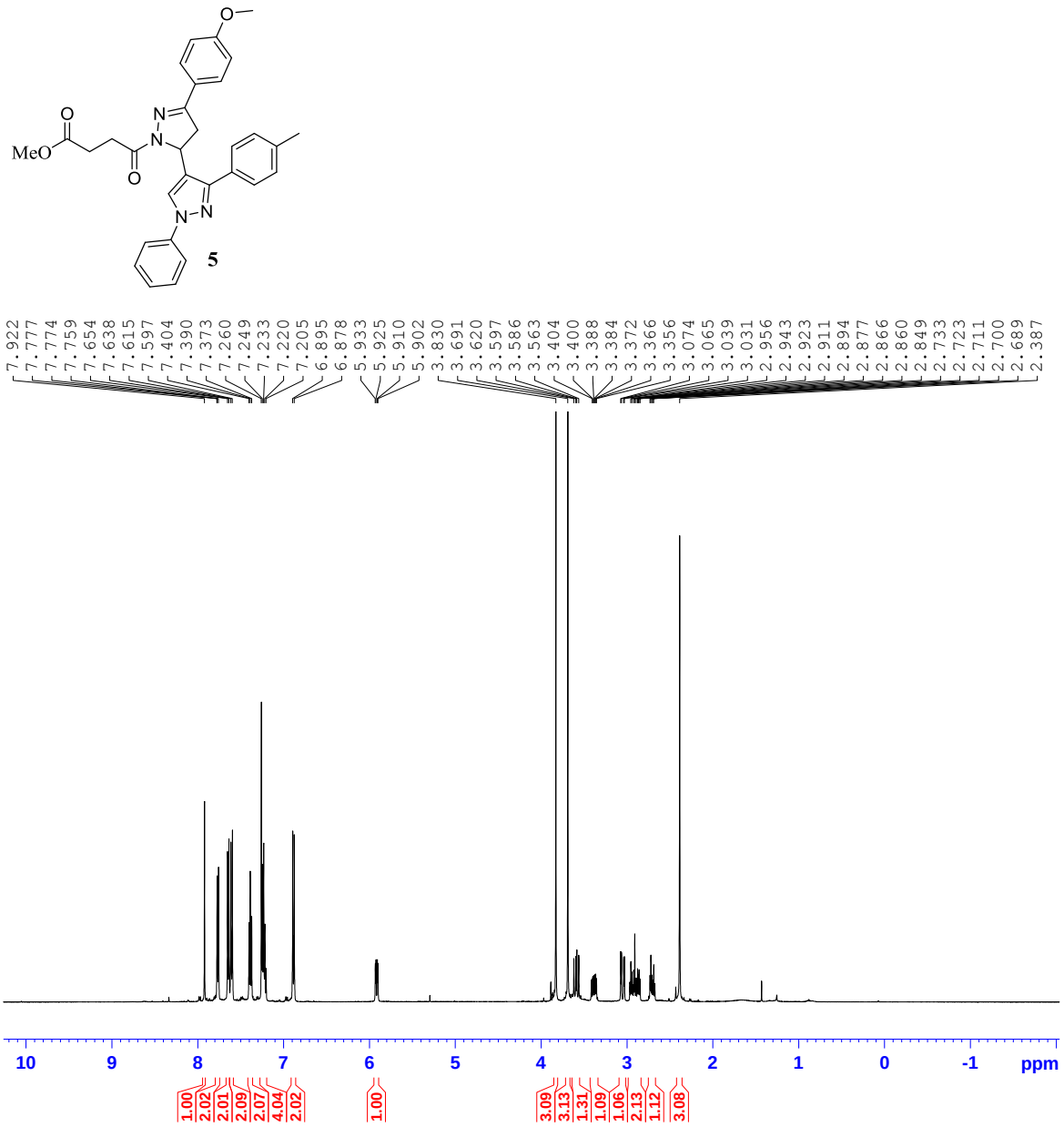

Figure A9. The 500 MHz ^{1}H NMR spectrum of **5** in $CDCl_3$

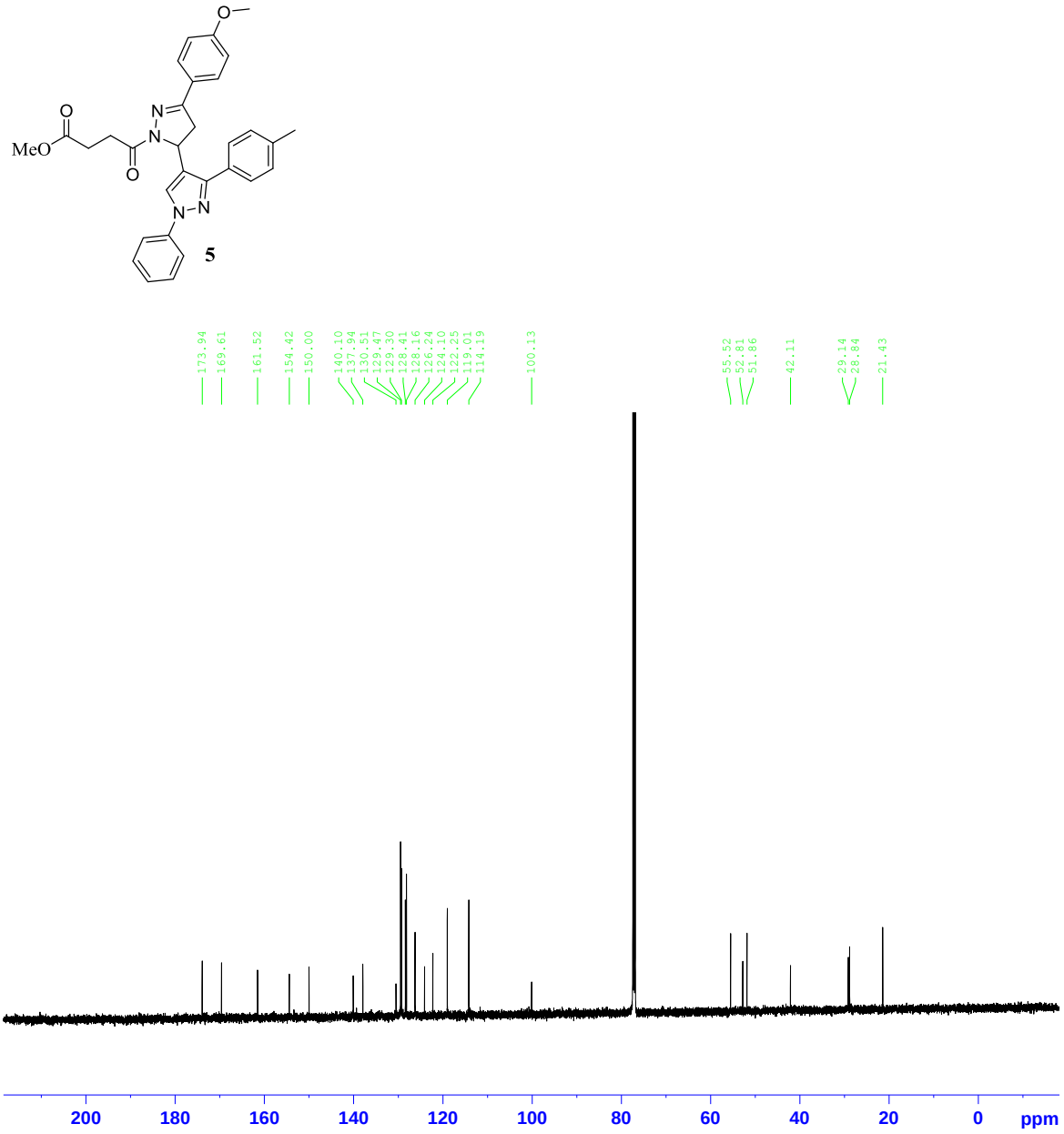

Figure A10. The 125 MHz ^{13}C NMR spectrum of **5** in $CDCl_3$

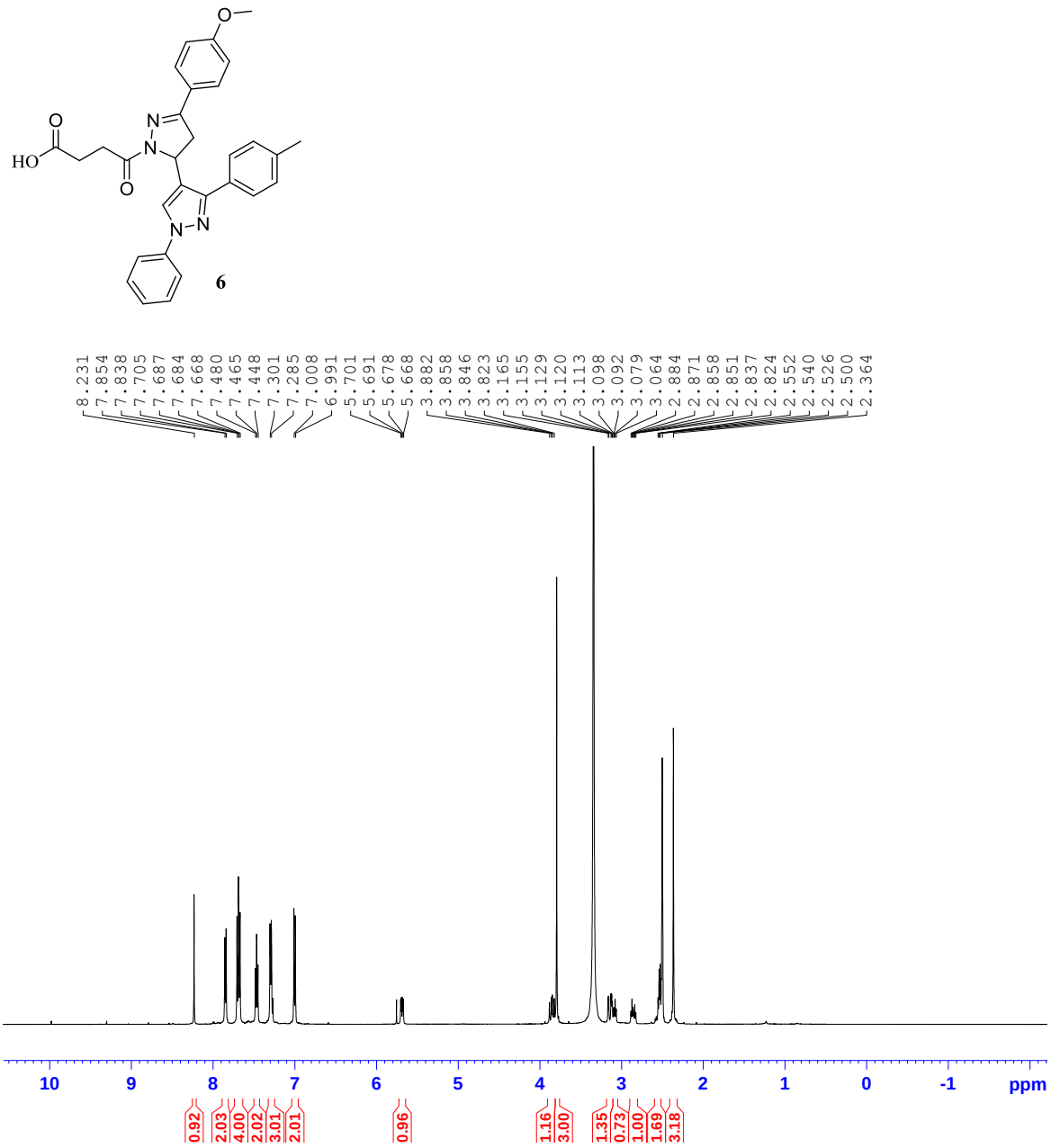

Figure A11. The 500 MHz ^{1}H NMR spectrum of **6** in DMSO-d_6

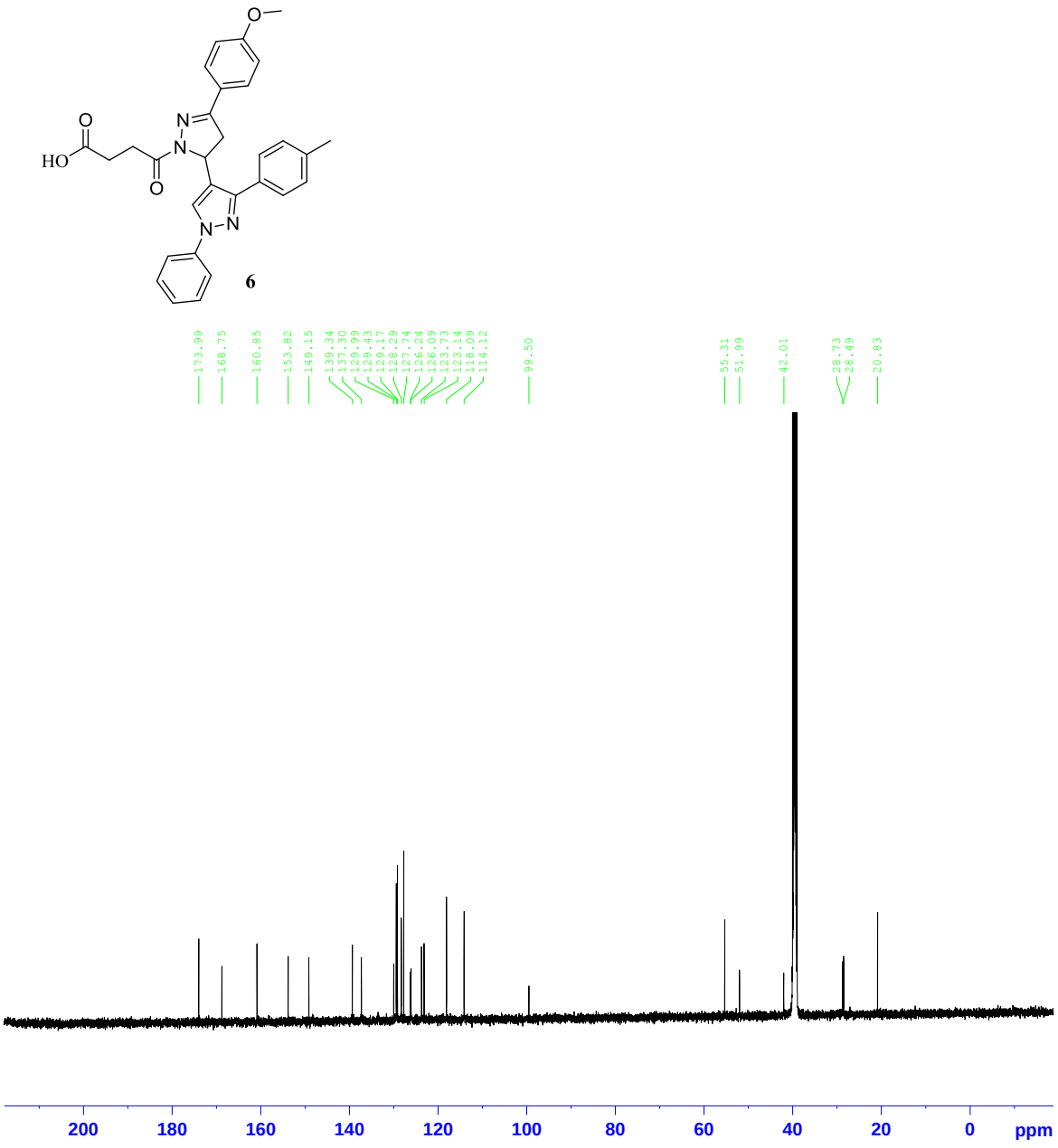

Figure A12. The 125 MHz ^{13}C NMR spectrum of **6** in DMSO-d_6

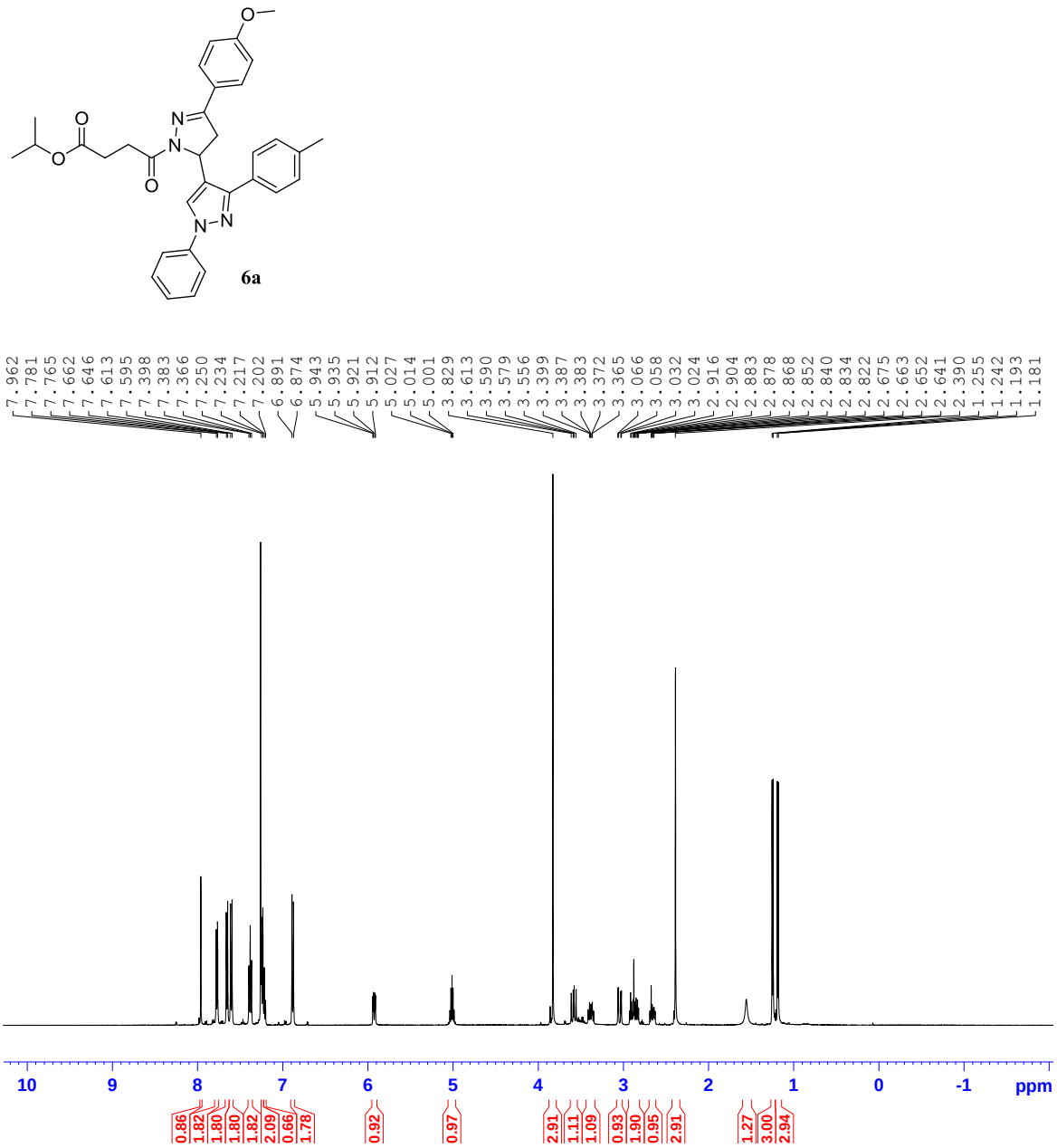

Figure A13. The 500 MHz ^{1}H NMR spectrum of **6a** in $CDCl_3$

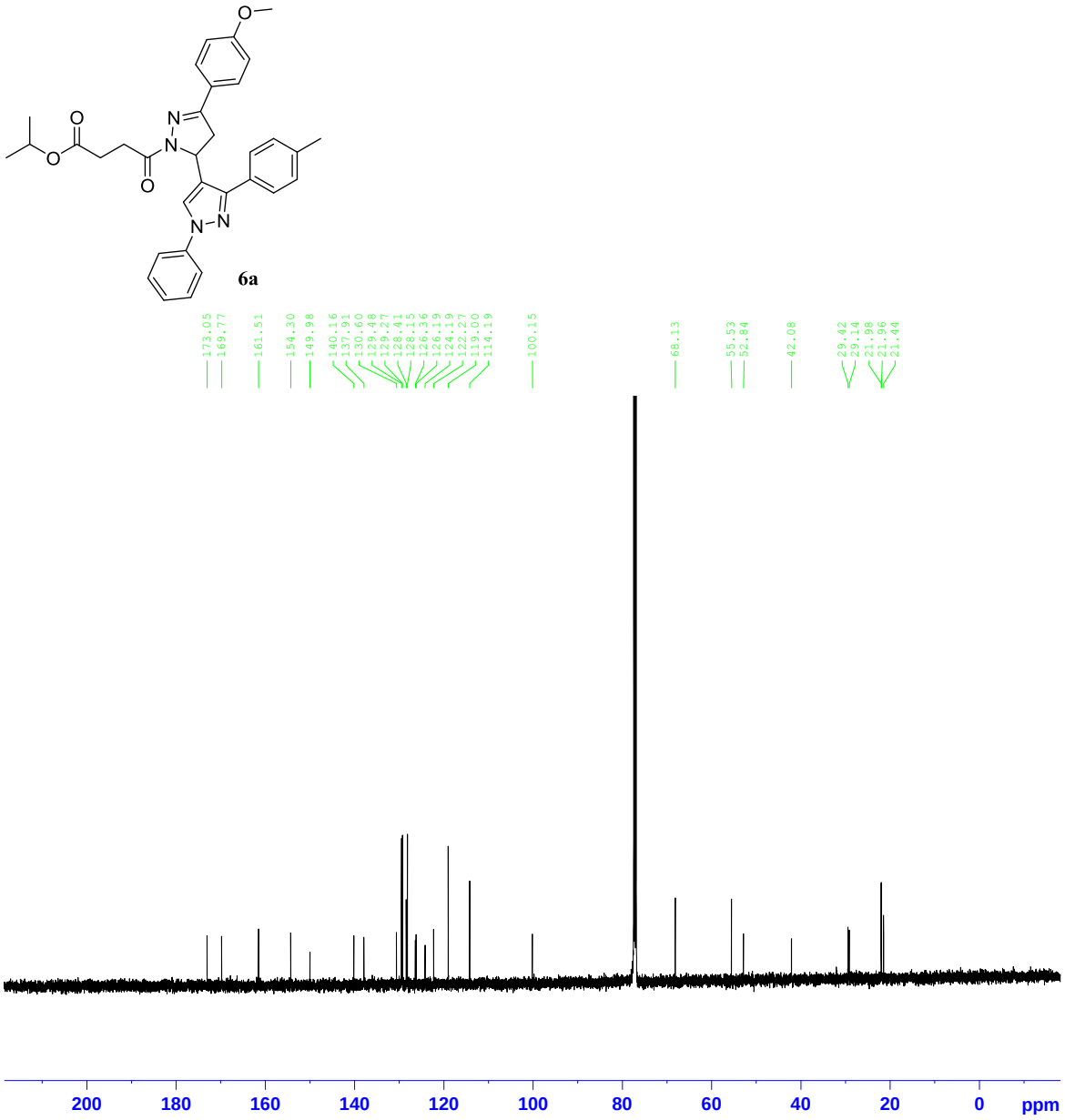

Figure A14. The 125 MHz ^{13}C NMR spectrum of **6a** in CDCl3

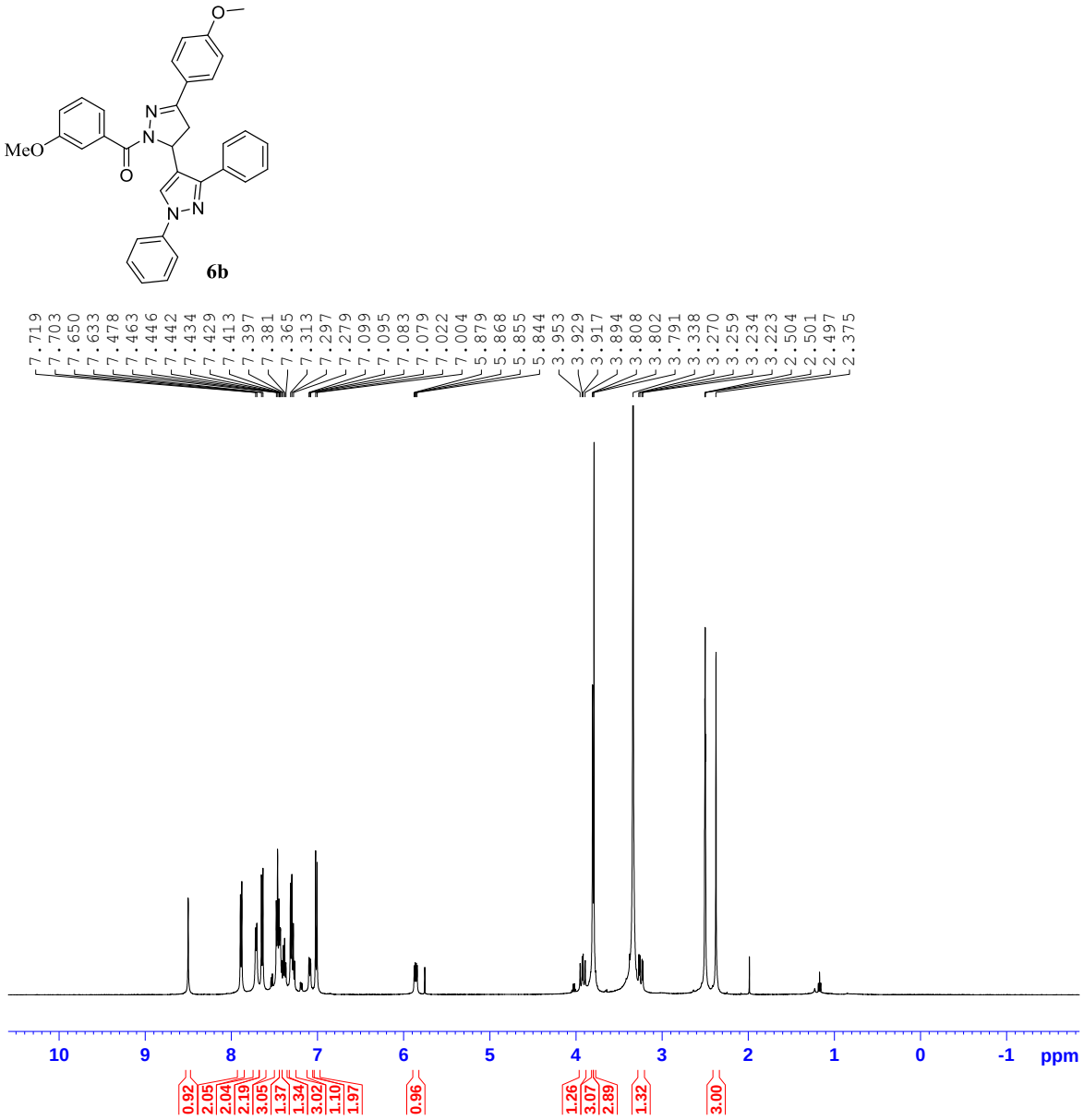

Figure A15. The 500 MHz ^{1}H NMR spectrum of **6c** in DMSO-d_6

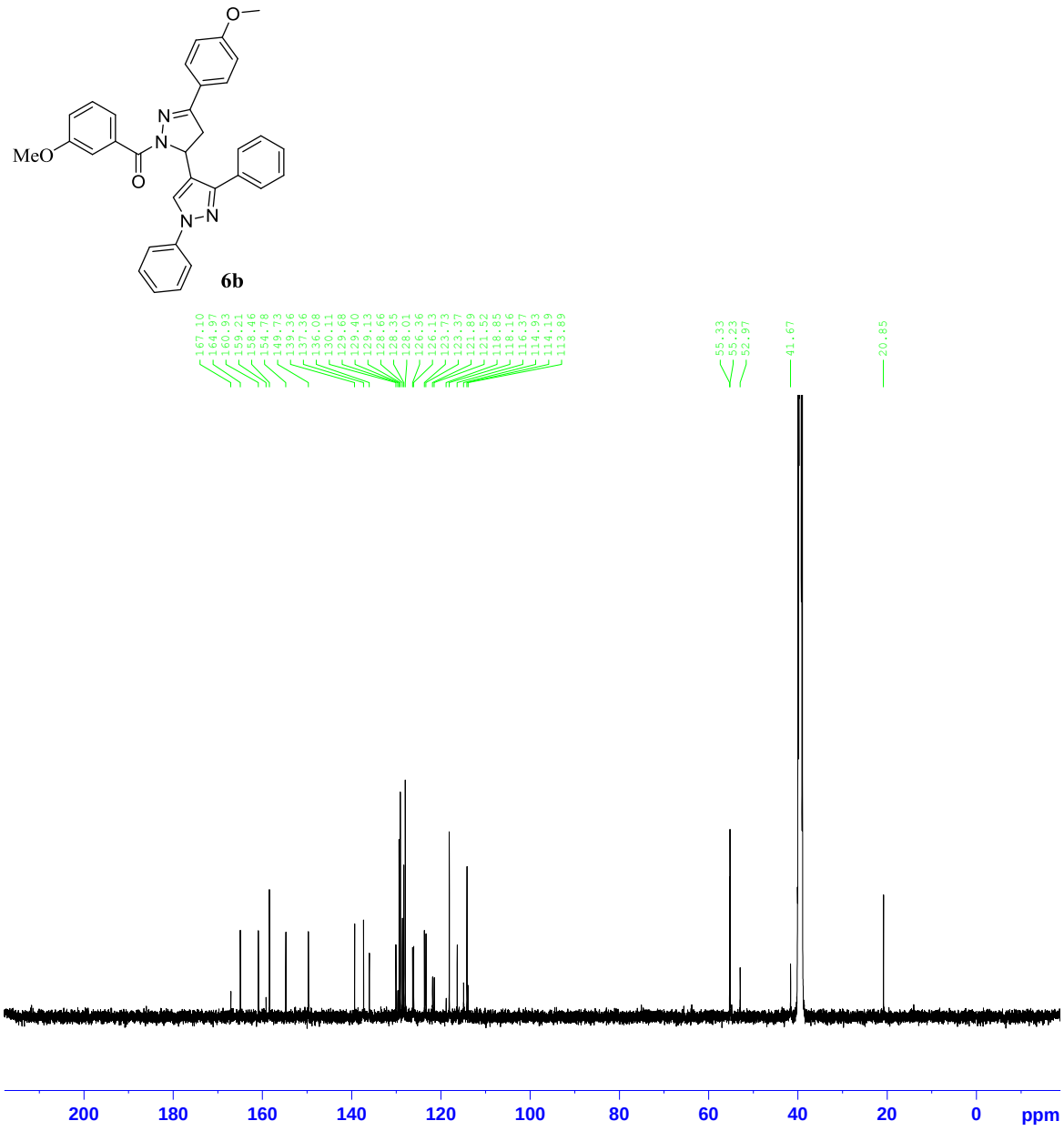

Figure A16. The 125 MHz ^{13}C NMR spectrum of **6b** in DMSO-d_6

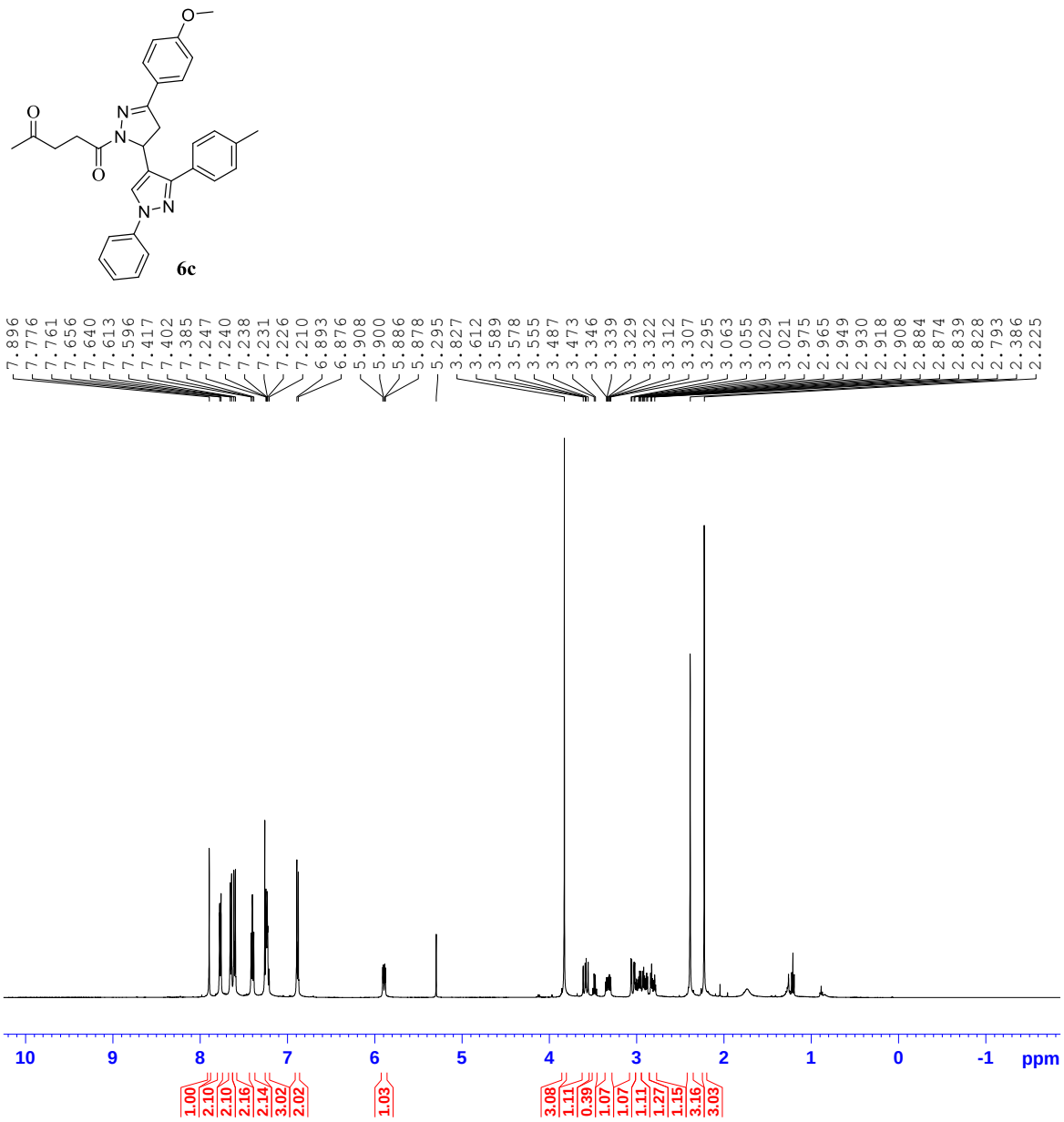

Figure A17. The 500 MHz ^{1}H NMR spectrum of **6c in** $CDCl_3$

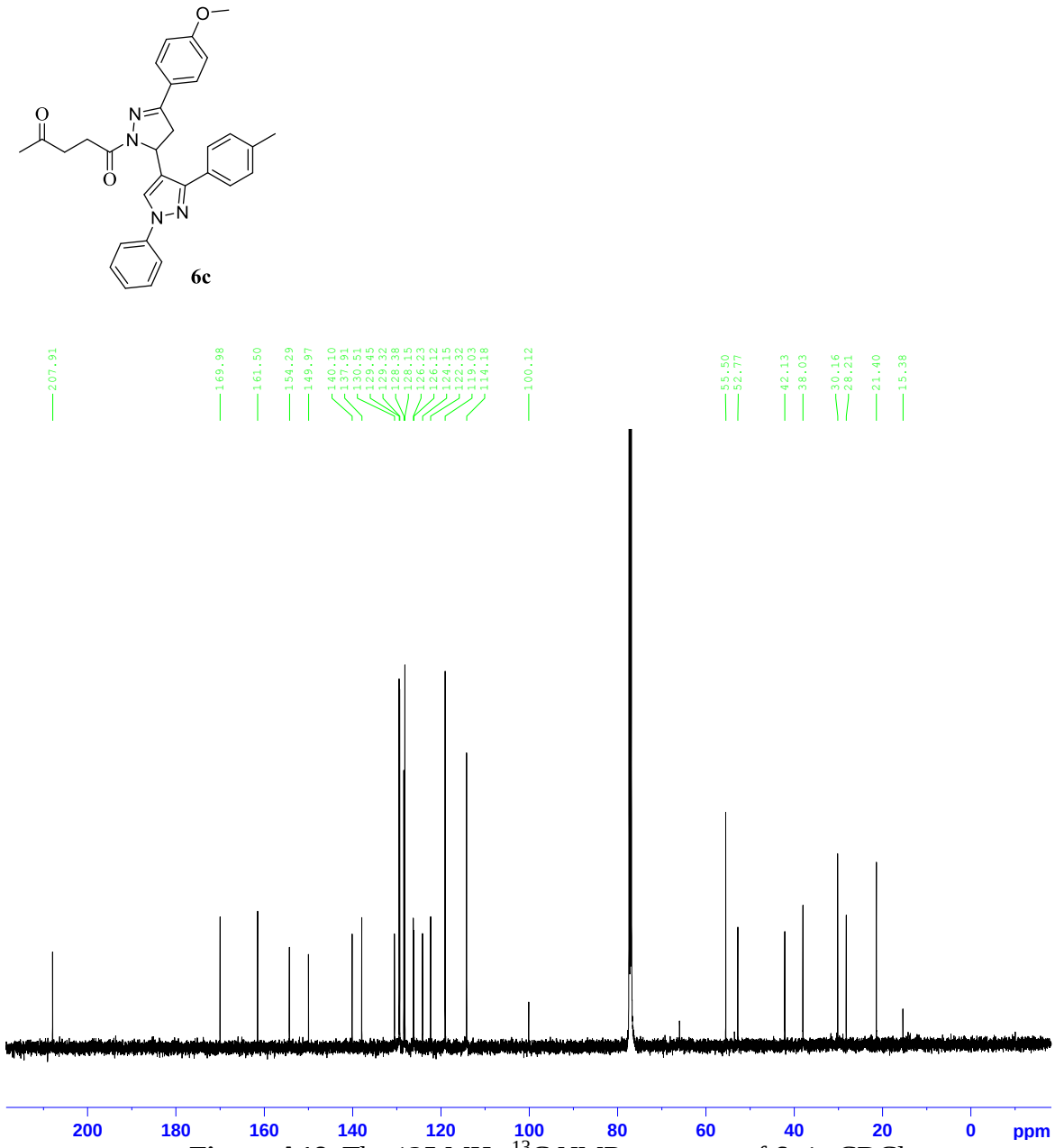

Figure A18. The 125 MHz ^{13}C NMR spectrum of **6c** in $CDCl_3$

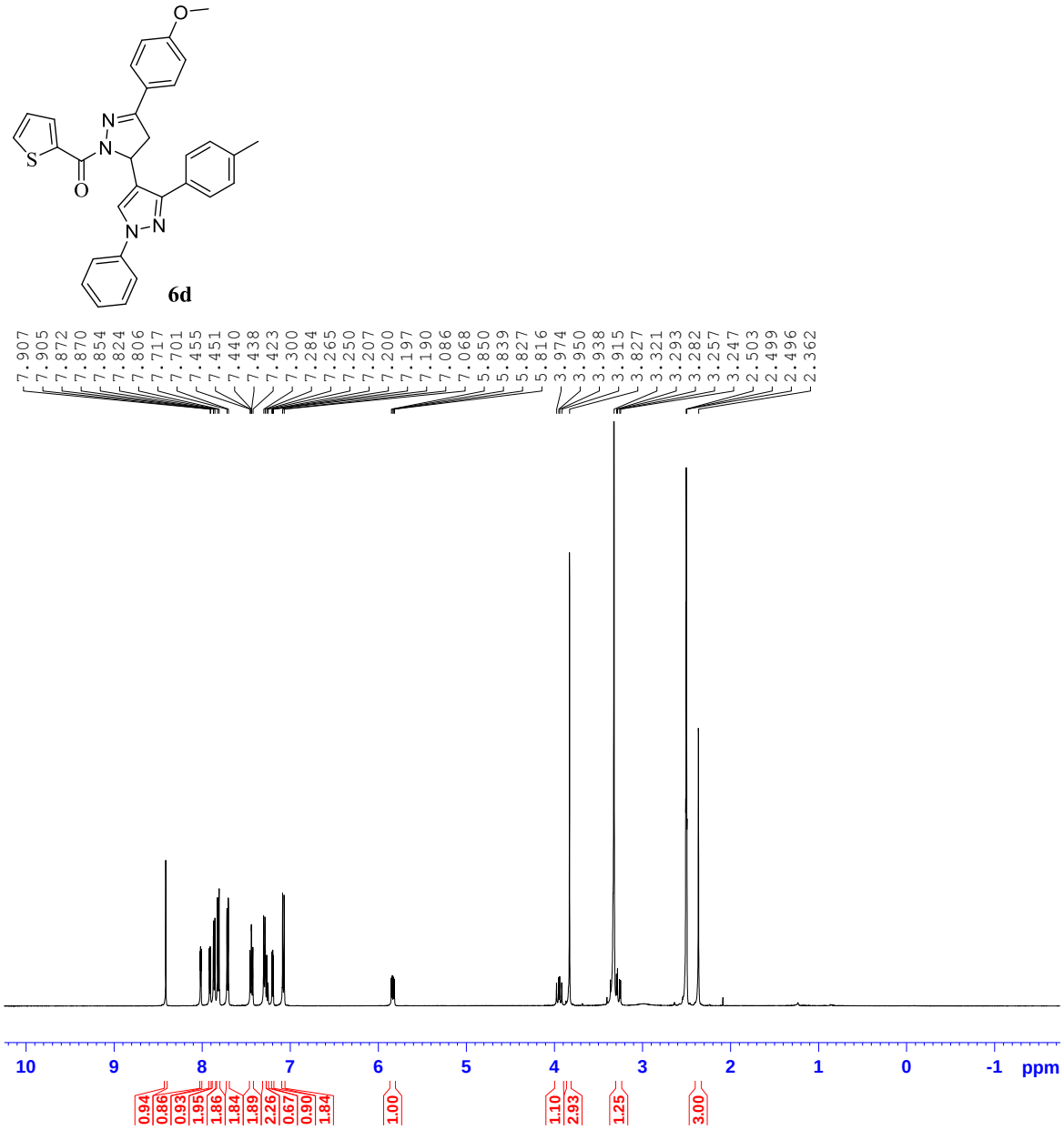

Figure A19. The 500 MHz ^{1}H NMR spectrum of **6d** in DMSO-d_6

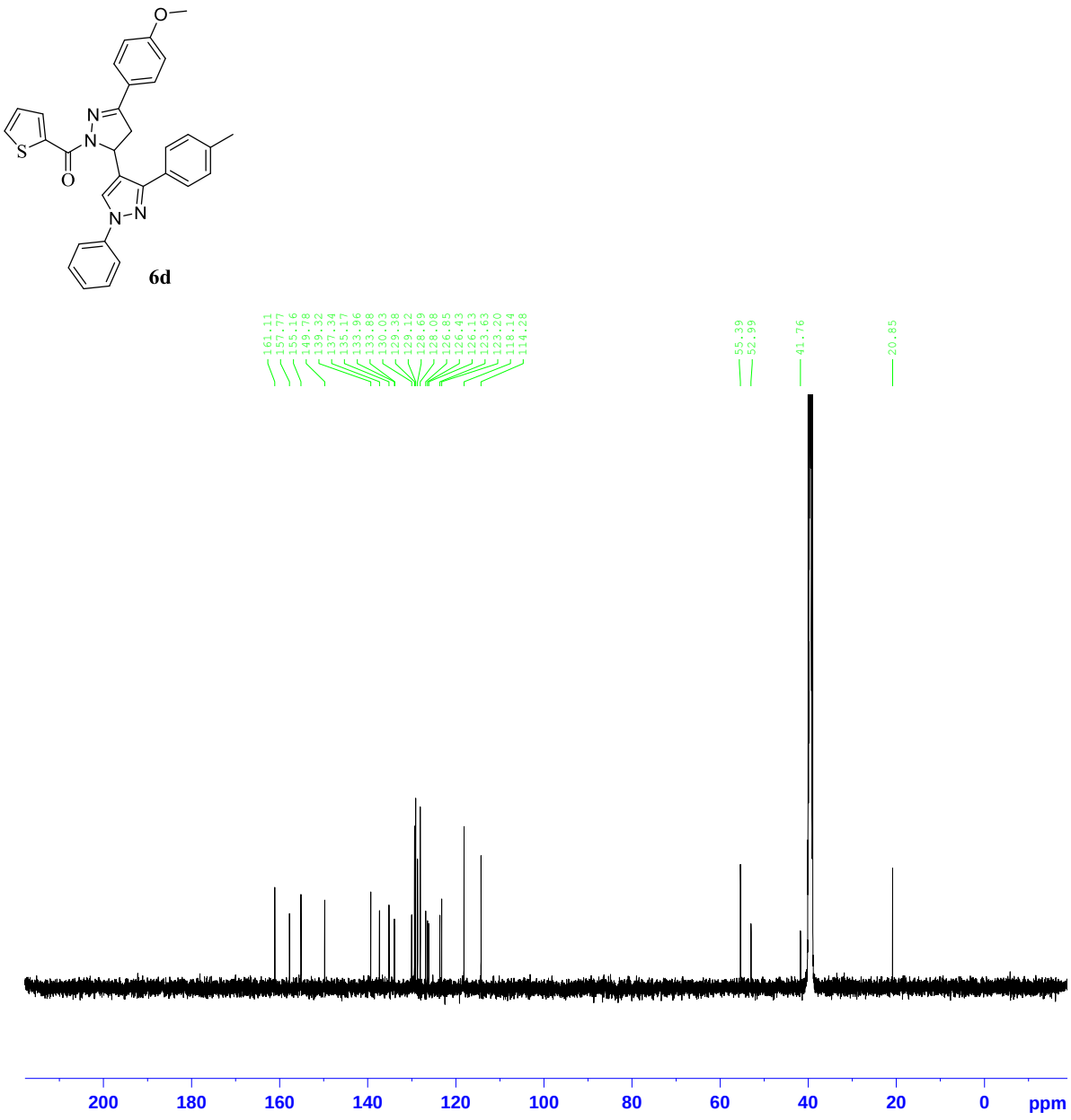

Figure A20. The 125 MHz ^{13}C NMR spectrum of **6d** in DMSO-d_6

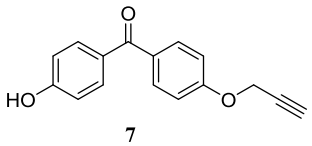

7

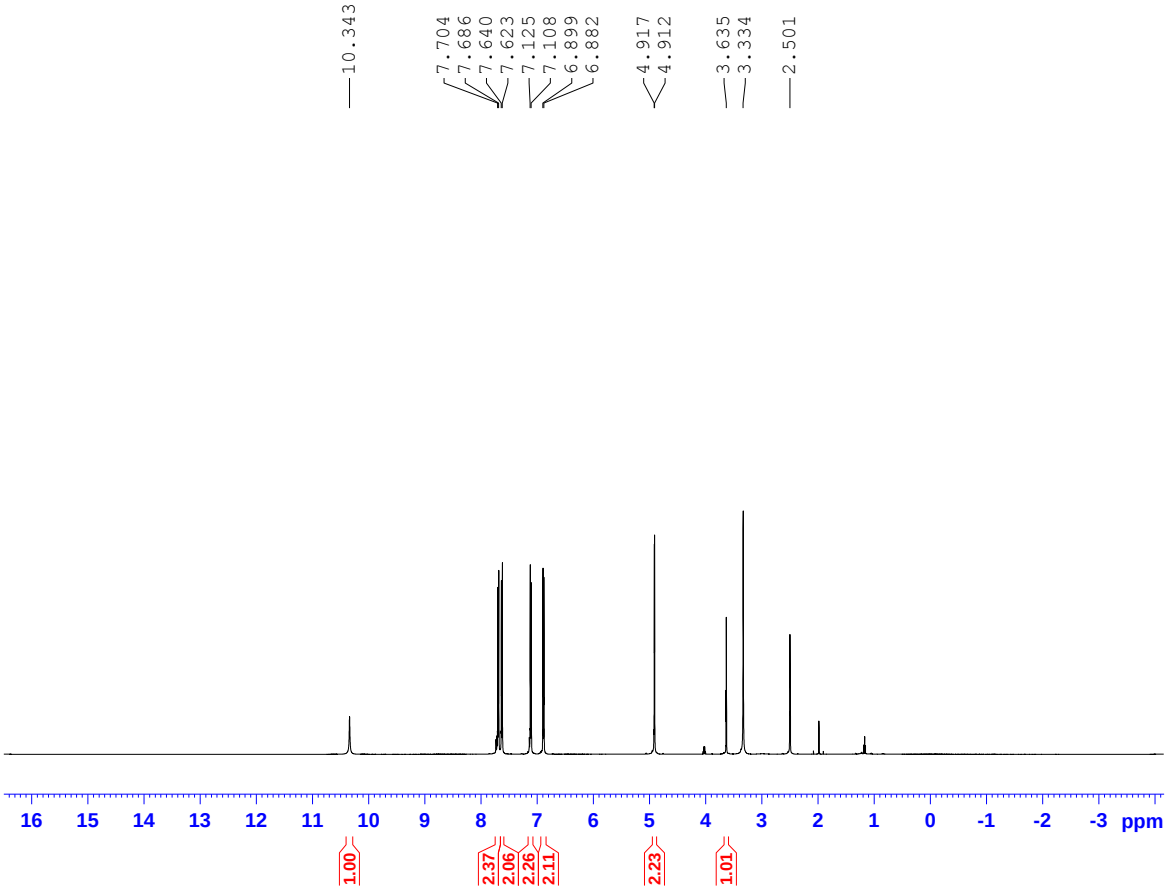

Figure A21. The 500 MHz ^{1}H NMR spectrum of **7** in DMSO-d_6

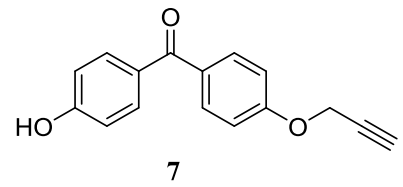

7

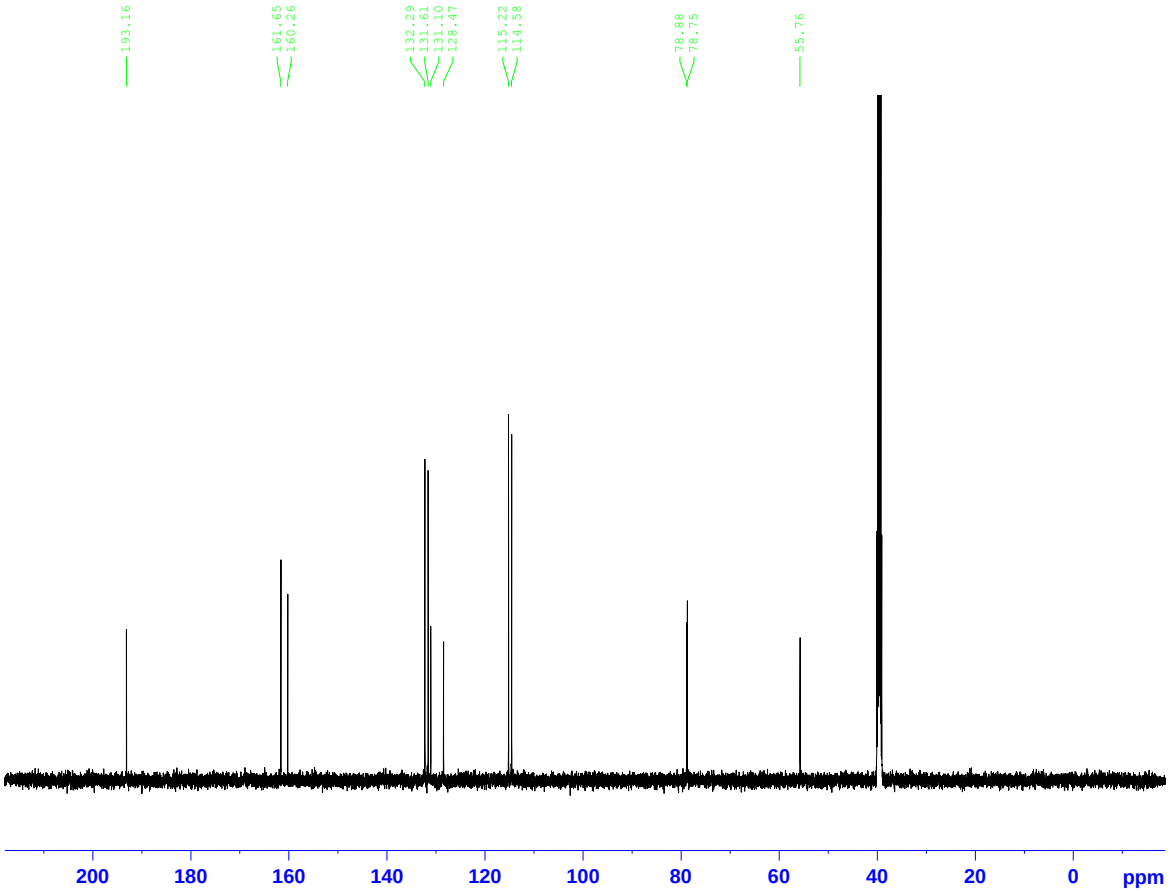

Figure A22. The 125 MHz ^{13}C NMR spectrum of **7** in DMSO-d_6

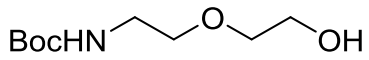

8

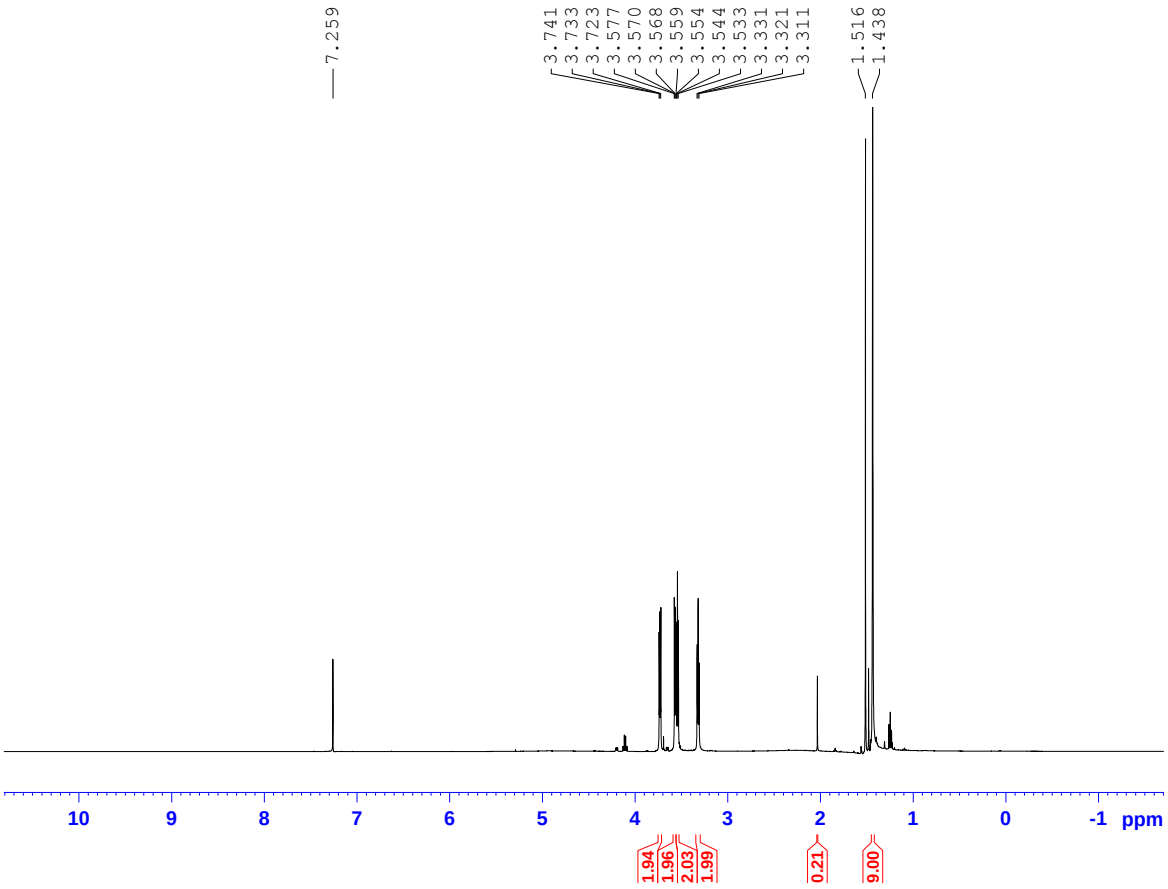

Figure A23. The 500 MHz ^{1}H NMR spectrum of **8** in $CDCl_3$

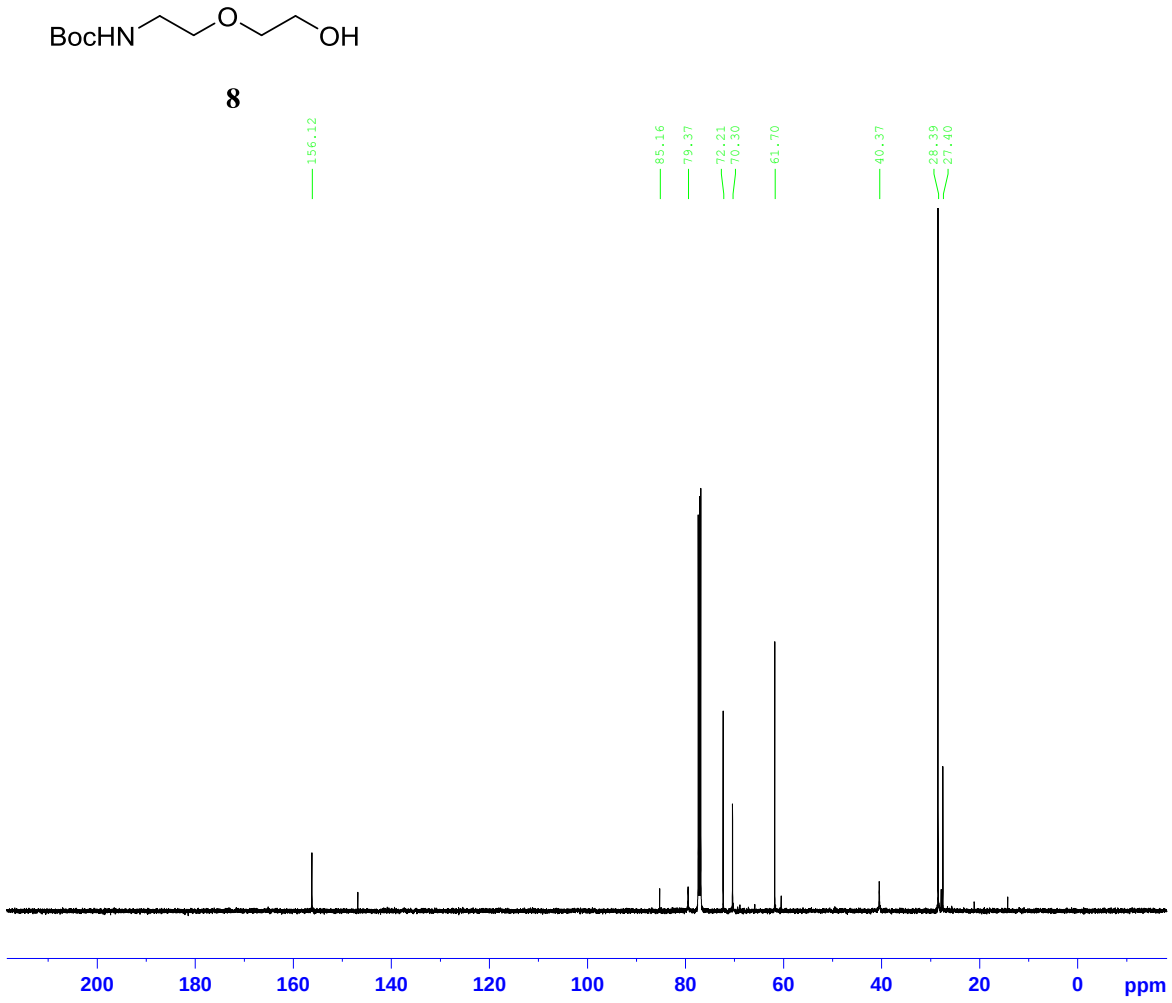

Figure A24. The 125 MHz ^{13}C NMR spectrum of **8** in $CDCl_3$

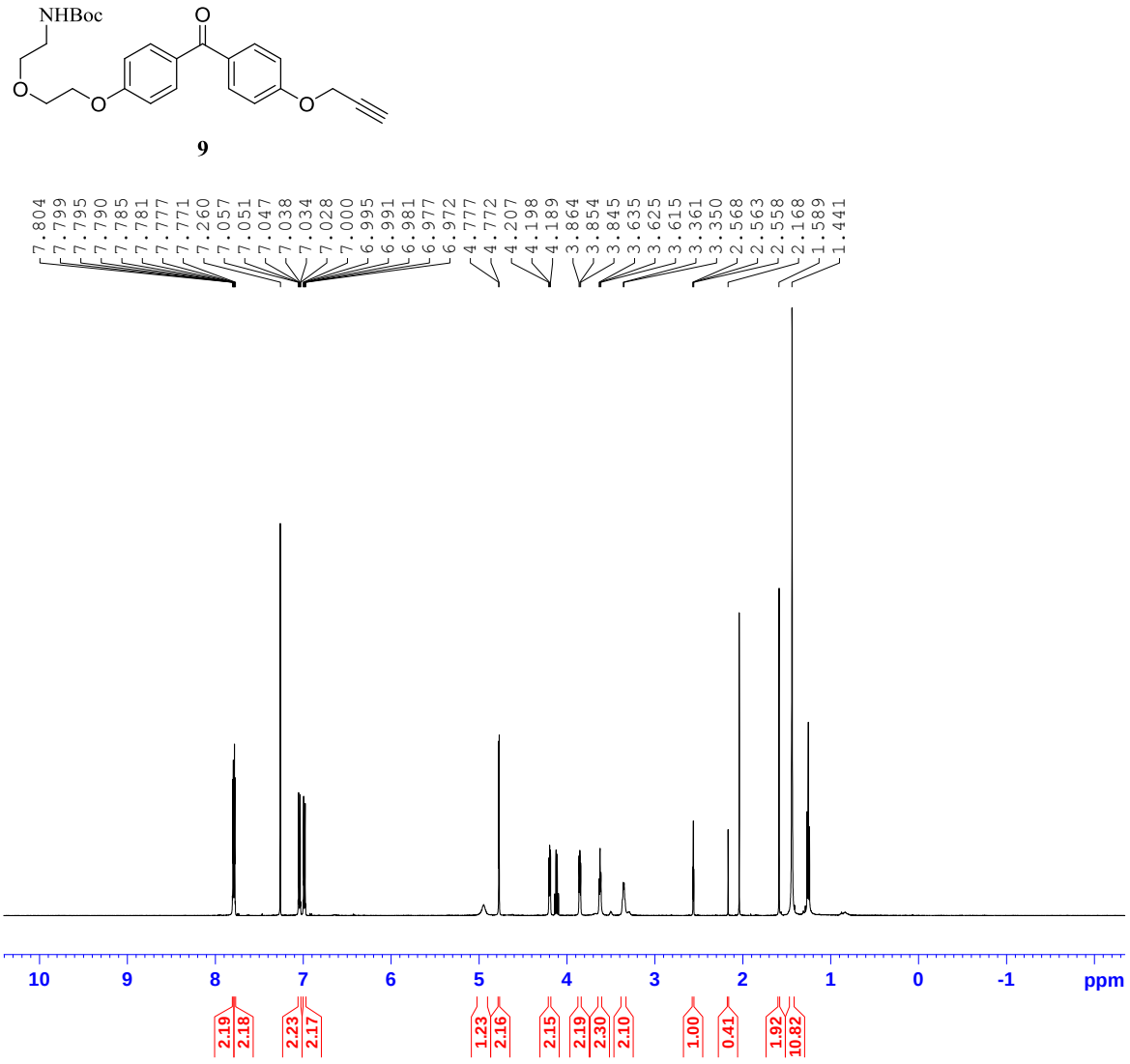

Figure A25. The 500 MHz ^{1}H NMR spectrum of **9** in $CDCl_3$

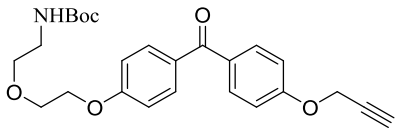

9

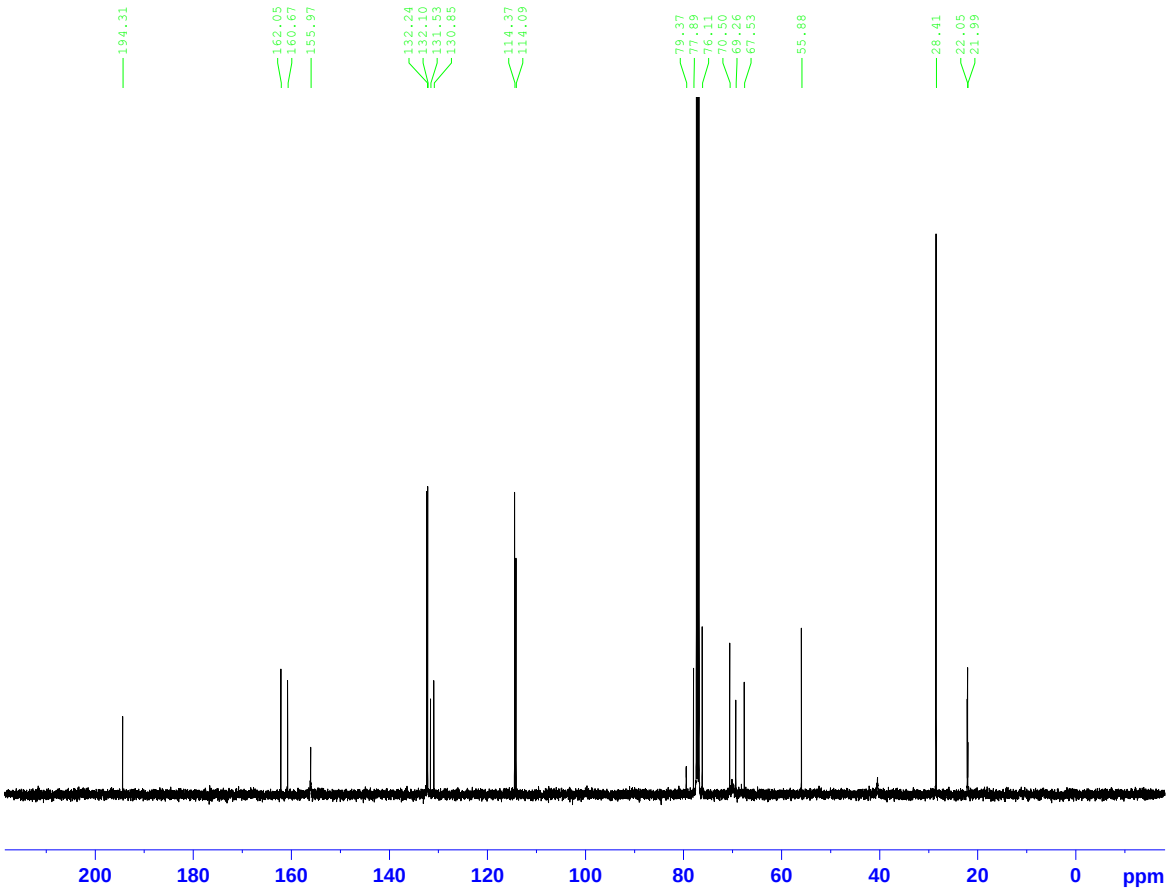

Figure A26. The 125 MHz ^{13}C NMR spectrum of **9** in $CDCl_3$

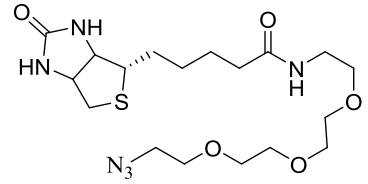

10

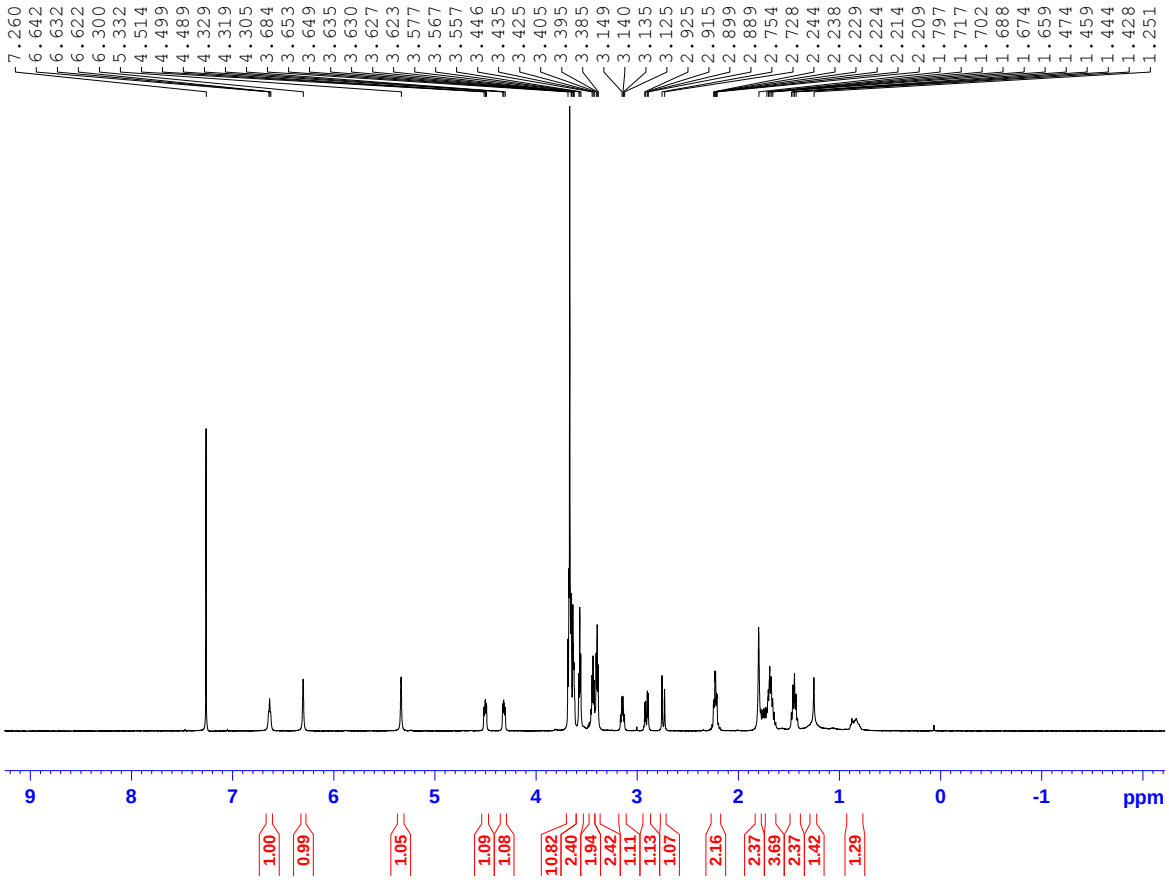

Figure A27. The 500 MHz ^{1}H NMR spectrum of **10** in $CDCl_3$

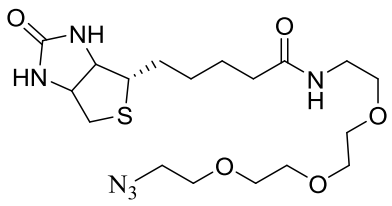

10

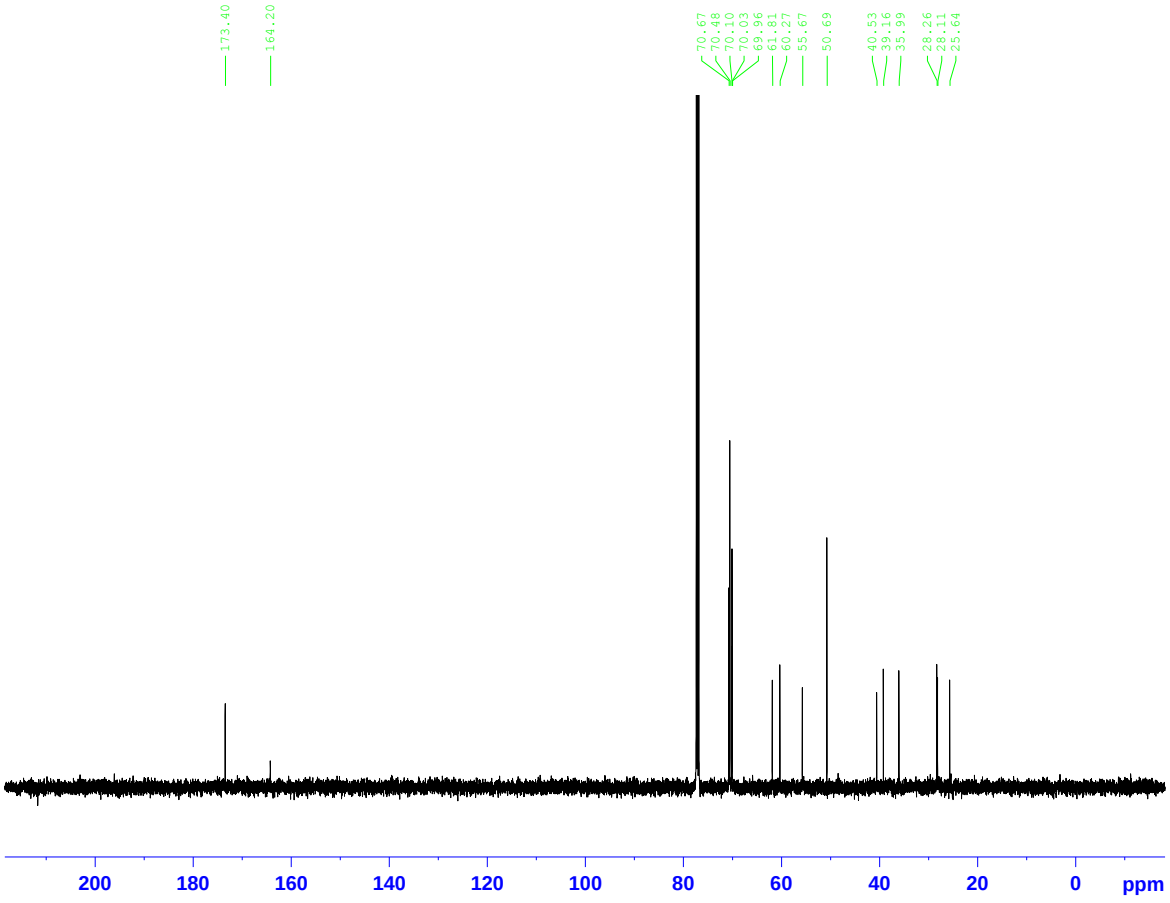

Figure A28. The 125 MHz ^{13}C NMR spectrum of **10** in $CDCl_3$

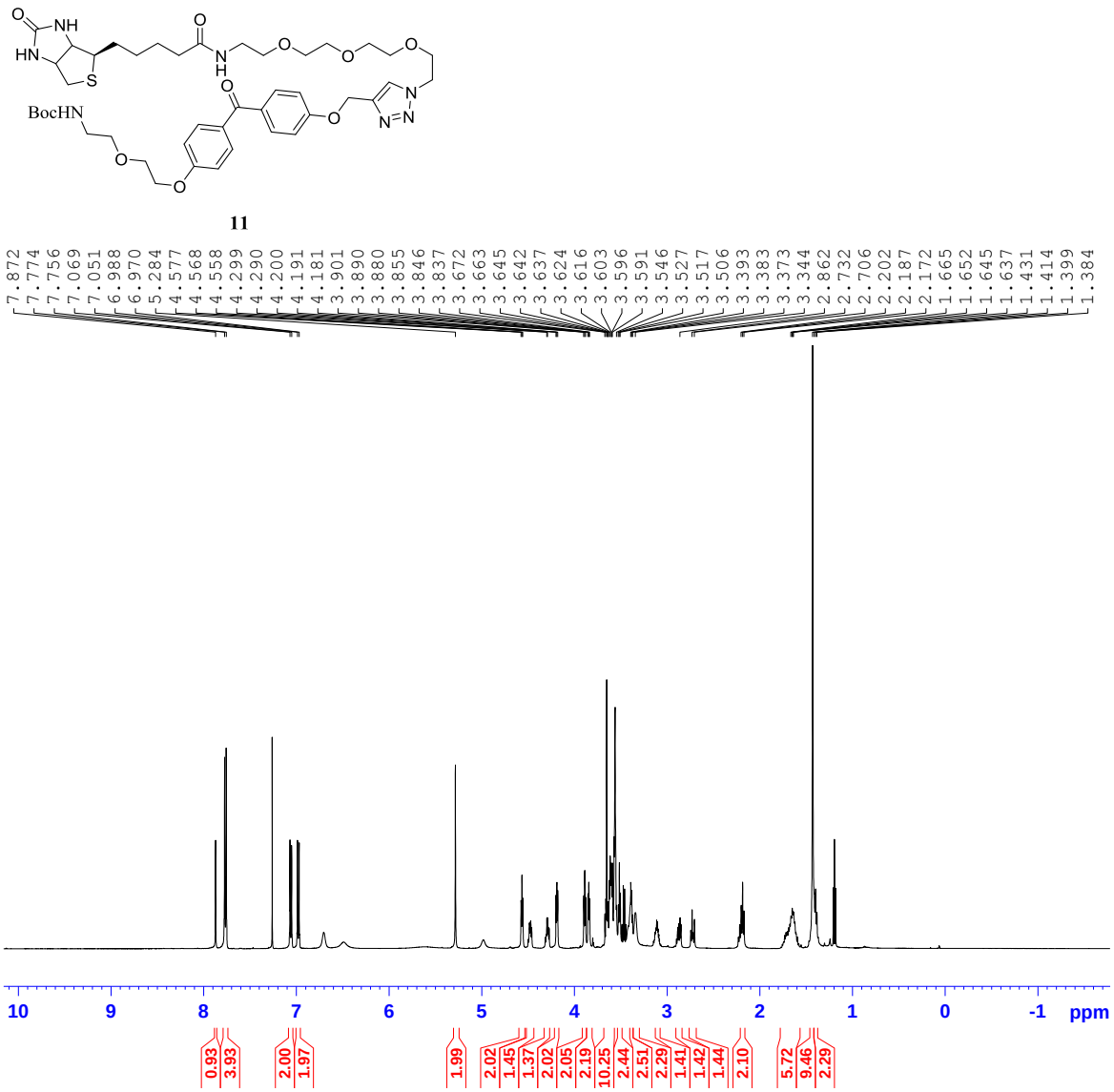

Figure A29. The 500 MHz ^{1}H NMR spectrum of **11** in $CDCl_3$

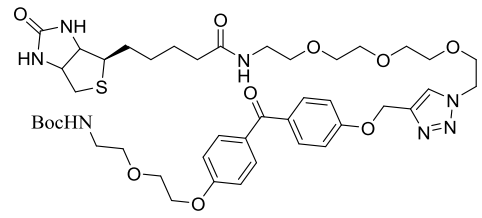

11

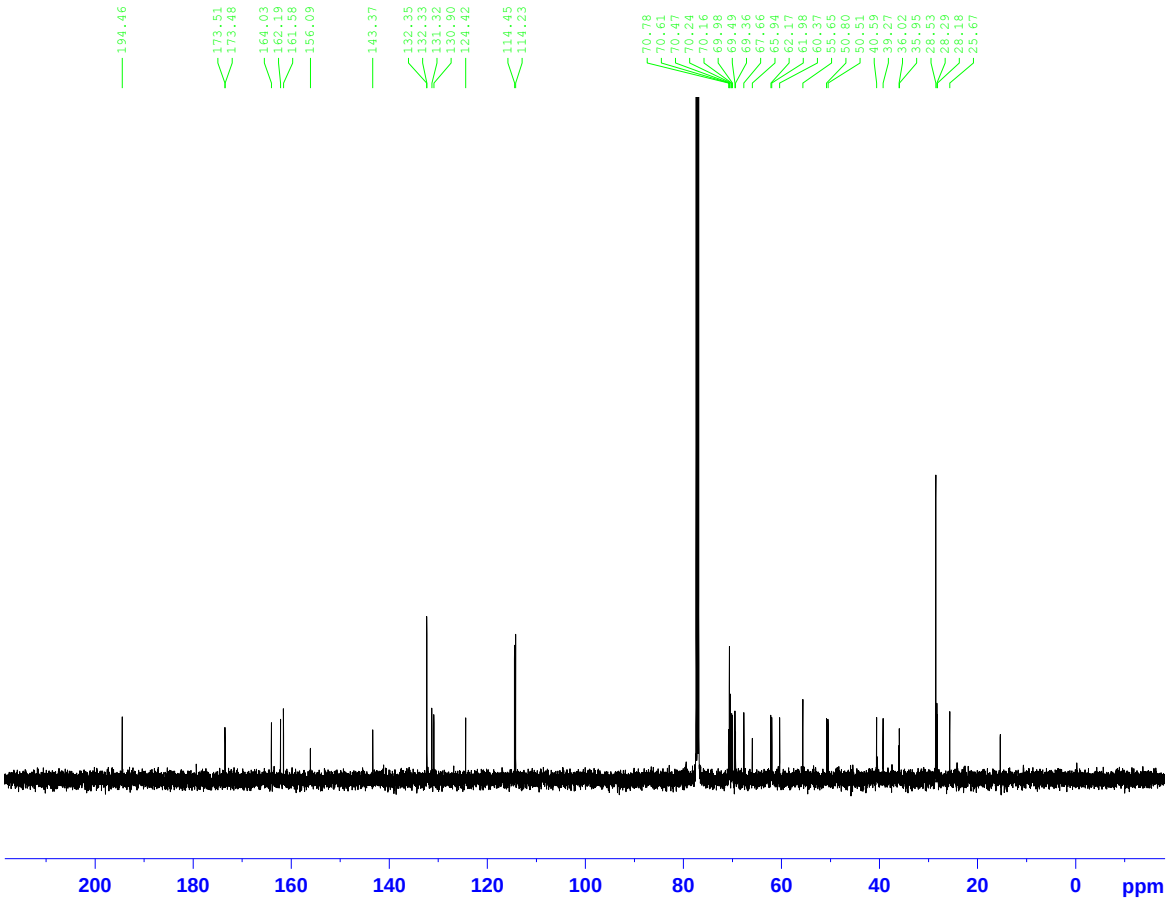

Figure A30. The 125 MHz ^{13}C NMR spectrum of **11** in $CDCl_3$

Appendix-B. ^{1}H NMR and ^{13}C NMR of Compounds in Chapter **2**

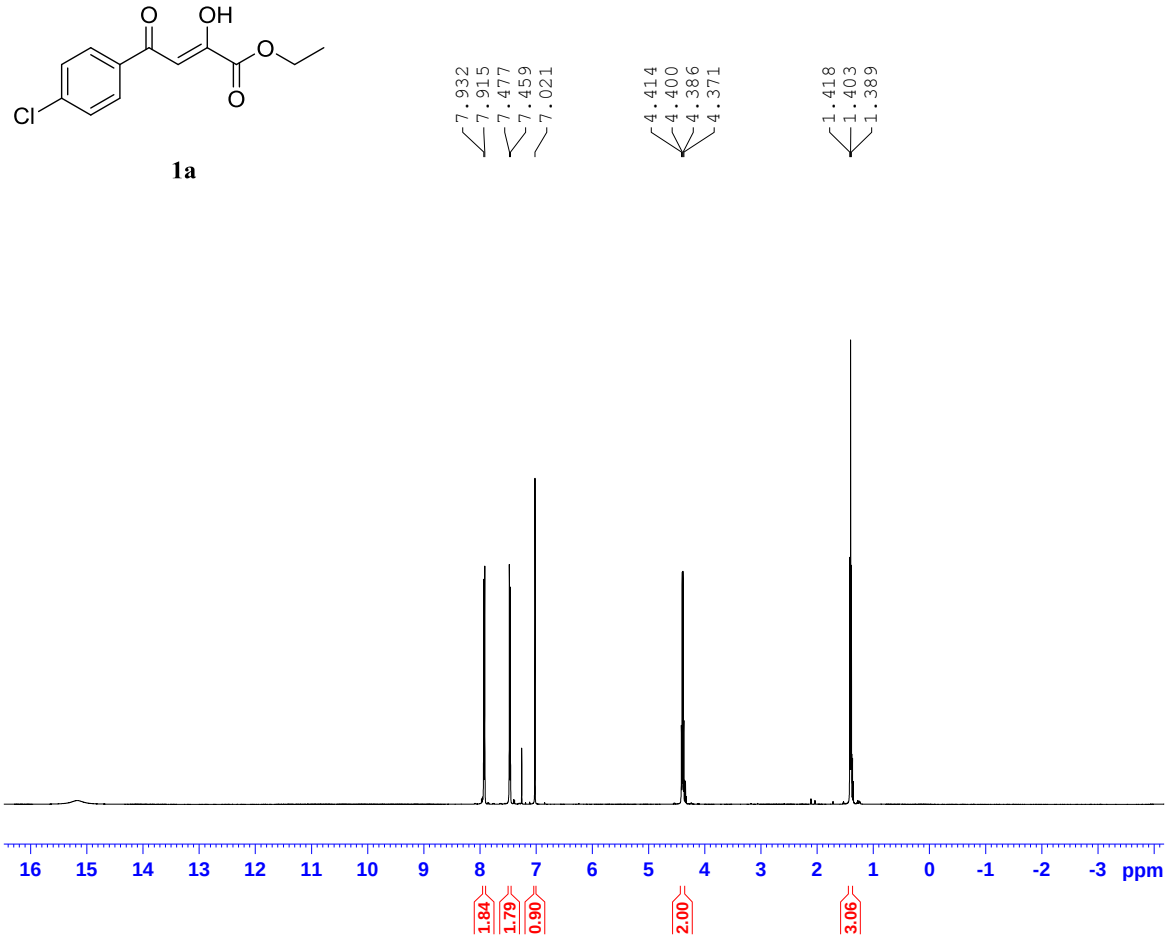

Figure B1. The 500 MHz ^{1}H NMR spectrum of **1a** in $CDCl_3$

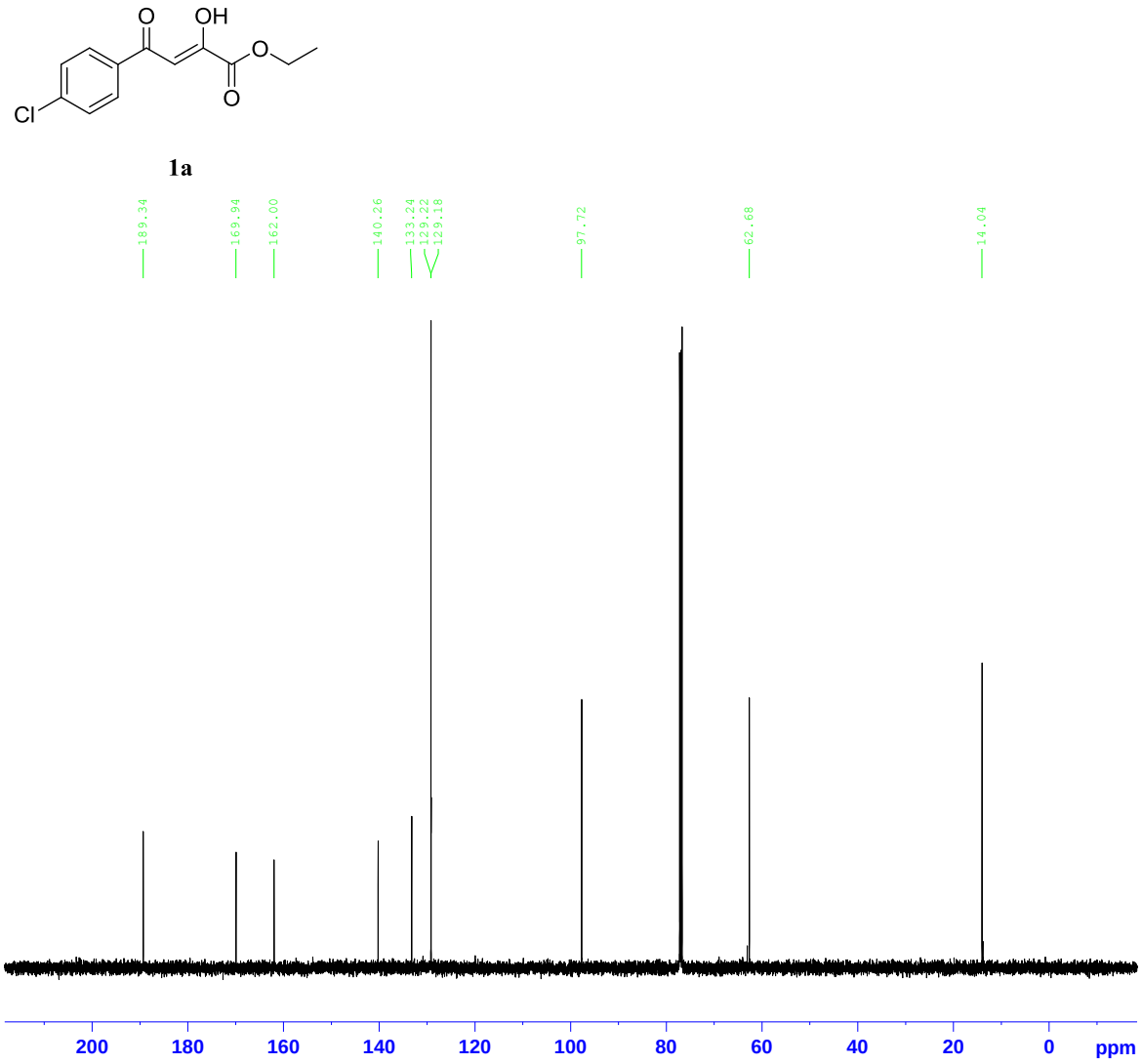

Figure B2. The 125 MHz ^{13}C NMR spectrum of **1a** in $CDCl_3$

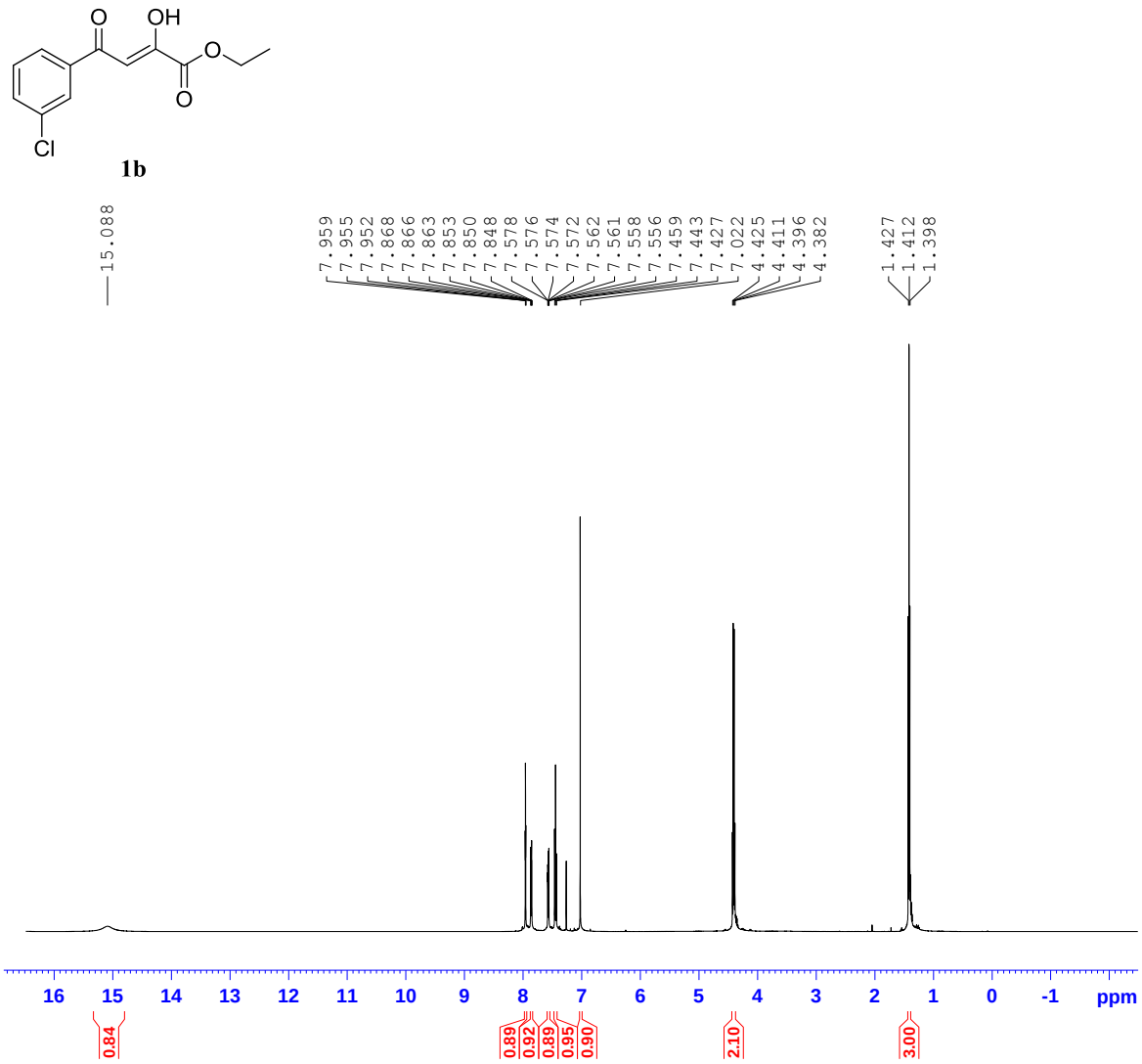

Figure B3. The 500 MHz ^{1}H NMR spectrum of **1b** in $CDCl_3$

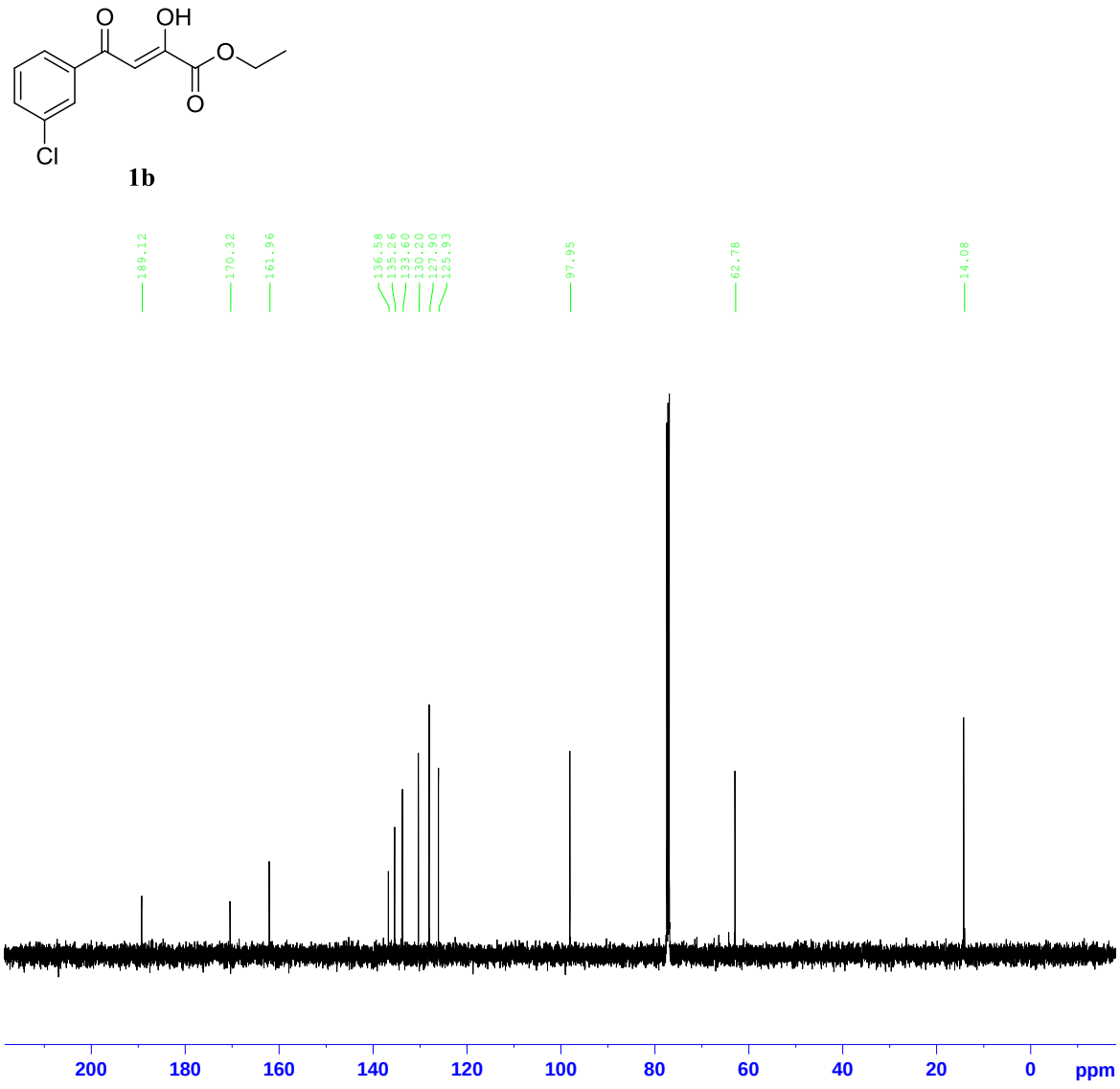

1b

Figure B4. The 125 MHz ^{13}C NMR spectrum of **1b** in $CDCl_3$

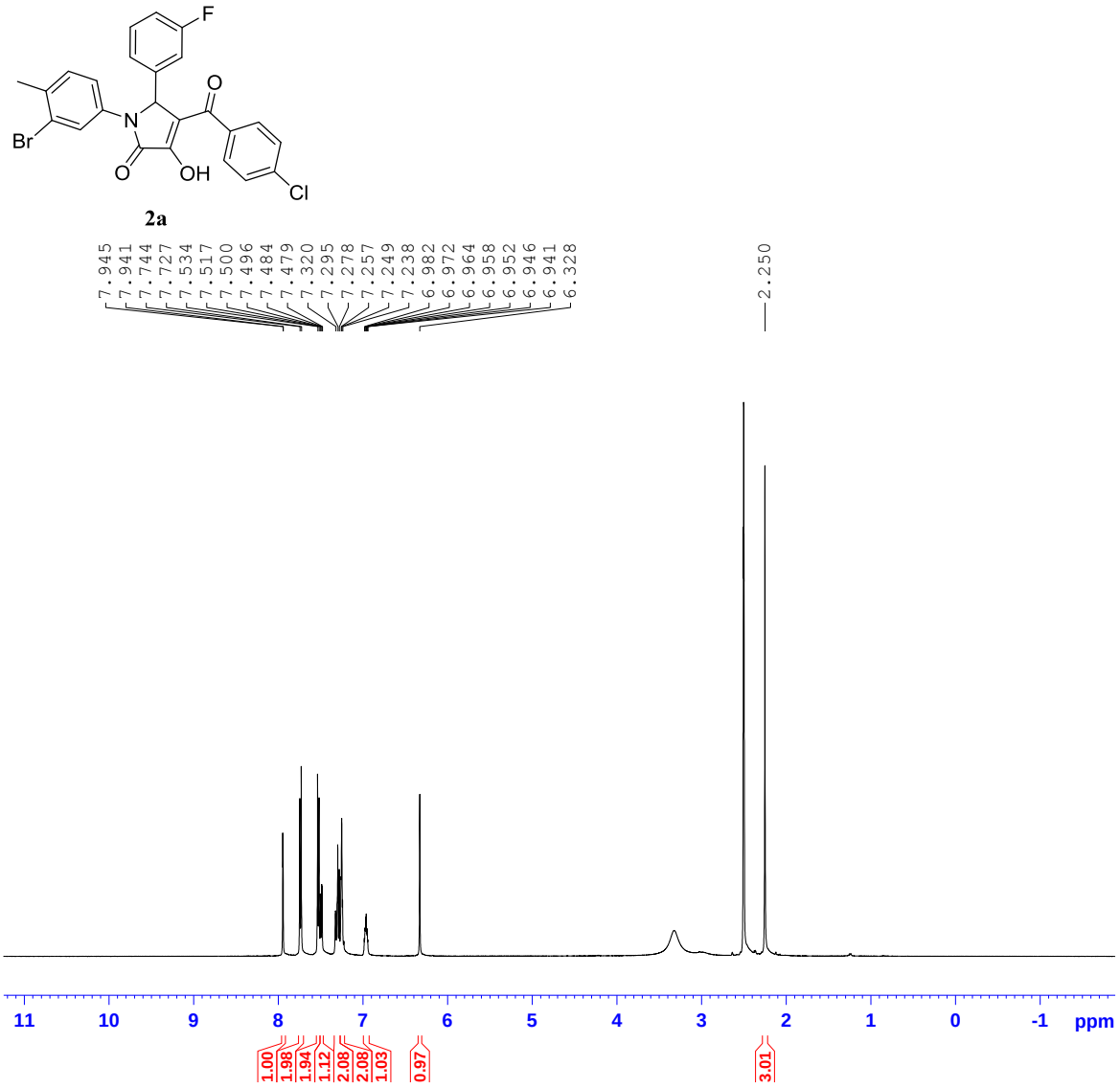

Figure B5. The 500 MHz ^{1}H NMR spectrum of **2a** in DMSO-d_6

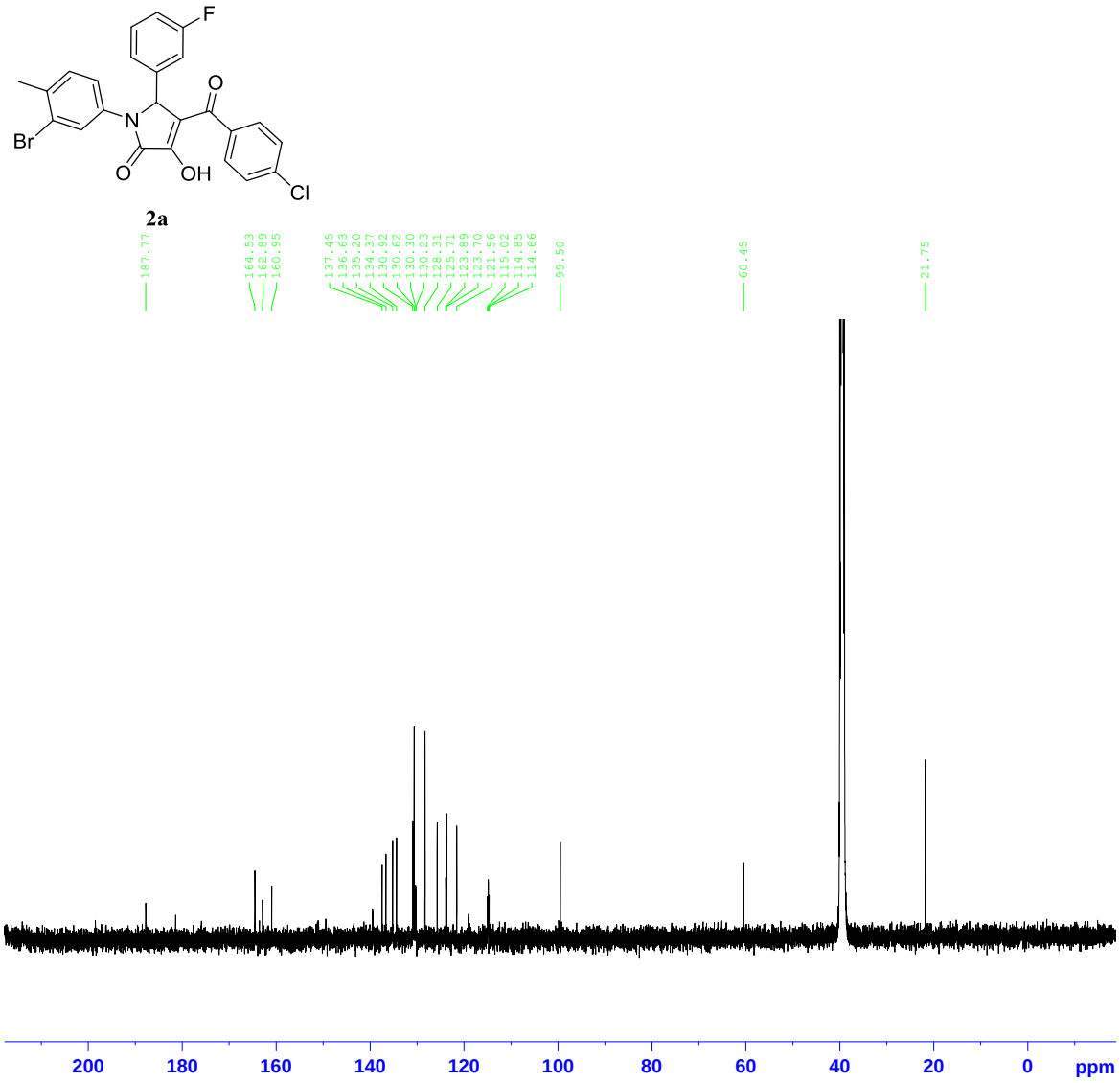

Figure B6. The 125 MHz ^{13}C NMR spectrum of **2a** in DMSO-d_6

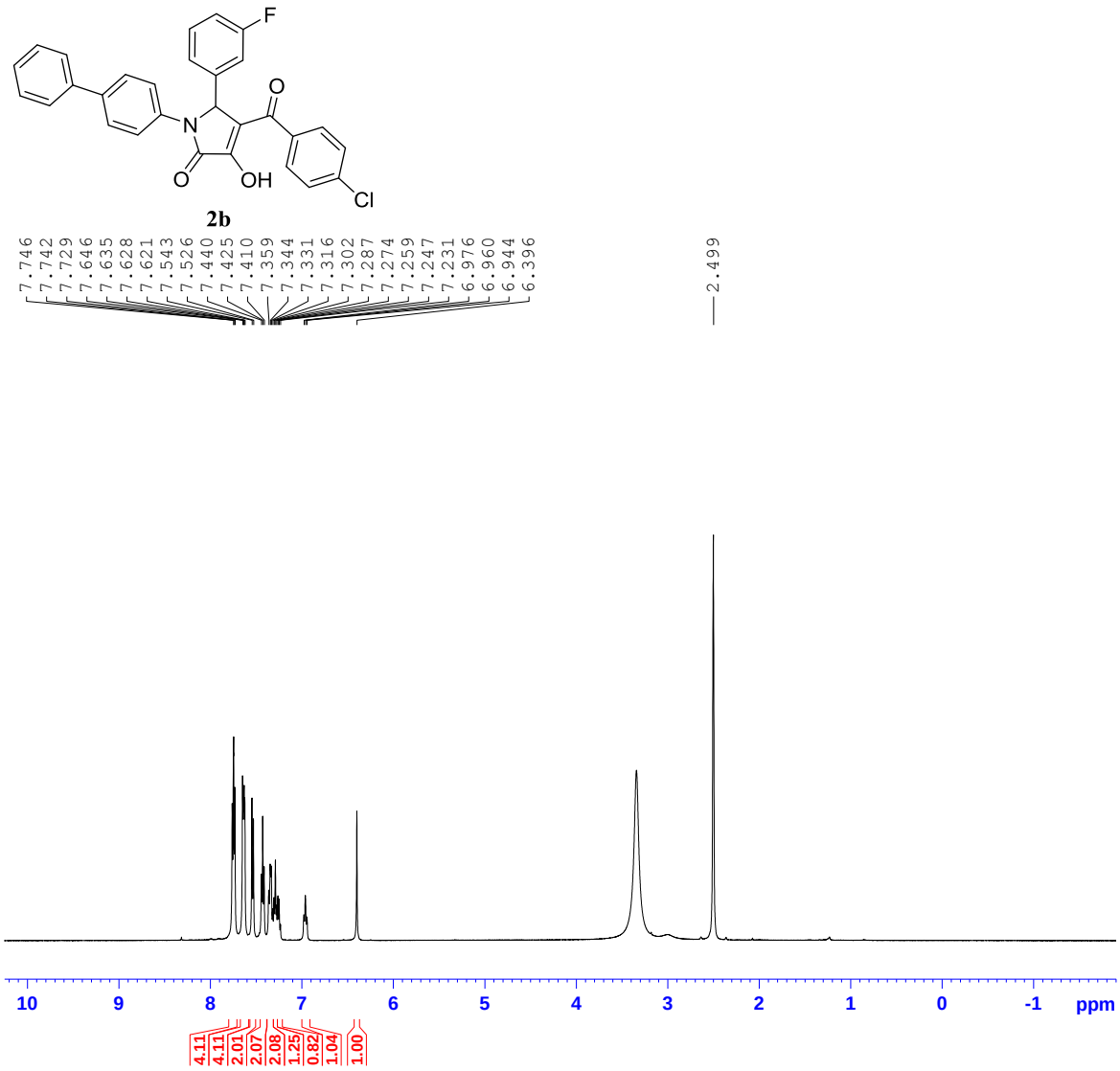

Figure B7. The 500 MHz ^{1}H NMR spectrum of **2b** in DMSO-d_6

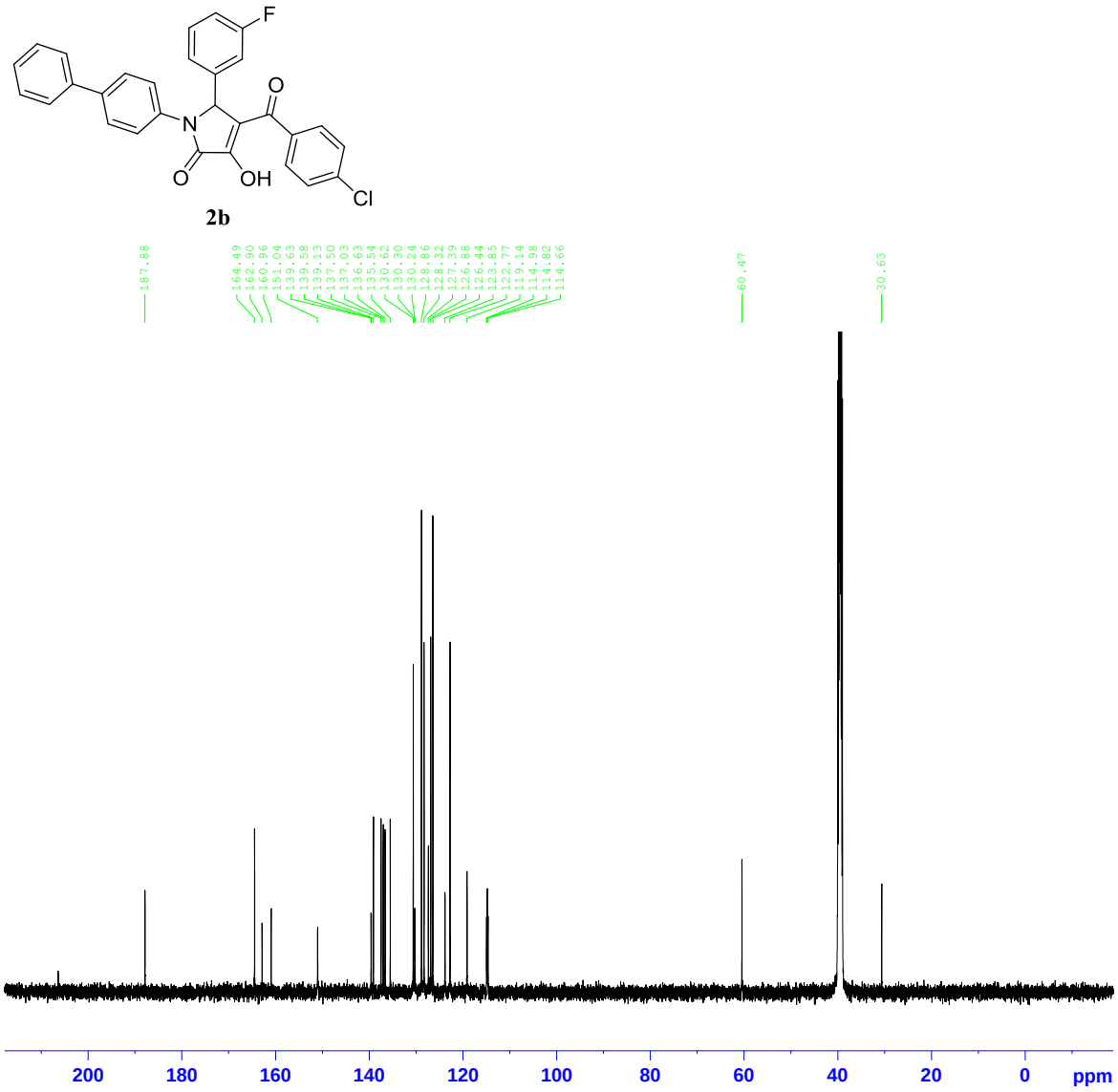

Figure B8. The 125 MHz ^{13}C NMR spectrum of **2b** in DMSO-d_6

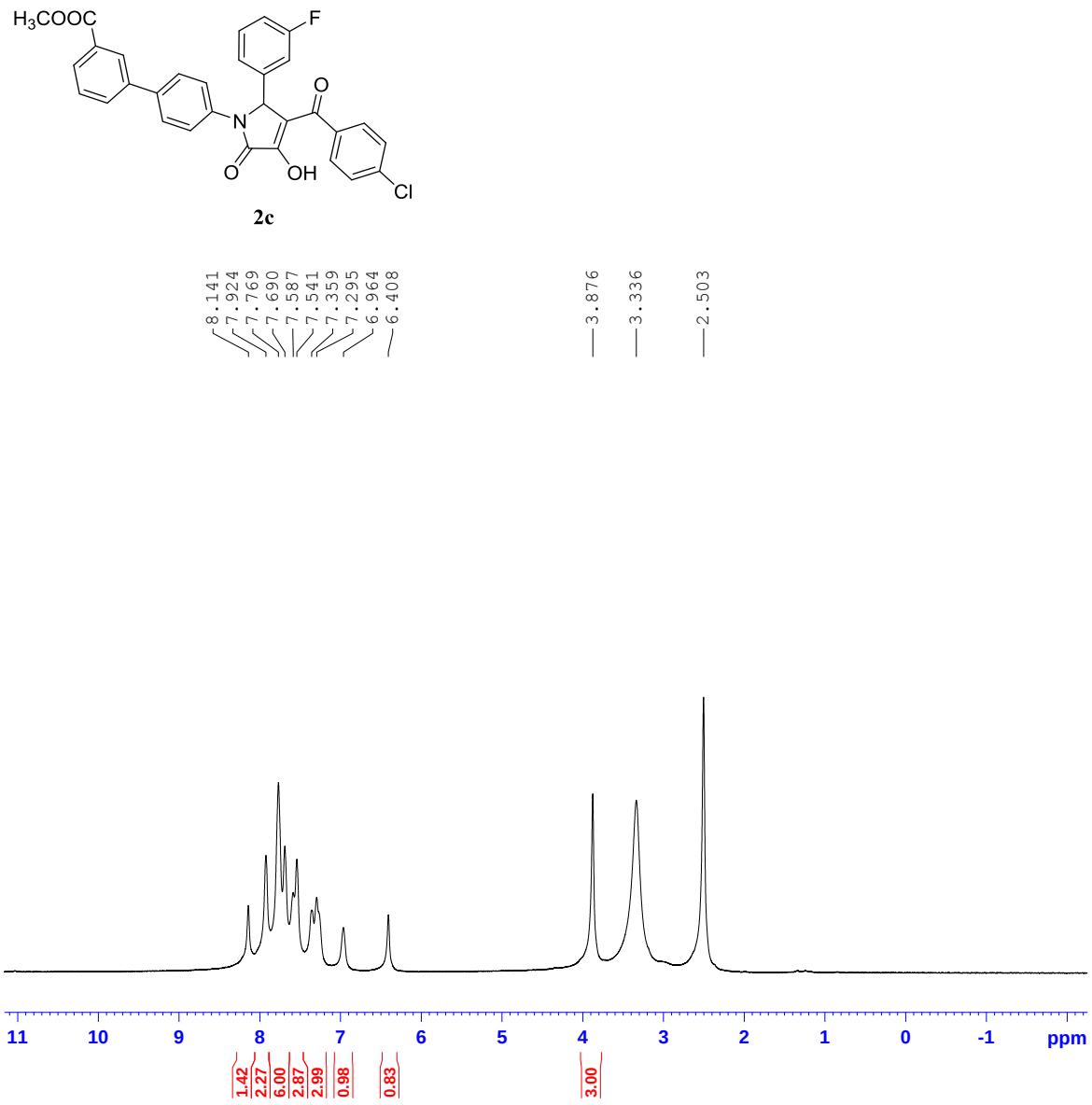

Figure B9. The 500 MHz ^{1}H NMR spectrum of **2c** in DMSO-d_6

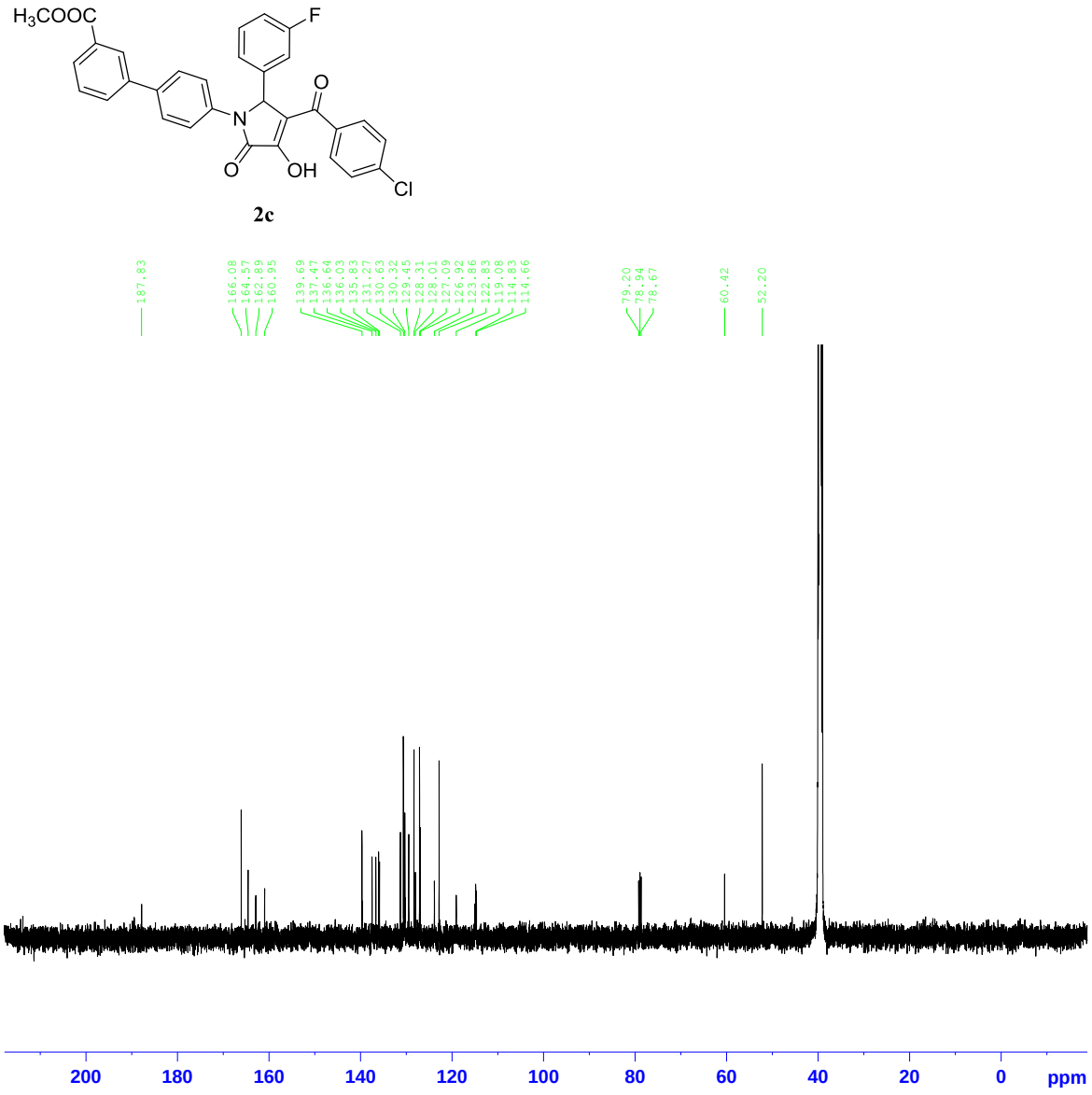

Figure B10. The 125 MHz ^{13}C NMR spectrum of **2c** in DMSO-d_6

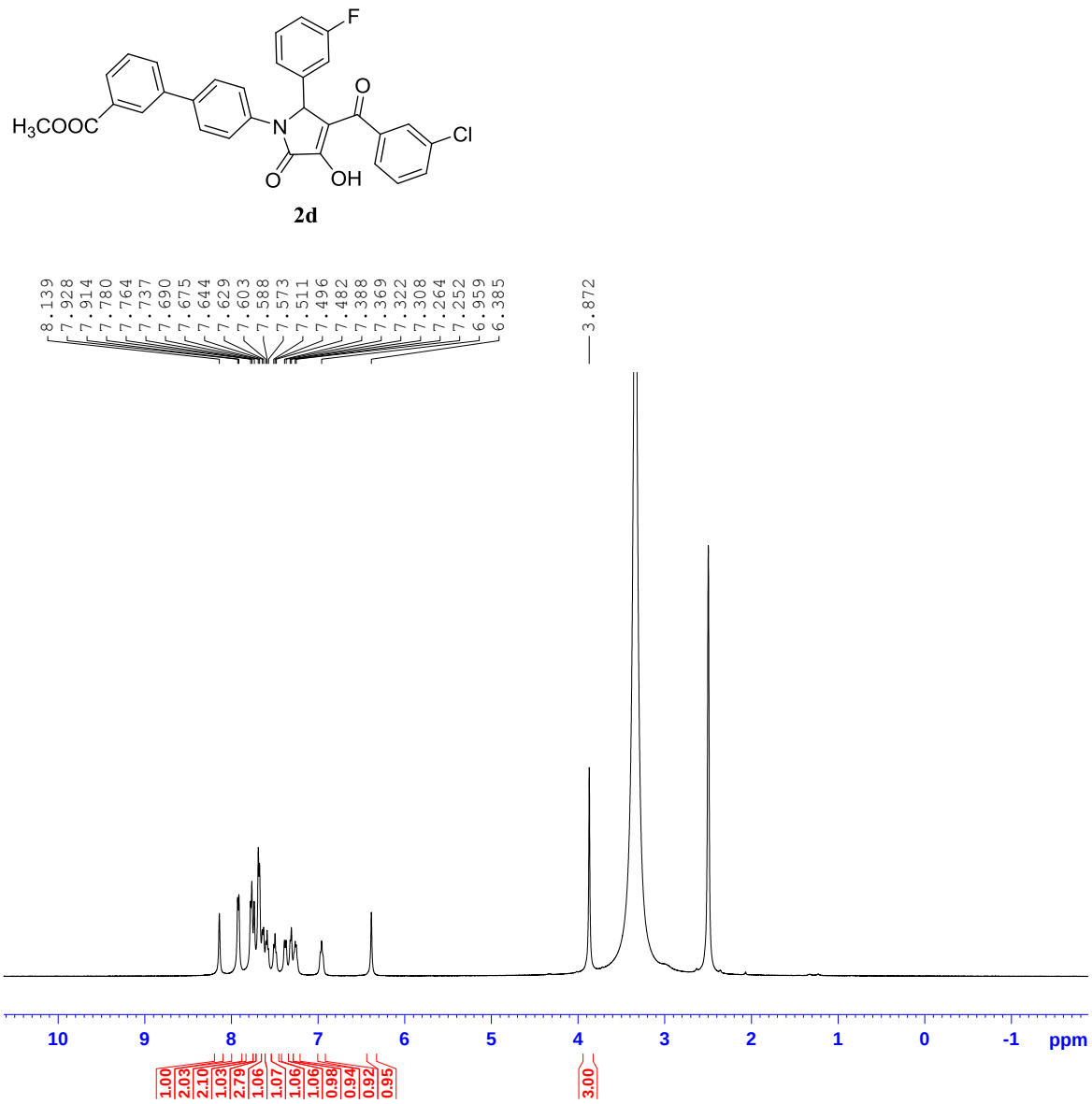

Figure B11. The 500 MHz ^{1}H NMR spectrum of **2d** in DMSO-d_6

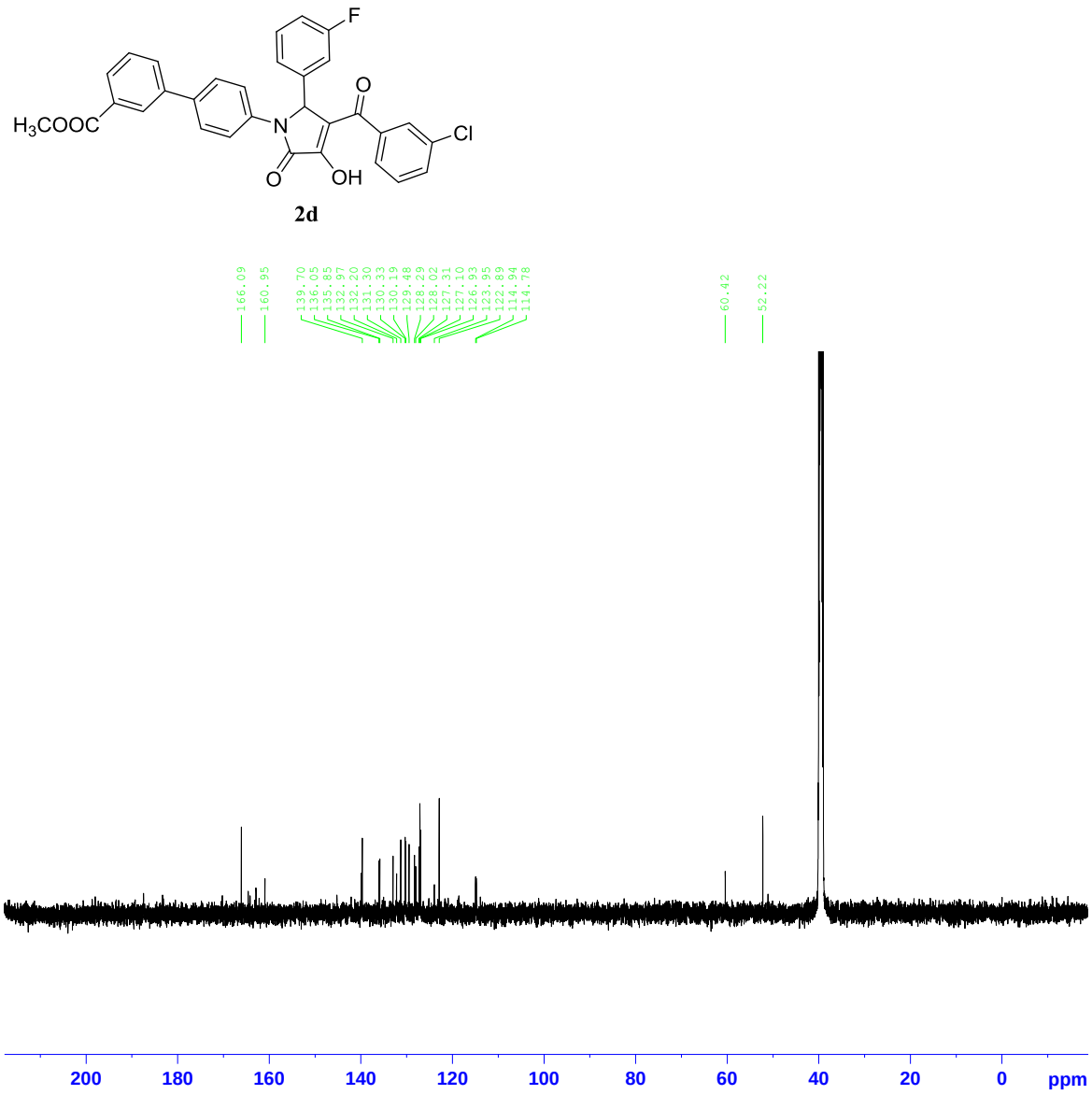

Figure B12. The 125 MHz ^{13}C NMR spectrum of **2d** in DMSO-d_6

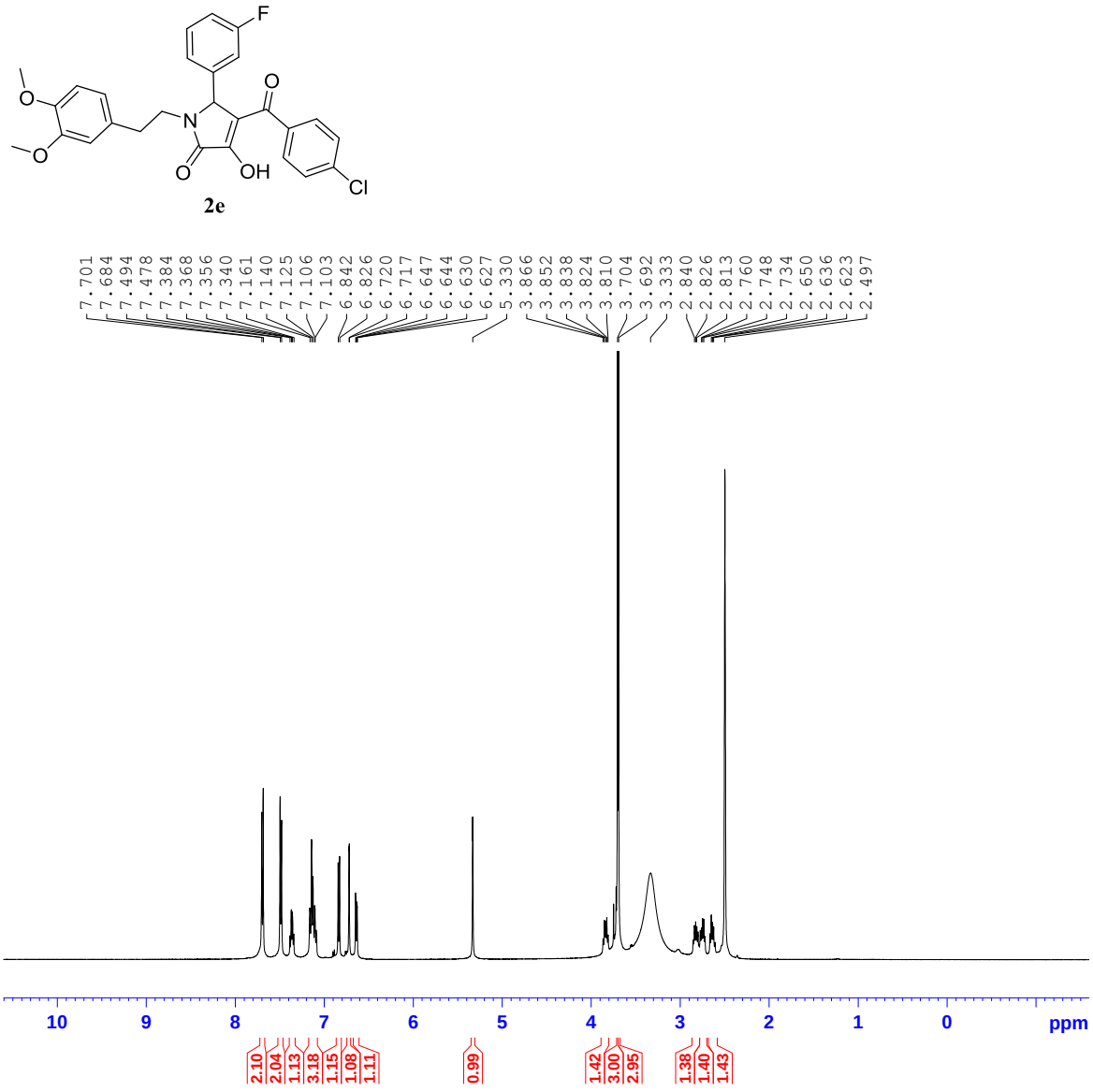

Figure B13. The 500 MHz ^{1}H NMR spectrum of **2e** in DMSO-d_6

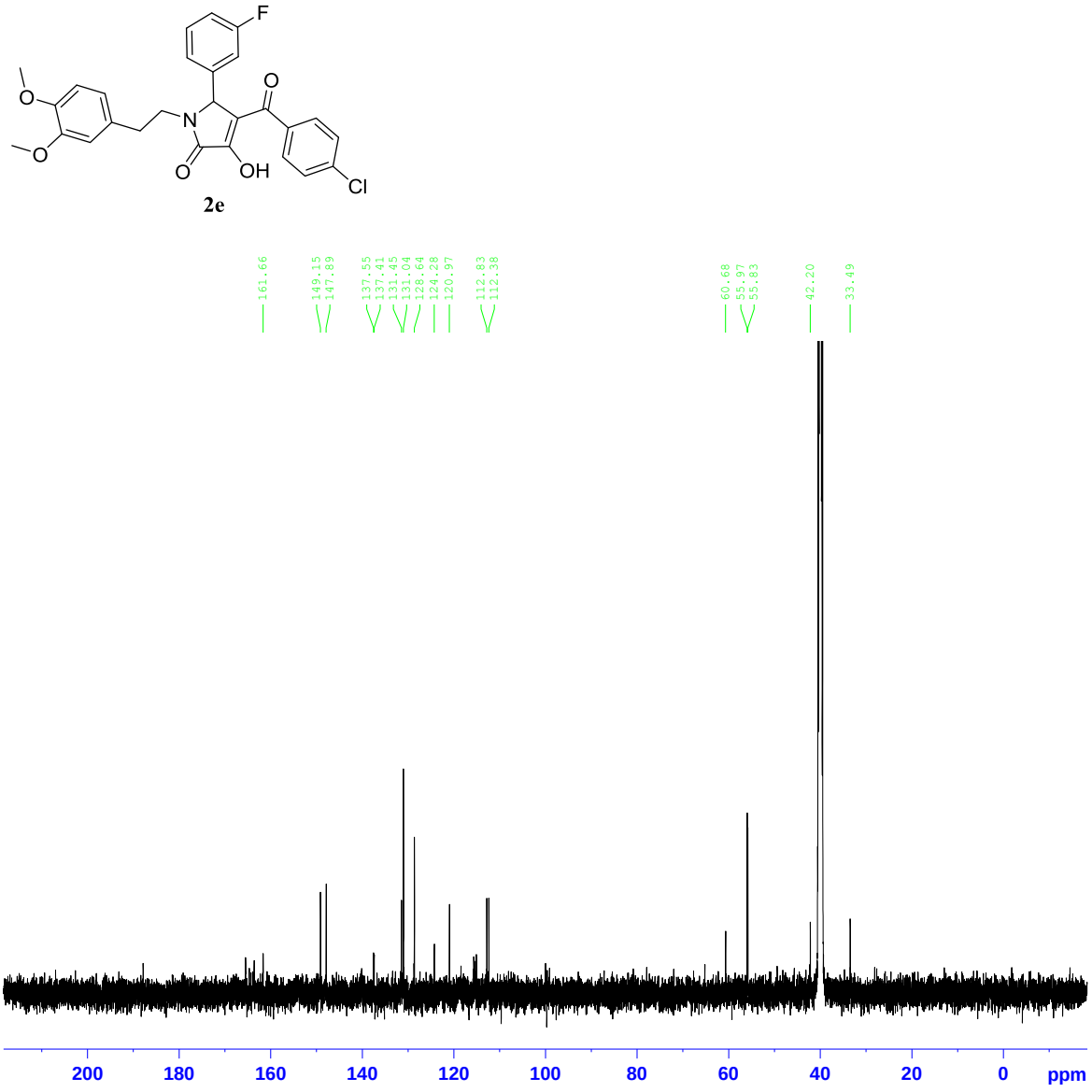

Figure B14. The 125 MHz ^{13}C NMR spectrum of **2e** in DMSO-d_6

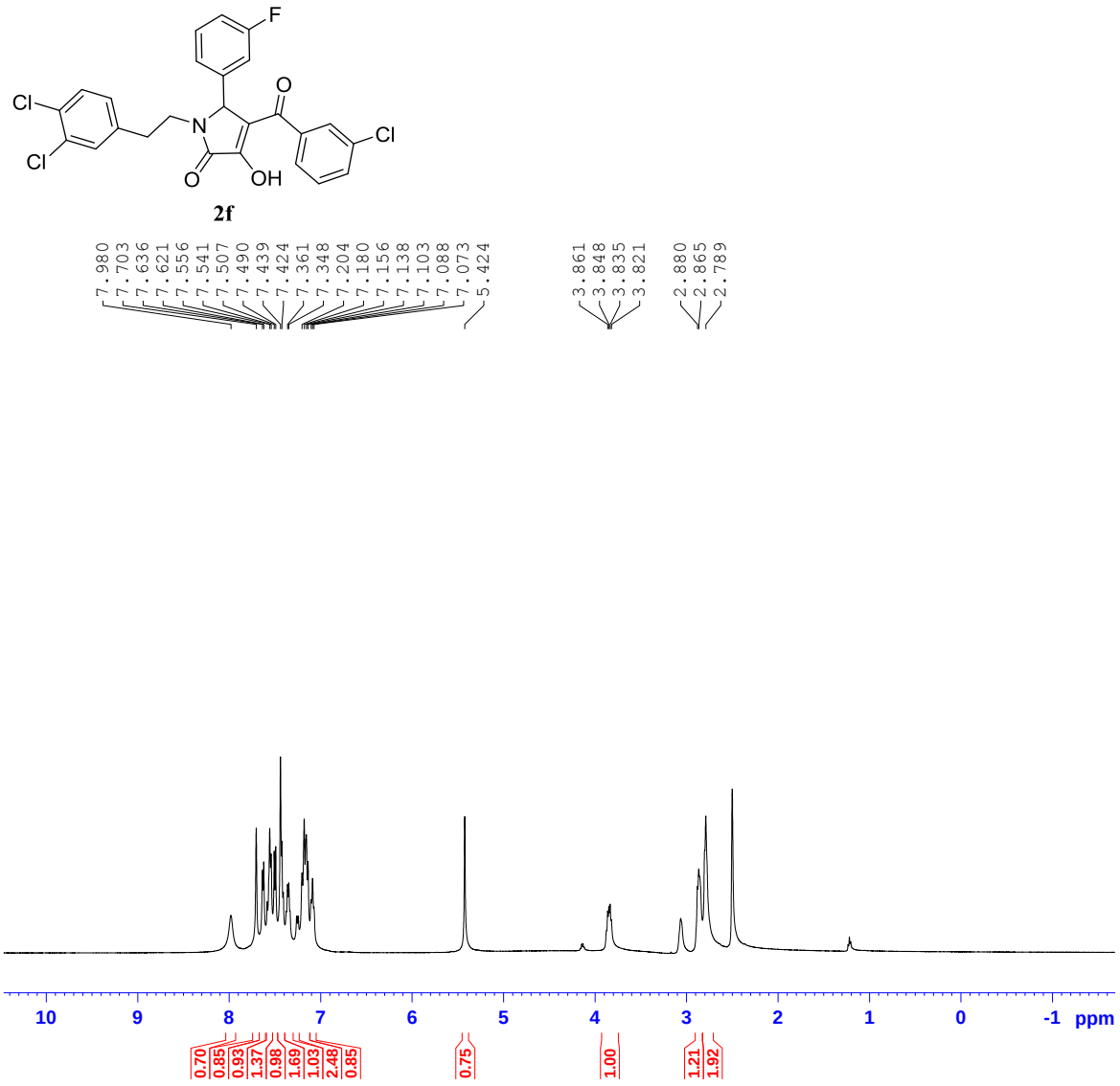

Figure B15. The 500 MHz ^{1}H NMR spectrum of **2f** in DMSO-d_6

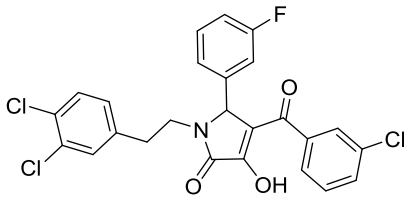

2f

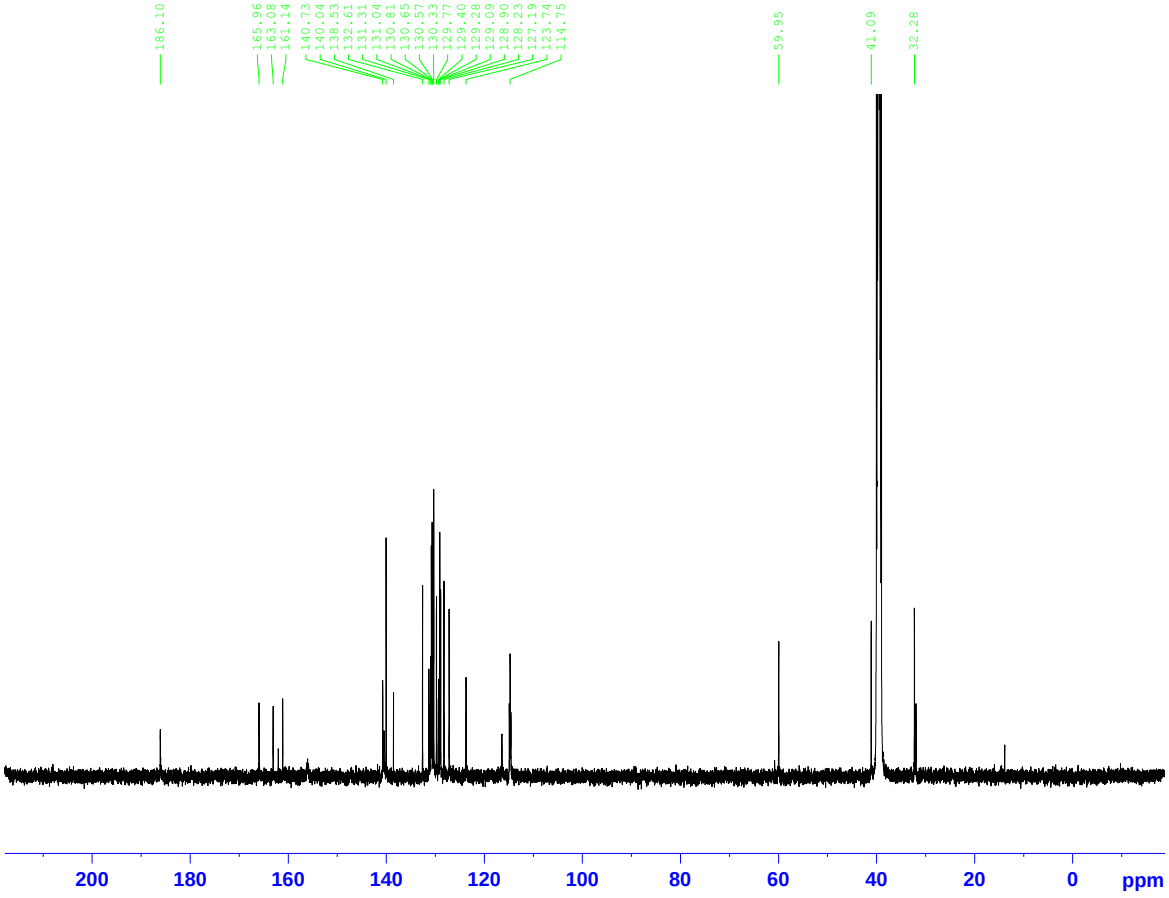

Figure B16. The 125 MHz ^{13}C NMR spectrum of **2f** in DMSO-d_6

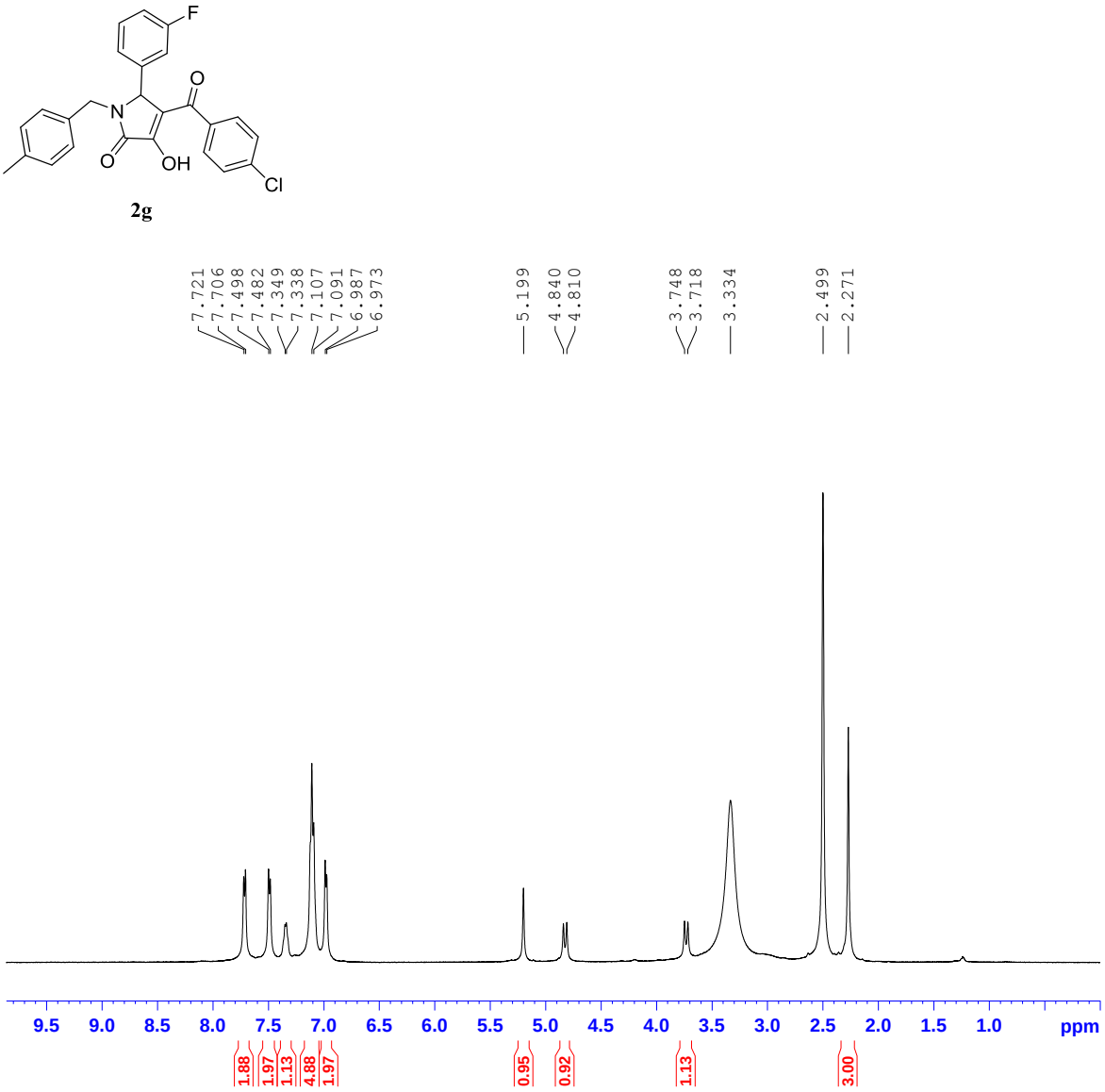

Figure B17. The 500 MHz ^{1}H NMR spectrum of **2g** in DMSO-d_6

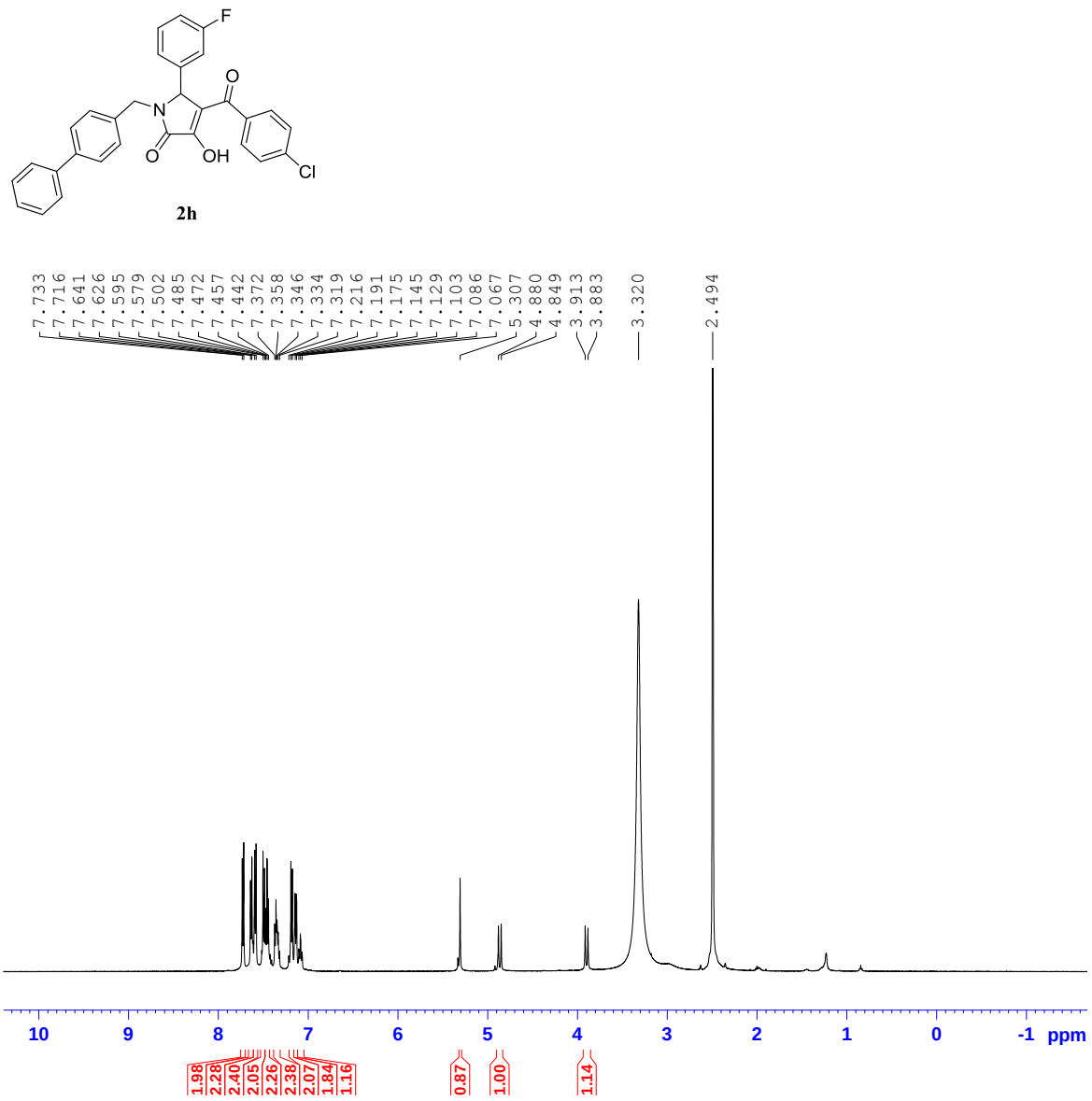

Figure B18. The 500 MHz ^{1}H NMR spectrum of **2h** in DMSO-d_6

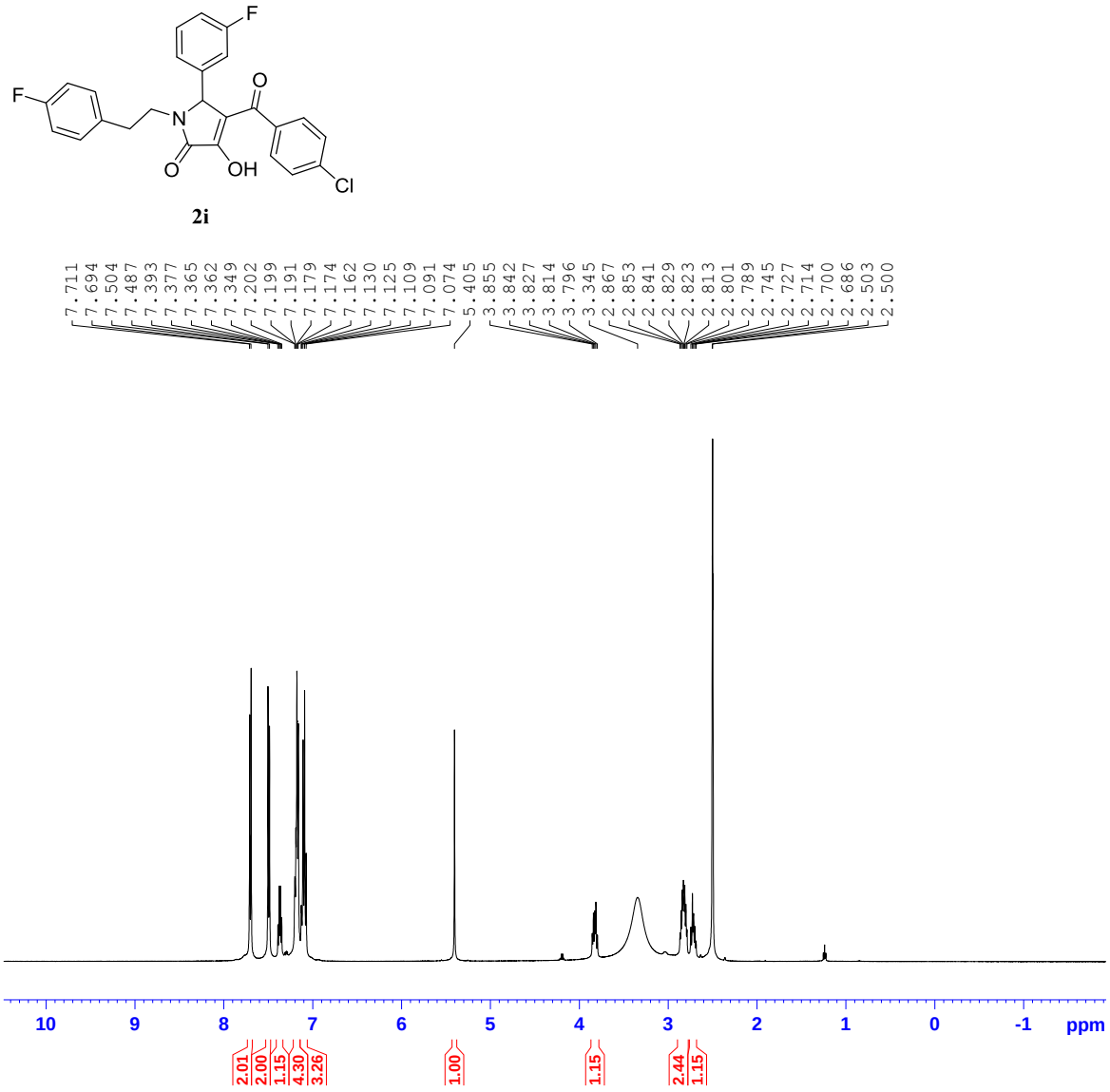

Figure B19. The 500 MHz ^{1}H NMR spectrum of **2i** in DMSO-d_6

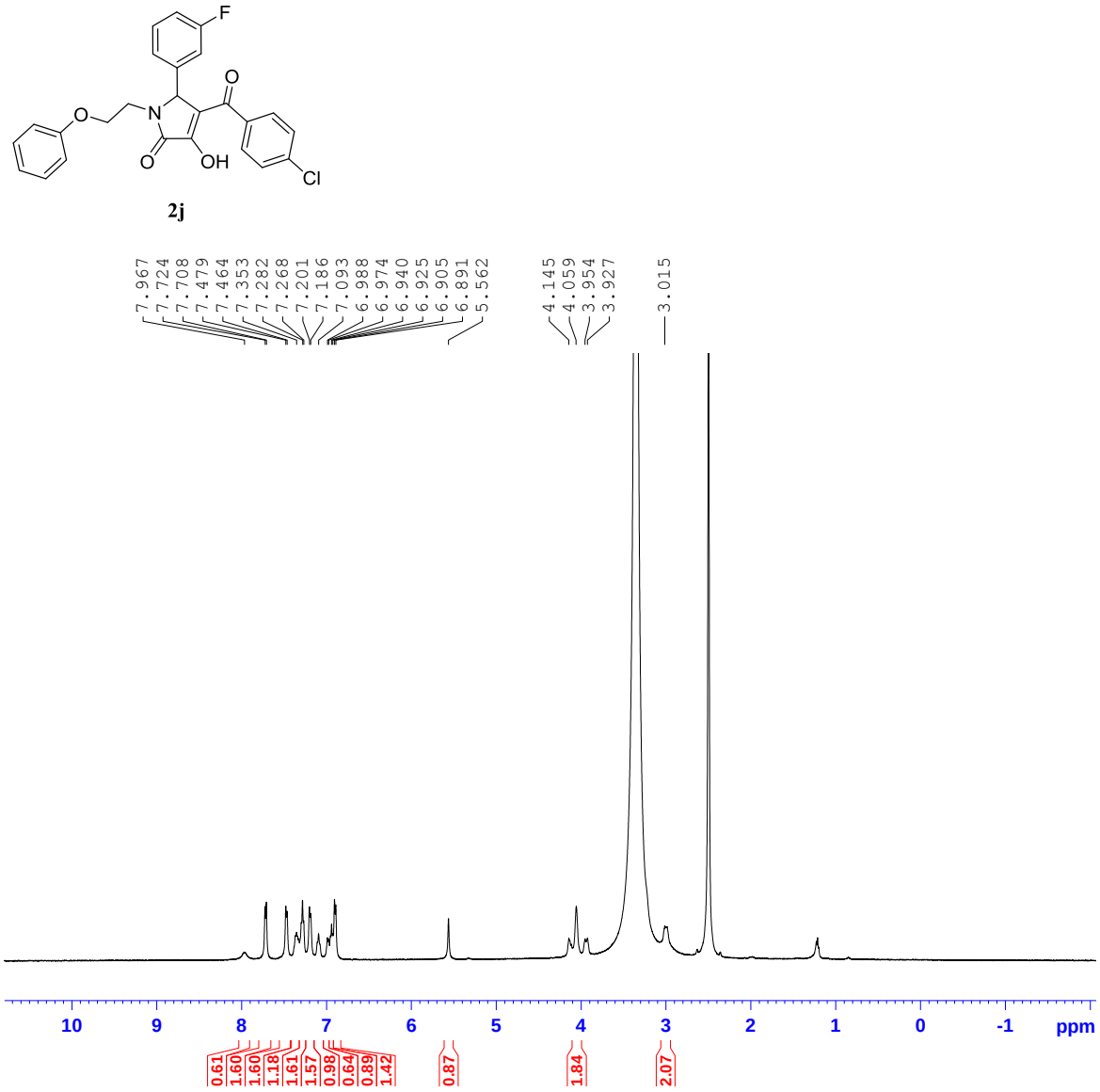

Figure B20. The 500 MHz ^{1}H NMR spectrum of **2j** in DMSO-d_6

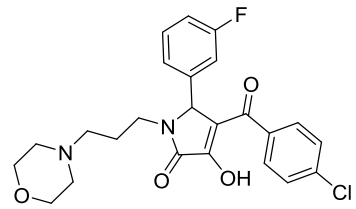

2k

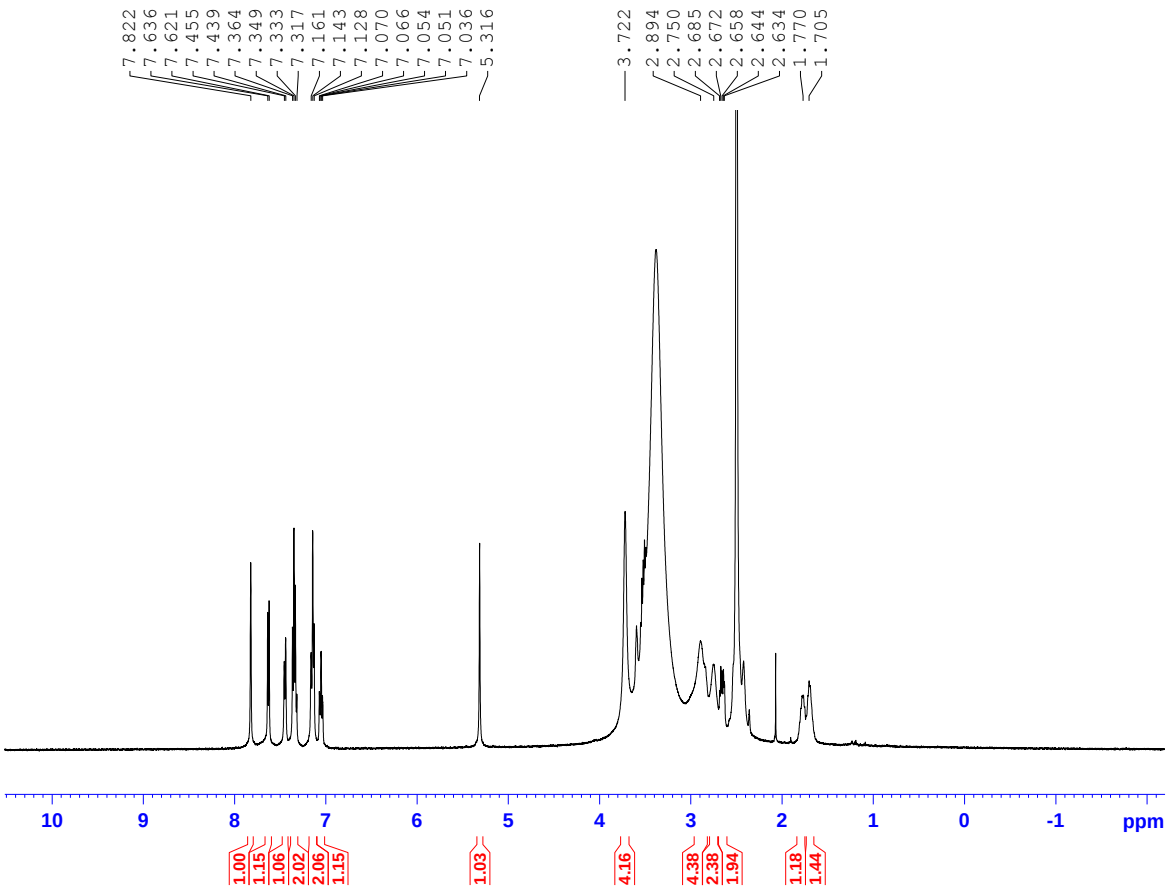

Figure B21. The 500 MHz 1H NMR spectrum of **2k** in DMSO-d_6

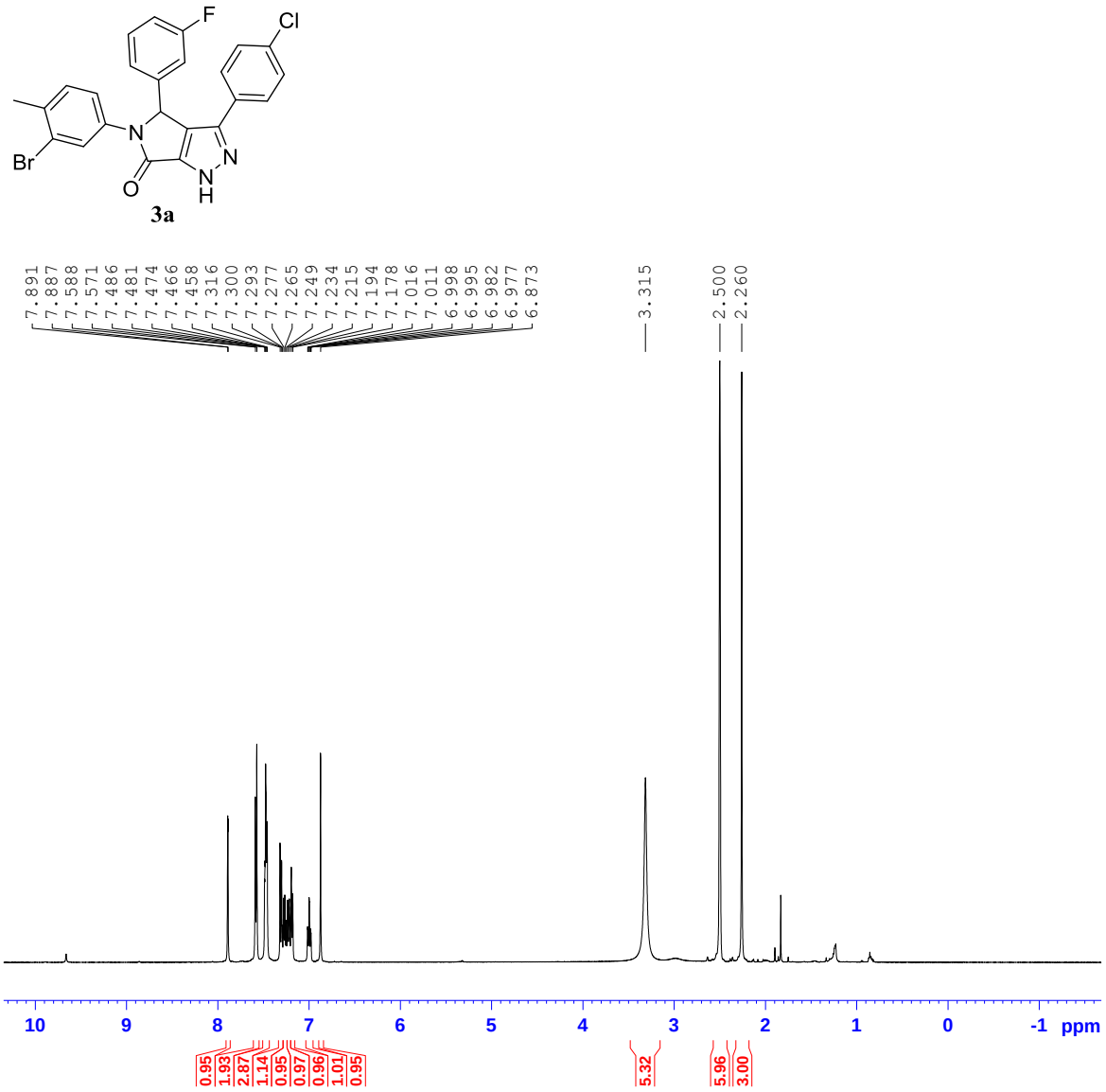

Figure B22. The 500 MHz ^{1}H NMR spectrum of **3a** in DMSO-d_6

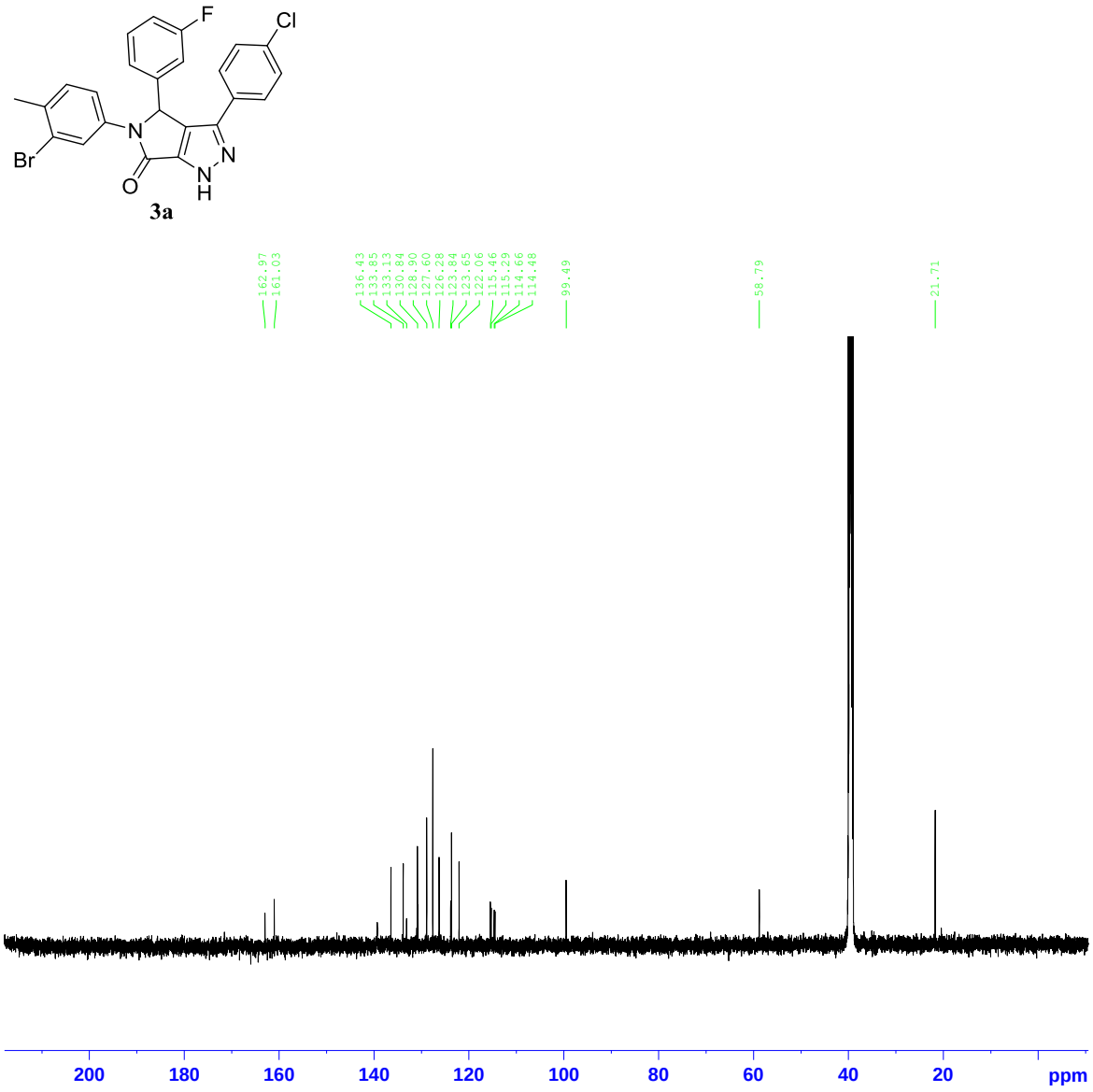

Figure B23. The 125 MHz ^{13}C NMR spectrum of **3a** in DMSO-d_6

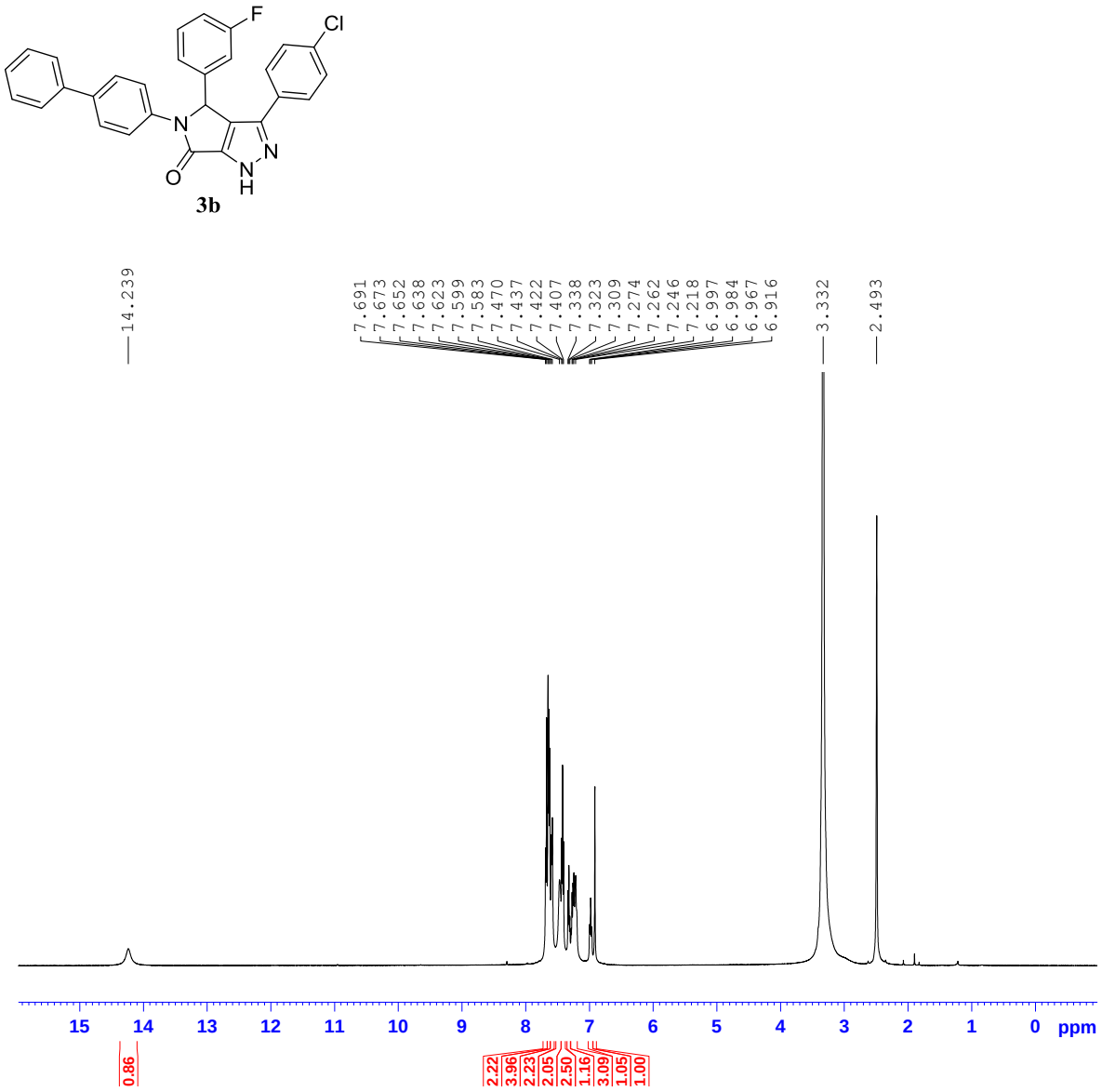

Figure B24. The 500 MHz ^{1}H NMR spectrum of **3b** in DMSO-d_6

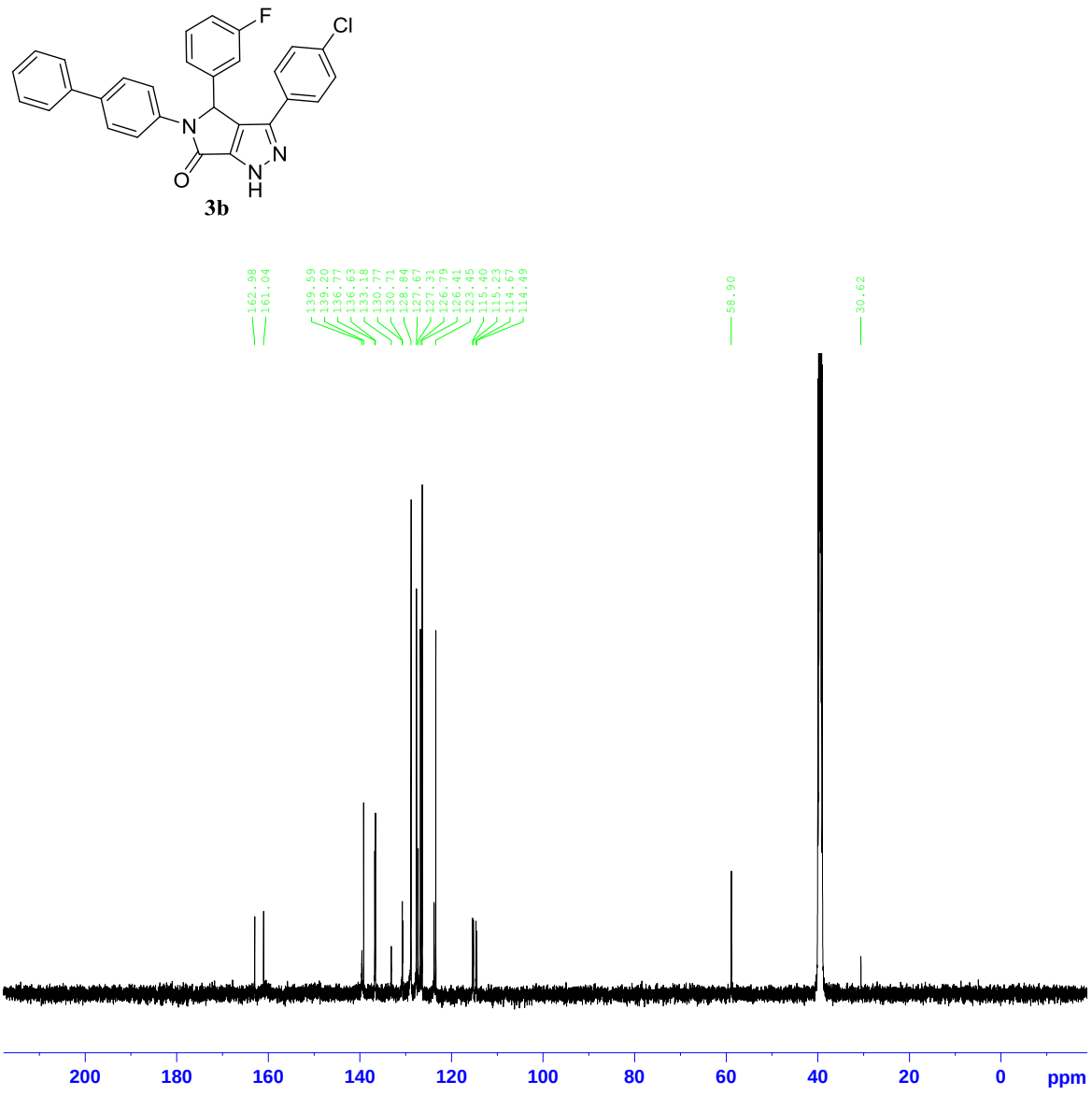

Figure B25. The 125 MHz ^{13}C NMR spectrum of **3b** in DMSO-d_6

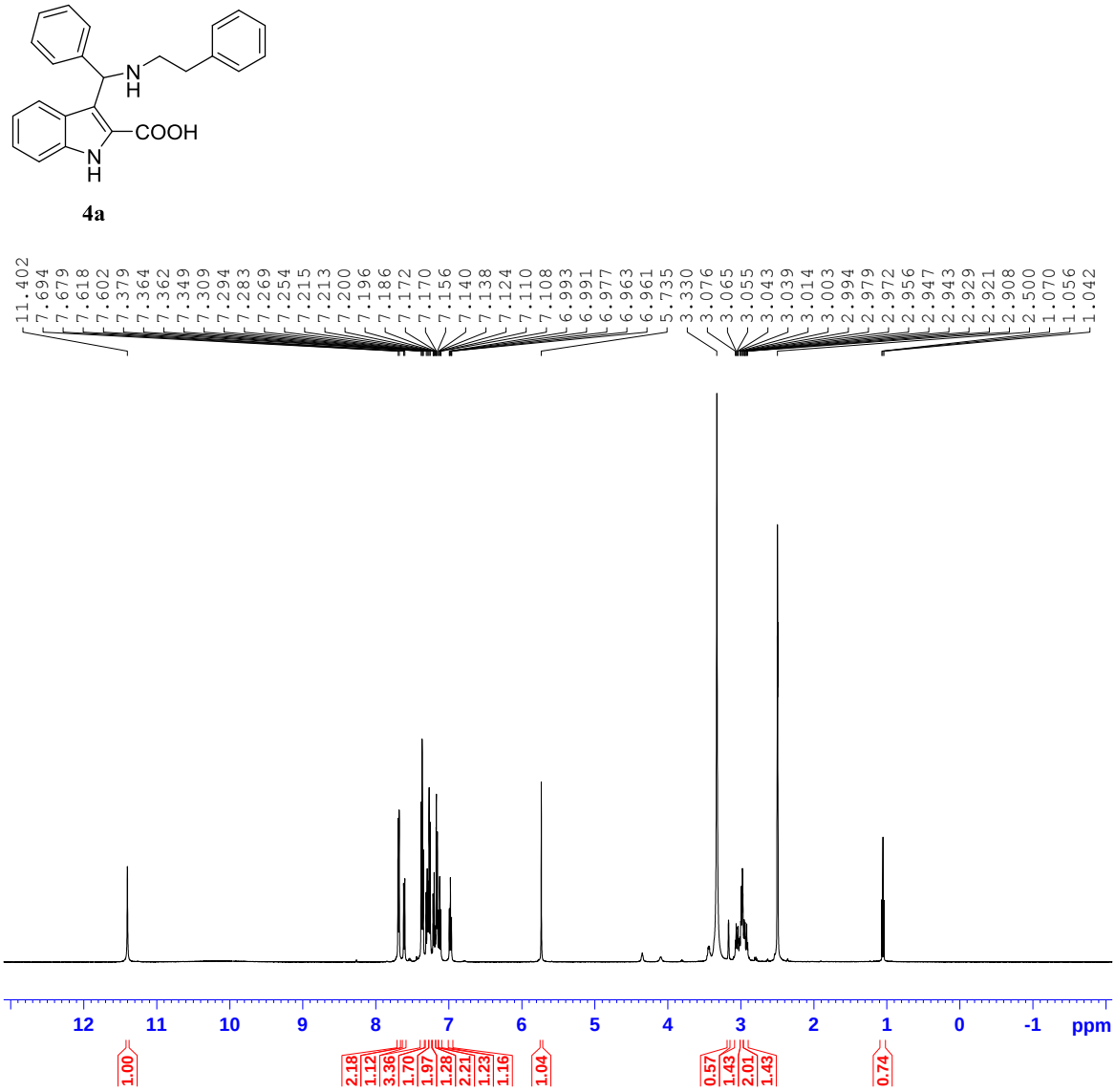

Figure B26. The 500 MHz ^{1}H NMR spectrum of **4a** in DMSO-d_6

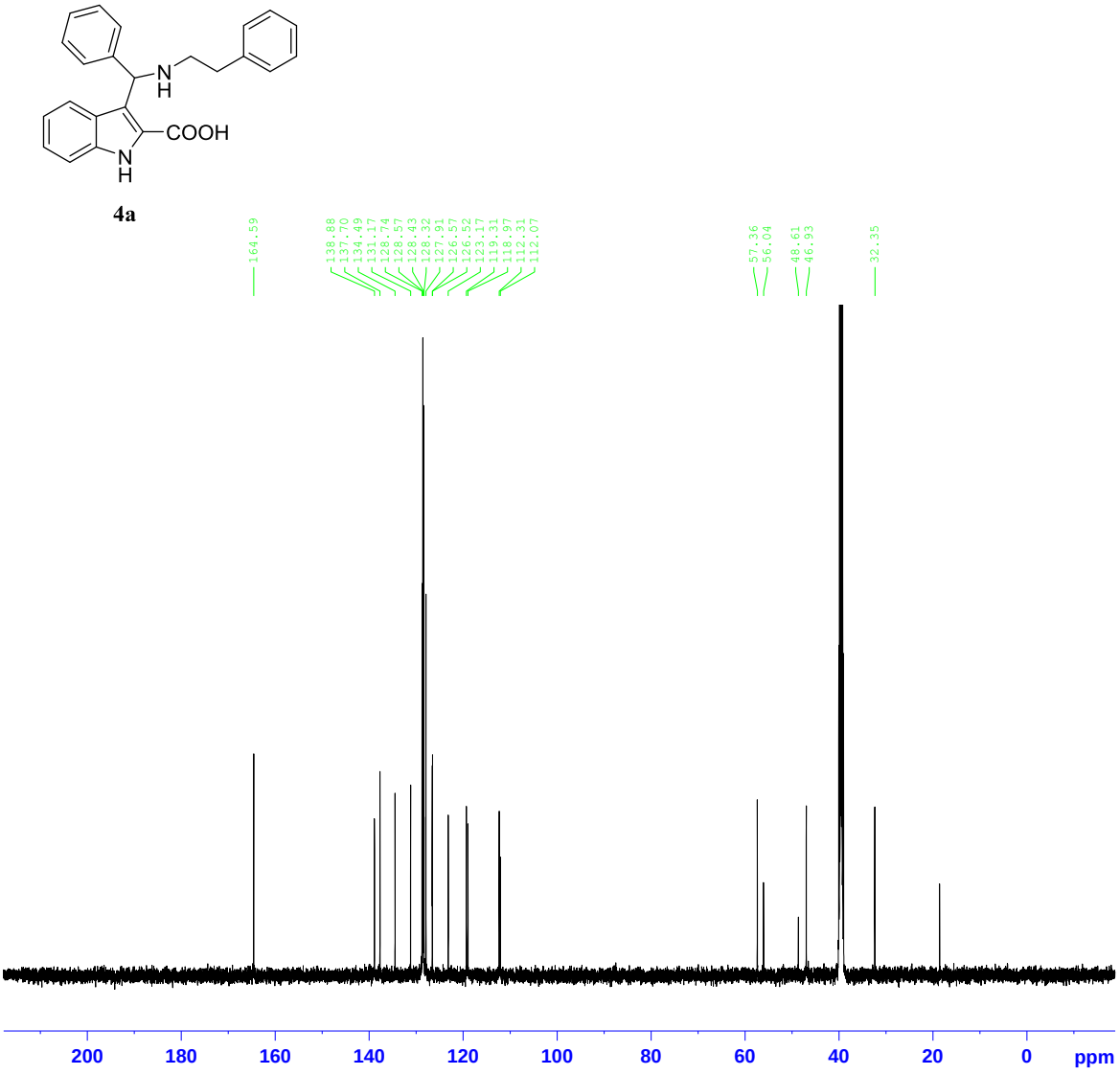

Figure B27. The 125 MHz ^{13}C NMR spectrum of **4a** in DMSO-d_6

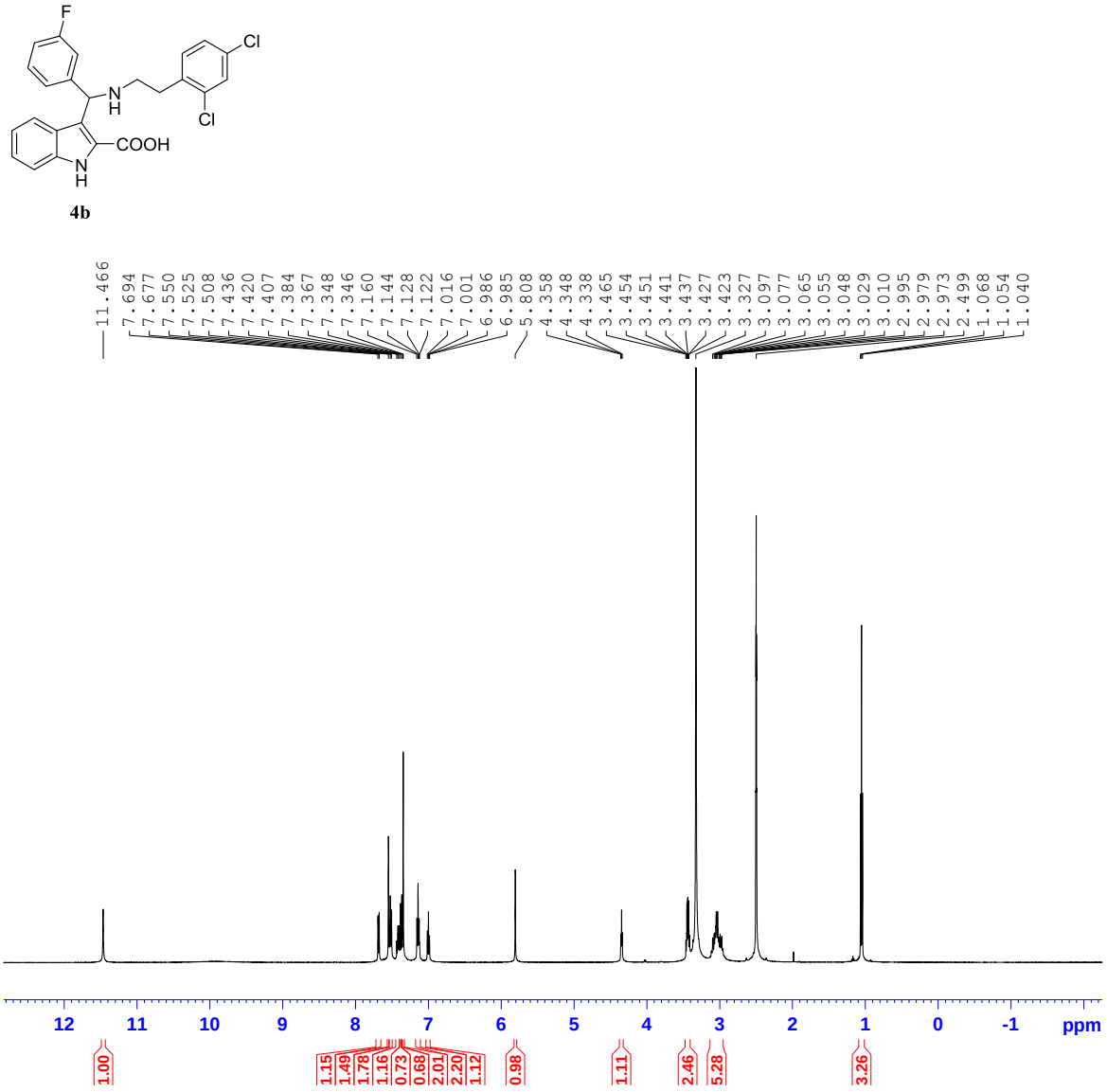

Figure B28. The 500 MHz ^{1}H NMR spectrum of **4b** in DMSO-d_6

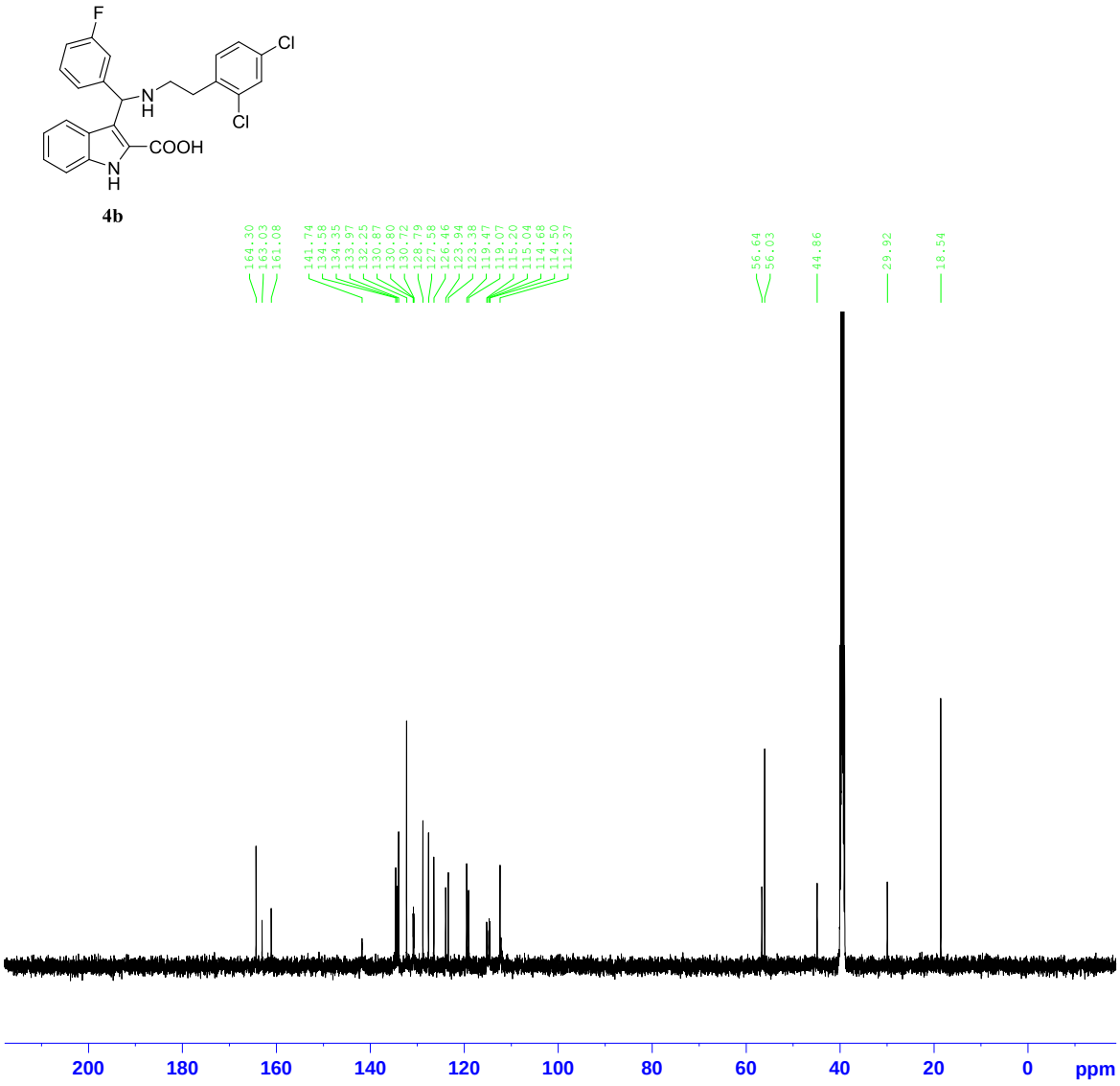

Figure B29. The 125 MHz ^{13}C NMR spectrum of **4b** in DMSO-d_6

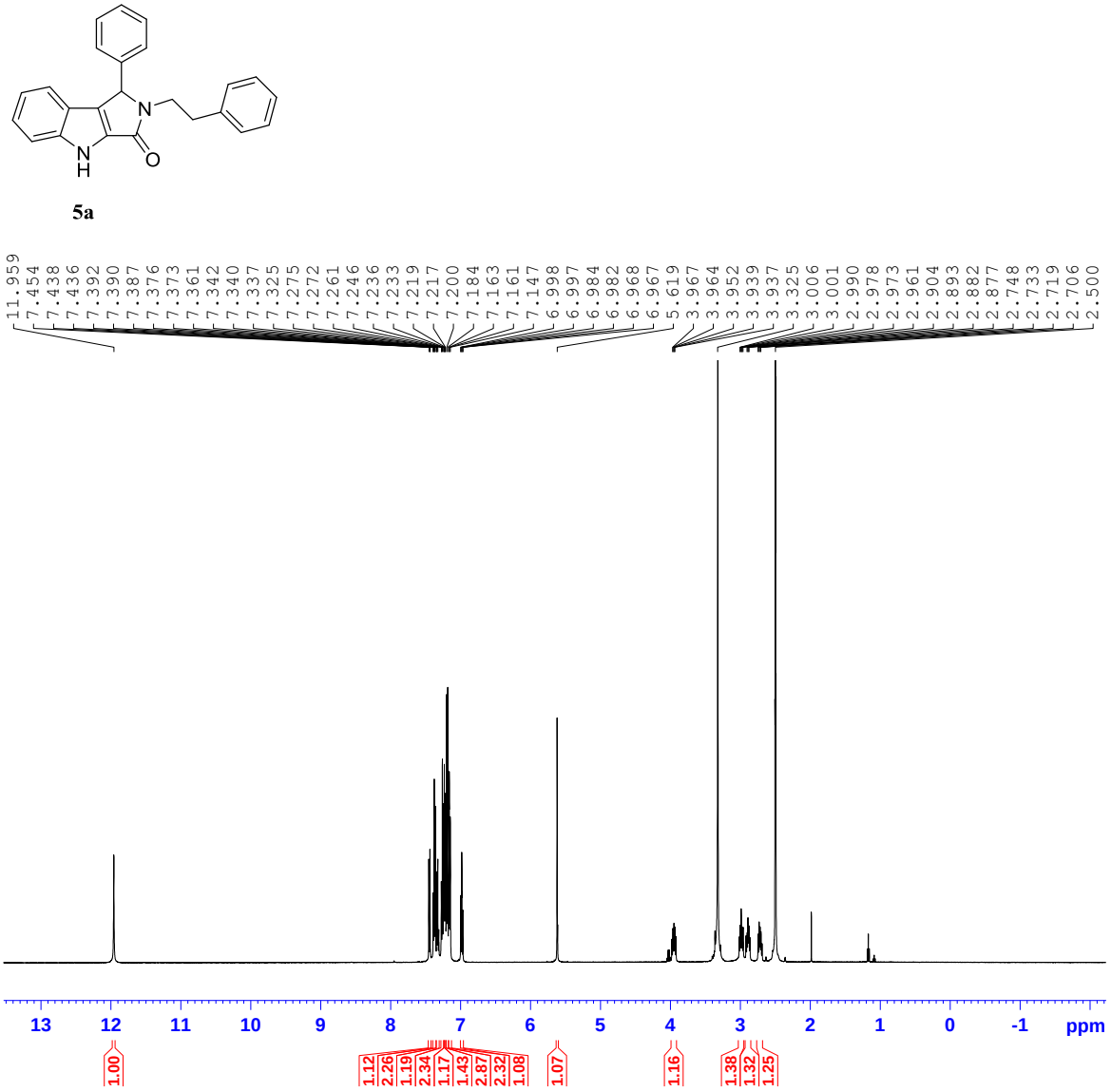

Figure B30. The 500 MHz ^{1}H NMR spectrum of **5a** in DMSO-d_6

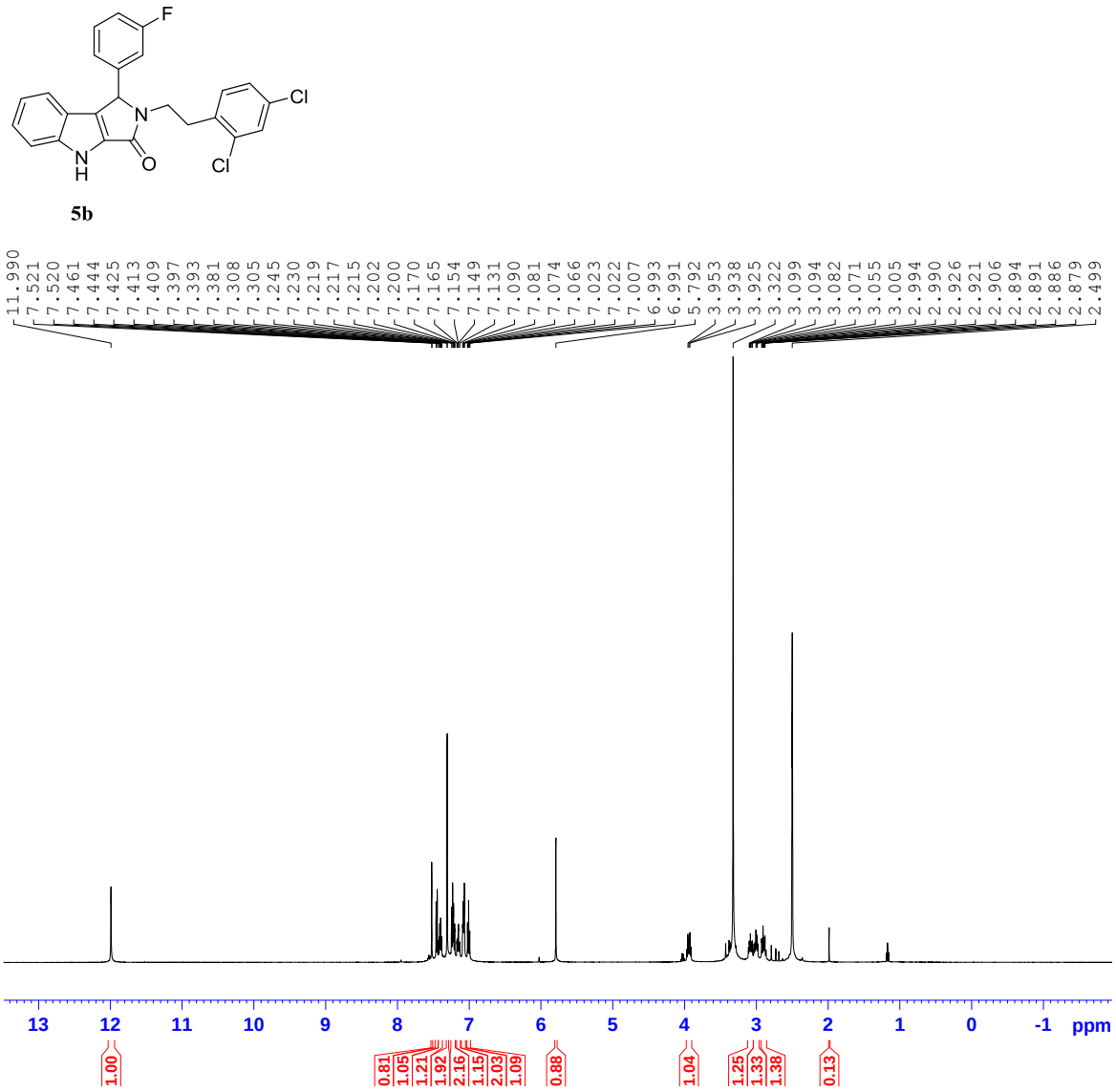

Figure B31. The 500 MHz ^{1}H NMR spectrum of **5b** in DMSO-d_6

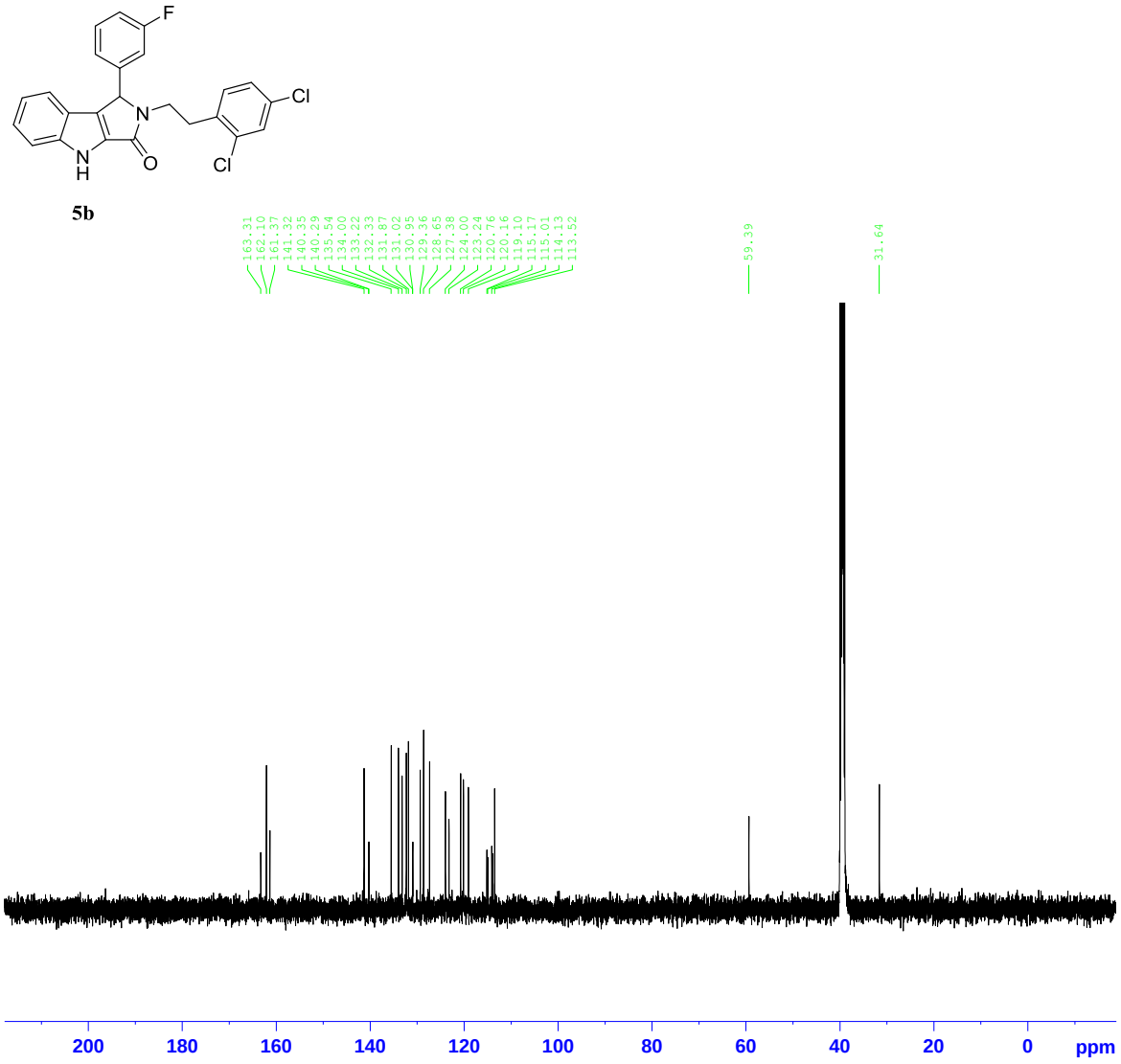

Figure B32. The 125 MHz ^{13}C NMR spectrum of **5b** in DMSO-d_6